UNIVERSITY OF TWENTE.

Faculty of Engineering Technology

BOSCH

Experimental Validation of Simulations on flow through Venturis and Diffusers

Bastiaan Drenth
Internship report
April 2016

Supervisors:
mw. dr. ir. D. van de Belt (Internship coordinator)
prof. dr. ir. H.W.M. Hoeijmakers (Mentor UT)
dr. ir. D. de Kleine (Mentor Bosch)

Faculty of Engineering Technology
Engineering Fluid Dynamics Group
University of Twente
P.O. Box 217
7500 AE Enschede
The Netherlands

Summary

The R&D department of Bosch Thermotechnology B.V. in Deventer focuses its research on wall mounted boilers. Wall mounted boilers are used in houses for central heating and the supply of hot water. Heat is generated by burning a mixture of air and gas. The hot gases pass a heat exchanger with metal pins which transfer the heat from the hot gases to the water. Mixing of the air and gas is done in a so called venturi pipe. A venturi is a section of pipe with a contraction. The velocity in this contraction is increased, which causes the static pressure to drop. This section of low pressure can be used to suck in the gas. The venturi will also ensure the right ratio of gas to air which is needed to ensure safe combustion and the right amount of emissions. Venturi pipes will induce a certain amount of pressure loss, caused mostly in the diverging part of the venturi. The EHC5 department in Deventer does simulations on the flow through venturis to try and minimize the amount of pressure loss and optimize venturis. Minimizing the amount of pressure loss will increase the modulation range of the boiler. The goal of this research is to validate these simulations by experiment by performing pressure measurements on diffusers and venturis.

A number of experiments will be performed to make sure the experimental set-up is reliable. The main set-up will consist of a fan to create an airflow and an orifice meter to measure the amount of mass flow. The challenge is to create a fully developed flow in the test section. This requires a certain amount of entry length of pipe. The accuracy of the pressure measurement will first be tested by measuring the pressure distribution on a section of PVC and copper pipe. Results showed variations in the pressure drop over small sections of pipe, which were accredited to defects in the manufacturing of the pressure taps. During the next experiments the pressure distribution was measured over a set of diffusers with and without gas inlet and with different diverging angles. For these experiments better care was taken in the manufacturing of the static pressure taps. Results of the pressure distribution of the diffusers without a gas inlet showed good agreement with simulations. The only large difference in static pressure between measurements and simulations occurred at the entry of the diffusers. This difference was due to a deviation in the diameter of the entry pipe, which caused a higher velocity and thus lower static pressure than expected. When the gas inlet was open, the results of the measurements showed large deviations with respect to the simulations. Simulations predicted a larger amount of pressure loss than observed during the measurements. For the final experiment a WB6 venturi was used. The measured static pressure was different from the theoretical value, as a far lower static pressure was observed in the throat of the venturi. Also, the amount of pressure loss was larger than expected.

Contents

Appendices

List of symbols

Symbol	**Quantity**	**Unit**
β	Ratio between orifice throat diameter and pipe diameter	-
δ	Boundary layer thickness	m
ϵ	Roughness height	m
ϵ_f	Expansion factor	-
κ	Isentropic component	-
μ	Dynamic viscosity	Pa s
ρ	Density	kg m^{-3}
τ_w	Wall shear stress	Pa
ϕ	Equivalence ratio	-
A	Cross-sectional area	m^2
C	Discharge coefficient	-
D	Diameter	m
L	Length	m
P	Static pressure	Pa
R_s	Specific gas constant	J kg^{-1} K^{-1}
Re	Reynolds number	-
Re_D	Reynolds number based on diameter D	-
$\overrightarrow{S}$	Area vector	m^2
Y	Mass fraction	-
d	Orifice throat diameter	m
f	Darcy friction factor	-
q	Dynamic pressure	Pa
q_m	Mass flow rate	kg s^{-1}
s	Mass stoichiometric ratio	-
$\overrightarrow{u}$	Velocity vector	m s^{-1}
v	Velocity	m s^{-1}

Chapter 1

Introduction

1.1 Company

The Bosch Group was founded in 1886 by Robert Bosch in Stuttgart. The company is a leading global supplier of technology and services and covers different business sectors including mobility solutions, industrial technology, consumer goods and energy and building technology.

The brands Bosch, Nefit and Buderus have been brought together in 2013 to form Bosch Thermotechniek B.V., which is located in Deventer. It has an R&D and production department, both focused on wall mounted boilers. Wall mounted boilers produced in Deventer are sold under the brand Nefit.

1.2 Wall mounted boilers

A schematic of a wall mounted boiler can be found in Figure 1.1. An airflow is generated by the fan and enters the set-up through the air intake. Mixing of the air and gas takes place in the venturi nozzle. When the airflow passes the contraction the velocity increases. This increase in velocity will cause the pressure to drop to a value which is lower then the ambient pressure. This underpressure is used to inject the gas in the flow of air. Mixing of the gas with the air is improved when the flow passes the fan. Heat is generated in the boiler by burning the air-gas mixture in the burner unit. The hot flue gas flows through a heat exchanger containing metal fins, which transfer the heat from the hot gases to water. The condensate which is formed when the temperature of the burned gases decreases, is collected in a condensate collector. The remaining gases exit the boiler through the exhaust.

There is a certain maximum and minimum output power that the boiler can deliver. Maximum output power is achieved when the fan operates at maximum power. The fan power can be decreased until at a certain point the amount of underpres-

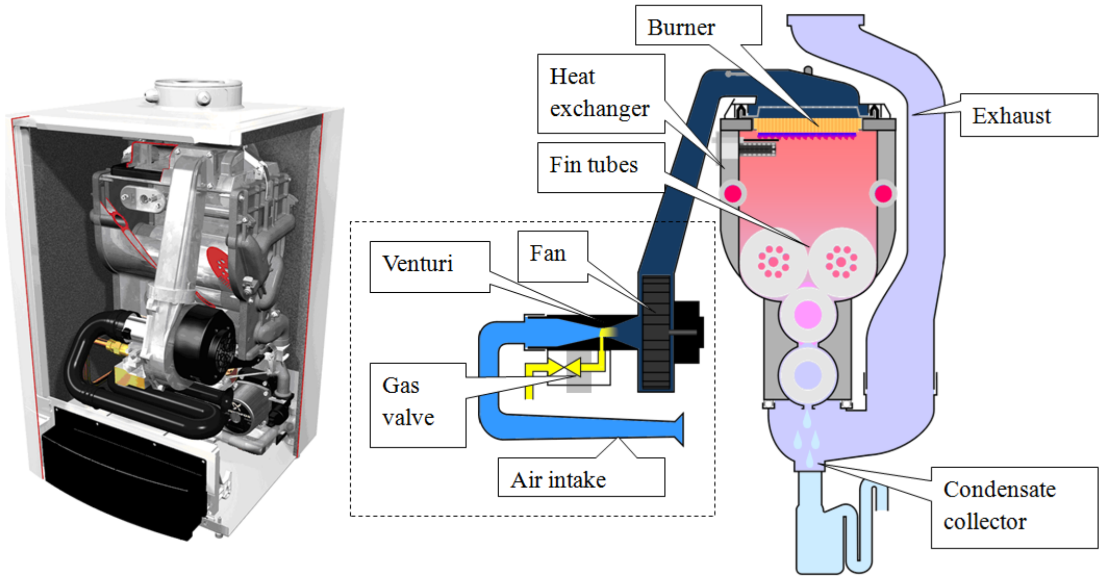

Figure 1.1: Schematic of a wall mounted boiler.

sure in the venturi will be too low to inject enough gas into the flow of air. Beyond this point the mixture of gas to air is too lean to ensure combustion. The ratio between the highest and lowest output power the boiler can deliver is known as the modulation range. A high modulation range is desired since it will reduce the amount of on/off cycling of the boiler, which improves the efficiency and the amount of wear on the boiler components.

The modulation range is affected by several factors. As the air flows through the boiler it will experience pressure losses, most of which occur in the venturi and the burner. Because of size and noise limitations, the fan can deliver a limited amount of pressure difference. By optimizing the flow through the venturi and heat exchanger the modulation range can be increased. The Reynolds numbers at which the appliances operate are depend on the output power. At 30 kW, the Reynolds number based on a pipe diameter of 3 cm is approximately 32000.

1.3 Research goal

The EHC5 department in Deventer performs simulations to try and optimize venturi designs by limiting the amount of pressure loss. The goal of this research is to make an experimental set-up to validate these simulations.

1.4 Report organization

The remainder of this report is organized as follows. In Chapter 2, some basic theory which is used for the experiments is explained. Chapter 3 will elaborate on the equipment that was used and the several experiments that were performed. The results of these experiments will be given in Chapter 4. Finally, in Chapter 5, conclusions and recommendations are given.

Chapter 2

Theory

2.1 Continuity equation

The relation between the velocity and cross-sectional area in a diffuser (Figure 2.1) can be determined by using the continuity equation which for steady flow yields:

$$\oiint \rho \overrightarrow{u} \cdot d\overrightarrow{S} = 0 \tag{2.1}$$

The integral can be evaluated over A_1, A_2 and the area of the wall to form a closed contour.

$$\oiint_{A_1} \rho \overrightarrow{u} \cdot d\overrightarrow{S} + \oiint_{A_2} \rho \overrightarrow{u} \cdot d\overrightarrow{S} + \oiint_{A_{wall}} \rho \overrightarrow{u} \cdot d\overrightarrow{S} = 0 \tag{2.2}$$

Assuming the velocity is always tangent along the wall, the third term will drop out. The resulting integrals can easily be evaluated since the areas are known and the assumption is made that there are no vertical velocity components. Assuming an incompressible fluid, this yields:

$$\oiint_{A_1} \rho \overrightarrow{u} \cdot d\overrightarrow{S} + \oiint_{A_2} \rho \overrightarrow{u} \cdot d\overrightarrow{S} = -A_1 v_1 + A_2 v_2 = 0 \tag{2.3}$$

$$A_1 v_1 = A_2 v_2 \tag{2.4}$$

The first term in Equation 2.3 is zero since $d\overrightarrow{S}$ always points outward.

2.2 Bernoulli's equation

Bernoulli's equation gives a relation between the pressure and velocity along streamlines. It is a simplified form of the Lamb-Gromeka form of the momentum equation.

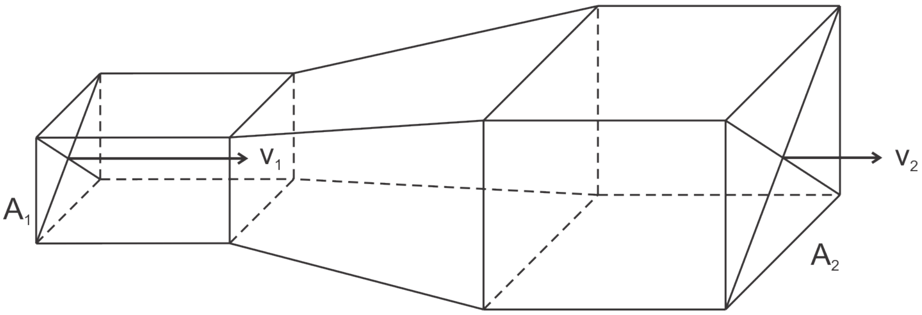

Figure 2.1: Schematic of a diffuser with increasing cross-sectional area.

If body forces are neglected, Bernoulli's equation for steady, inviscid, incompressible flow is given by:

$$p + \frac{1}{2}\rho v^2 = \text{constant along streamlines} \tag{2.5}$$

Where p is the static pressure and v is the fluid velocity. The second term in Bernoulli's equation is also known as the dynamic pressure. Rewriting Bernoulli's equation and combining it with the Continuity equation gives the pressure in dimensionless form:

$$v_E A_E = v_x A_x \tag{2.6}$$

$$v_x = v_E \frac{A_E}{A_x} \tag{2.7}$$

$$P_E + \frac{1}{2}\rho v_E^2 = P_x + \frac{1}{2}\rho v_x^2 = P_x + \frac{1}{2}\rho v_E^2 \left(\frac{A_E}{A_x}\right)^2 \tag{2.8}$$

$$P_x - P_E = \frac{1}{2}\rho v_E^2 \left(1 - \left(\frac{A_E}{A_x}\right)^2\right) \tag{2.9}$$

$$\frac{P_x - P_E}{\frac{1}{2}\rho v_E^2} = 1 - \left(\frac{A_E}{A_x}\right)^2 \tag{2.10}$$

Where P_E and A_E are the pressure and cross-sectional area at the diffuser entry and P_x and A_x are the pressure and cross-sectional area at location x in the diffuser. The right-hand side of Equation 2.10 is a measure for the pressure increase in the diffuser without frictional losses and losses due to flow separation.

2.3 Boundary layers

If a viscous flow moves over a body, the assumption is made that the fluid velocity u at the surface of the body will be zero due to adhesion to the surface. This effect is also known as the ”no-slip” condition. The thin layer with reduced fluid velocity above the surface of the body is known as the velocity boundary layer. Figure 2.2 shows the flow over a flat plate with corresponding boundary layer. The velocity at the surface of the flat plate is zero due to the no slip condition. With increasing y, u also increases. At a certain point above the plate the velocity will reach the value of $u_e = 0.99u$, where u is the free-stream velocity. u_e Is the velocity at the edge of the boundary layer. The thickness of the boundary layer is often expressed as δ. Downstream of the leading edge, the flow will be retarded due to skin friction at the surface of the plate. The extent of this retarded flow above the plate will grow larger with increasing x, which means an increase in the boundary layer thickness. The flow just downstream of the leading edge of the plate will be laminar. After a certain distance, instabilities will form in the laminar flow which will cause the boundary layer to experience a transition from laminar to turbulent flow. This transition occurs in a finite region called the transition region. Flow will generally be turbulent at Reynolds numbers greater than 2000.

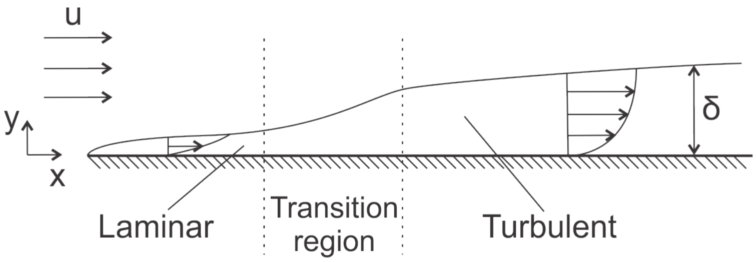

Figure 2.2: Transition from laminar to turbulent boundary layer, from [1].

The transition from a laminar to turbulent boundary layer can be stimulated by using tripping devices which disturb the flow [2]. Examples of such tripping devices include tripping wires, sandpaper and silicon granule strips. In the research of Rona [2], the most effective tripping device was found to be a strip of silicon granules which increased the boundary layer thickness by more than 200 percent. The tripping devices were tested at Reynolds numbers ranging from Re $= 0.145 \cdot 10^6$ to Re $= 0.58 \cdot 10^6$.

2.4 Flow through a pipe

The situation sketched in Figure 2.2 also occurs for flows entering a pipe. At a certain length downstream in the pipe, the boundary layers will come together. At this point the flow will be fully developed. The distance needed for the flow to become fully developed is known as the entrance length of the pipe (Figure 2.3). During the development of the boundary layer the velocity gradients near the wall will be very steep due to the small thickness of the boundary layer. These high gradients will cause large shear stresses and subsequently higher pressure drops than in fully developed flow. The wall shear stress is defined as:

$$\tau_w = \mu \left(\frac{\partial u}{\partial y} \right) \tag{2.11}$$

Where μ is the viscosity and u is the velocity parallel to the wall.

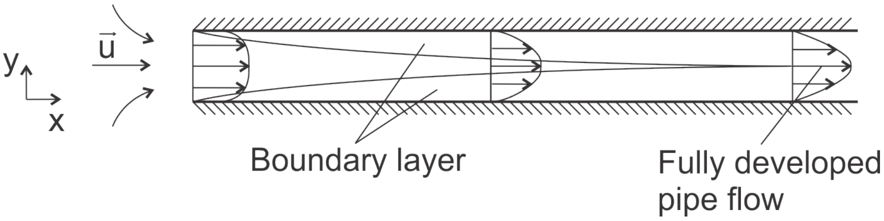

Figure 2.3: Boundary layer development a pipe.

The entrance length for fully developed pipe flow has been thoroughly investigated and several values of the entry length have been found. 25 to 40 diameters have been found by J. Nikuradse [3]. In the experiment of C. Parchen et al. [4] the entry length was found to be Reynolds number dependent and approximately 140 pipe diameters at Reynolds numbers in the order of 10^5. This value was also observed by K. Lien et al. [5]. Velocity measurements were performed in a rectangular duct with a width of 1170 mm and height of 100 mm. The Reynolds numbers based on channel height were approximately 40,000, 105,000 and 185,000. The resulting entrance length was found to be approximately 130 diameters for all three cases. In the experiments mentioned further in this report, an entry length of 33 diameters is used. The reason for this entry length is the limited amount of space and the amount of pressure loss a longer pipe will induce. This entry length should however be long enough according to [3].

2.5 Pressure losses

According to Bernoulli's equation there is no pressure loss in a pipe or venturi. However, this is an ideal situation where viscosity is neglected and flow separation is left out of regard. In reality, pressure losses will occur because of energy dissipation due to skin friction with the wall and due to flow separation [6].

2.5.1 Skin friction

The pressure loss due to skin friction can be calculated by using the Darcy-Weisbach equation for pressure loss in a pipe [7].

$$\Delta P = f\frac{L}{D}\frac{\rho v_{avg}^2}{2} \tag{2.12}$$

v_{avg} is the average velocity in the pipe, L is the length and D is the diameter. f is the Darcy friction factor, which for laminar flow is defined as:

$$f = \frac{8\tau_w}{\rho v_{avg}^2} \tag{2.13}$$

Where τ_w is the wall shear stress as defined in Equation 2.11. Several experiments have been performed to obtain an expression for the friction factor in turbulent flow by measuring the flow rate and pressure drop. The experimental data was combined by C.F. Colebrook to obtain a function form of the friction factor for turbulent flow, known as the Colebrook equation:

$$\frac{1}{\sqrt{f}} = -2.0\log\left(\frac{\epsilon/D}{3.7} + \frac{2.51}{\mathrm{Re}\sqrt{f}}\right) \tag{2.14}$$

Where ϵ is the roughness height. For smooth pipes, the roughness height is assumed to be approximately zero. The Colebrook equation has to be solved iteratively because of its implicit form. An approximate explicit form of the Colebrook equation was given bij S.E. Haaland:

$$\frac{1}{\sqrt{f}} \approx -1.8\log\left[\frac{6.9}{\mathrm{Re}} + \left(\frac{\epsilon/D}{3.7}\right)^{1.11}\right] \tag{2.15}$$

$$f \approx \frac{1}{3.24\log\left[\frac{6.9}{\mathrm{Re}} + \left(\frac{\epsilon/D}{3.7}\right)^{1.11}\right]^2} \tag{2.16}$$

The pressure loss in a diffuser can be calculated by taking the integral over the diffuser length L (Figure 2.4). This yields:

$$\Delta P_{diffuser} = \int_0^L \frac{x\rho v_{avg}(x)^2}{6.48D(x)\log\left[\frac{6.9}{\mathrm{Re}} + \left(\frac{\epsilon/D(x)}{3.7}\right)^{1.11}\right]^2}dx \tag{2.17}$$

Since the integral is too hard to compute analytically it will be approximated by calculating the average values of the pressure drop per meter over small increments of x multiplied with dx (Figure 2.4). This yields:

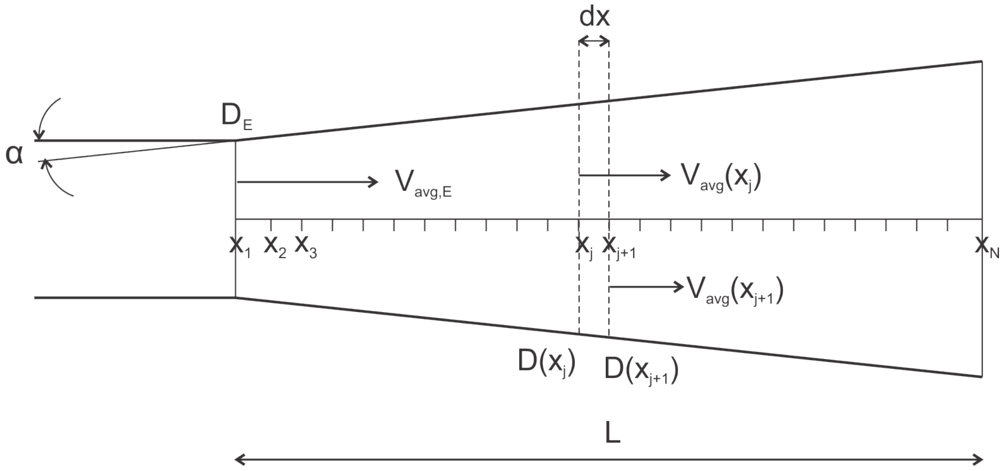

Figure 2.4: Diffuser geometry.

$$\Delta P_{diffuser} = \sum_{j=1}^{N-1}(x_{j+1}-x_j)\frac{1}{2}\left[\frac{\rho v_{avg}(x_j)^2}{6.48D(x_j)\log\left[\frac{6.9}{\mathrm{Re}}+\left(\frac{\epsilon/D(x_j)}{3.7}\right)^{1.11}\right]^2}\right. \tag{2.18}$$

$$\left.+\frac{\rho v_{avg}(x_{j+1})^2}{6.48D(x_{j+1})\log\left[\frac{6.9}{\mathrm{Re}}+\left(\frac{\epsilon/D(x_{j+1})}{3.7}\right)^{1.11}\right]^2}\right]$$

Where j runs from 1 to $N-1$ and x runs from 0 to L. The diameter and velocity can be expressed in terms of x in the following way:

$$D(x) = \frac{D_{exit}-D_E}{L}x + D_E \tag{2.19}$$

$$v_{avg}(x)A(x) = v_{avg,E}A_E \tag{2.20}$$

$$v_{avg}(x) = \frac{v_{avg,E}D_E^2}{\left(\frac{D_E-D_{exit}}{L}x+D_E\right)^2} \tag{2.21}$$

2.5.2 Flow separation

Another form of pressure loss is the formation of flow separation. Flow separation can occur when air flows over a region with an adverse pressure gradient, i.e. where the pressure increases. An example of such a region is a diffuser. The adverse pressure gradient will cause a reduction in the velocity. At a certain point, the velocity will be zero, which is the starting point of flow separation. After this point there will be a negative velocity component, resulting in an area of reversed flow [1]. The wake that results from the flow separation will result in a pressure loss. Figure 2.5 elaborates this effect.

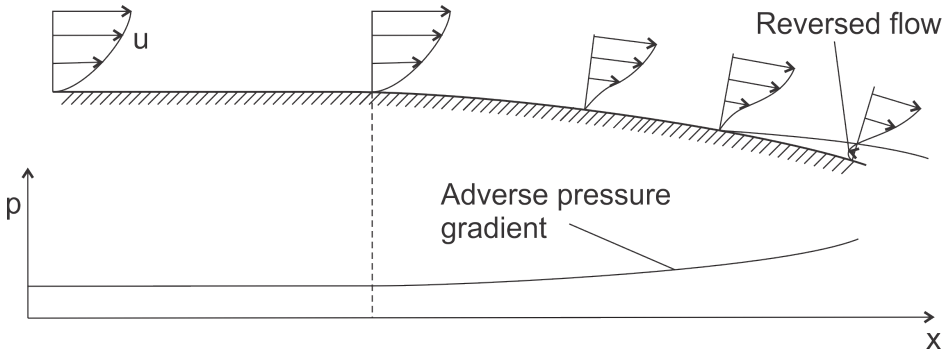

Figure 2.5: Separated flow induced by an adverse pressure gradient. [1]

2.6 Reference experiments

Several detailed experiments have been performed on diffusers, which can serve as a comparison for the experiments performed in this report.

H. Sprenger performed static pressure measurements on several curved and straight conical diffusers [8]. These diffusers were tested at Reynolds numbers ranging from 56,000 to 800,000. One diffuser used in the experiments has an angle of 4 degrees and an inlet and outlet diameter of 100 mm and 120 mm, respectively (Figure 2.6) and will be used as a comparison for the experiment mentioned in Chapter 3.5 and 3.6. Pressure taps were positioned at intervals of 2 mm along the wall of the diffuser. Results were presented in terms of the dimensionless pressure versus dimensionless position, where the pressure was made dimensionless according to Equation 2.10.

A similar experiment was performed by R.K. Singh and R.S. Azad [9]. Velocity and pressure measurements were performed on an eight degree conical diffuser with fully developed turbulent entry flow. All measurements were performed at a Reynolds number of 69,000 based on the entry diameter of the diffuser. Some quantitive information about instantaneous flow reversals in the diffuser was obtained through pulsed-wire anemometry. Mean velocity profiles were measured with hot-wire anemometry. The static pressure along the wall of the diffuser was measured at different locations through static pressure taps with an internal diameter of 0.70 mm. The hot-wire and pulsed-wire measurements showed good agreement within experimental uncertainty, even in the region of high turbulence intensity.

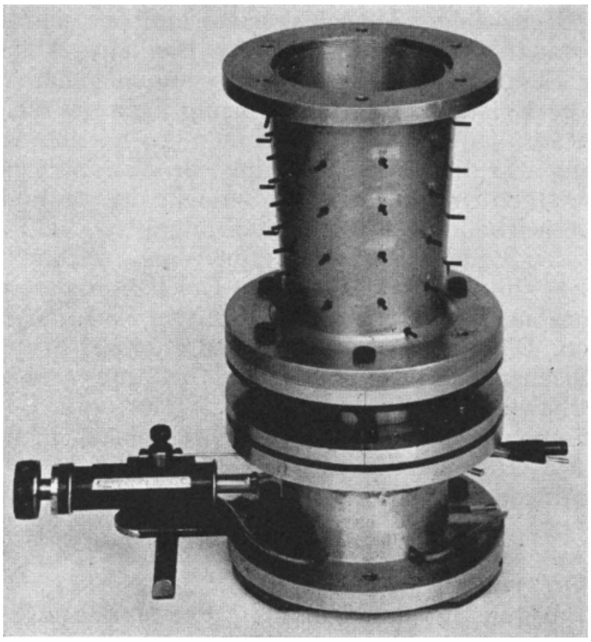

Figure 2.6: Conical diffuser used in the experiments of Sprenger [8].

For extreme turbulence intensity and appreciable instantaneous flow reversals the pulsed-wire technique was found superior to the hot-wire technique.

Measurements on the flow through a conical contraction and a 20 degree diffuser were performed by Spencer et al. [10]. Measurements were performed both with air and water at Reynolds number ranging from 100,000 to 200,000. Velocity measurements were performed with a LDV system and by a hot-wire probe. Intercomparison between measurements and simulations showed that the velocity profile through a 20 degree conical diffuser could be predicted with reasonable accuracy when using standard turbulence models and a sound numerical scheme.

The turbulent separating flow in an asymmetric plane diffuser was tested by S. Obi et al. [11]. The experimental set-up consisted of a wind tunnel containing a settling chamber with several screens and a honeycomb. The test section contained a diffuser which had only one diverging wall with a diverging angle of approximately 10 degrees, as shown in Figure 2.7. The diffuser has fully-developed inlet flow due to the entry length of 110 times the entry channel height. The diffuser encounters flow separation from the diffuser wall. Simulating this flow separation can be a challenge for turbulence models. Velocity measurements were performed by using an LDV system. Mean velocity components in two directions and three Reynolds stress components were obtained along the center of the channel span through vector operation from three different velocity components. These results along with measured wall pressure profiles were compared with a variety of turbulence models. A detailed explanation of the numerical procedure can be found in [11]. Experiments were performed at a Reynolds number of 20,000, based on channel height.

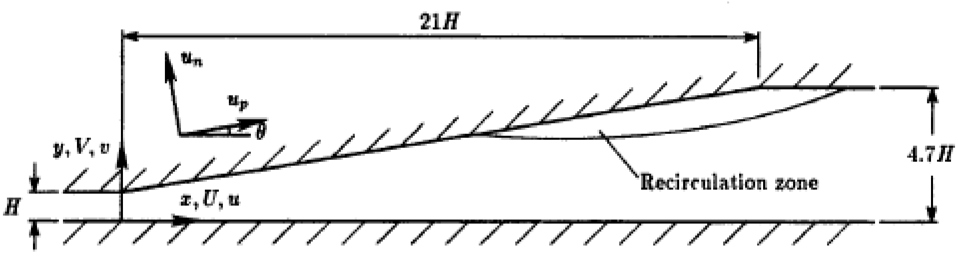

Figure 2.7: Diffuser geometry used in the experiments of Obi et al., from [11]

.

C.U. Buice and J.K. Eaton also investigated the flow through the asymmetric plane diffuser in Figure 2.7 [12], to try and re-create the experiments of Obi et al. [11]. Wall pressure measurements were performed and compared compared with Large Eddy Simulations and a $k - \epsilon - v^2$ turbulence model. Good similarity could be observed between the pressure coefficient obtained from measurements and simulations.

A combination of a nozzle and conical diffuser with diverging angle of 4 degrees was tested in the experiments of Means et al. [13]. A momentum-integral boundary layer method was used to study the relative importance of various boundary layer parameters in correlating unstalled diffuser performance. The momentum-integral method appeared to be in good agreement with the experimental results regarding the prediction of the pressure recovery to the point of boundary-layer separation at inlet Reynolds numbers of 144,000 and 169,000.

Chapter 3

Experimental set-up

The main experimental set-up can be seen in Figure 3.1. The main set-up consists of a fan controlled by a control unit and an orifice meter. The test section is fitted to the end of this set-up and can easily be removed. The ambient pressure and temperature are measured by the test rigs present in the lab. The density can be calculated by using the ideal gas law: $\rho = P/R_sT$, where R_s is the specific gas constant.

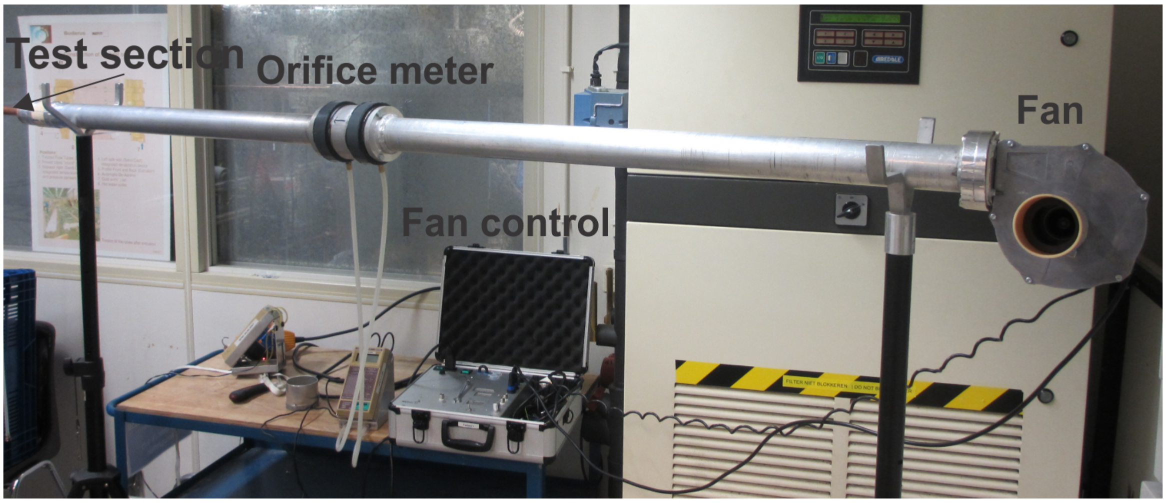

Figure 3.1: Main experimental set-up.

3.1 Equipment

3.1.1 Fan

The airflow is generated by an RG128 centrifugal fan (Figure 3.2). Some important characteristics of the fan can be found in Table 3.1. The fan is controlled by a control unit. The input power can be set as a percentage of the maximum power at a

Speed	7400	rpm
Power input	67	W
Air flow	134	m^3/h
Back pressure	2000	Pa

Table 3.1: Nominal data of the RG128 fan.

resolution of 1 percent. This percentage corresponds to a certain rotational speed, which is displayed on the control unit (Figure 3.3).

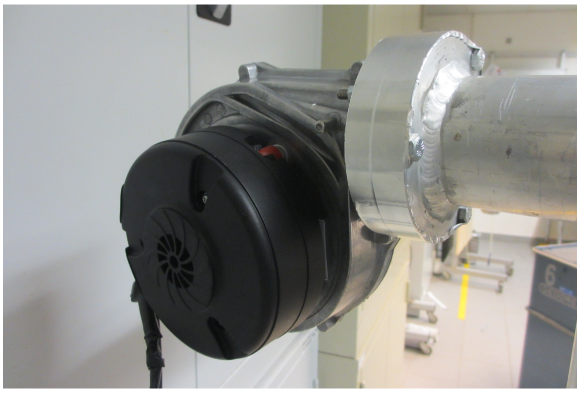

Figure 3.2: RG128 fan.

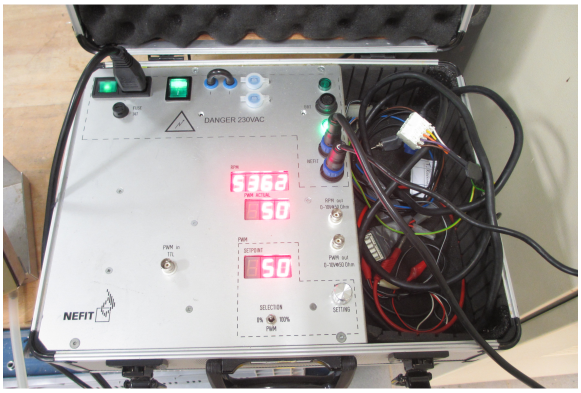

Figure 3.3: Control unit for the fan.

3.1.2 Orifice flow meter

An orifice meter was used to measure the mass flow generated by the fan. It contains an orifice plate with pressure meters on each side (Figure 3.4). As the flow passes the orifice the cross-sectional area decreases, which causes a rise in velocity and thus a drop in static pressure (according to the conservation of mass and Bernoulli's law). The pressure drop in the two pressure chambers is measured and can be linked to the mass flow rate according to the following formula [14]:

$$q_m = \frac{C\epsilon_f}{\sqrt{1-\beta^4}} \frac{\pi d^2}{4} \sqrt{2\rho_1 \Delta P} \tag{3.1}$$

Where C is the discharge coefficient (ratio between actual flow rate and theoretical flow rate), ϵ_f is the expansion factor, which serves as a correction for the compressibility of the gas, β is the ratio between the orifice throat diameter d and pipe diameter D, ΔP is the static pressure difference between measuring point 1 and 2 and ρ_1 is the density at measuring point 1.

The orifice meter used in the experiments has been made according to the ISO 5167-2 standard (International Organization for Standardization). Extensive experiments on orifice meters made according to this standard have resulted in equations

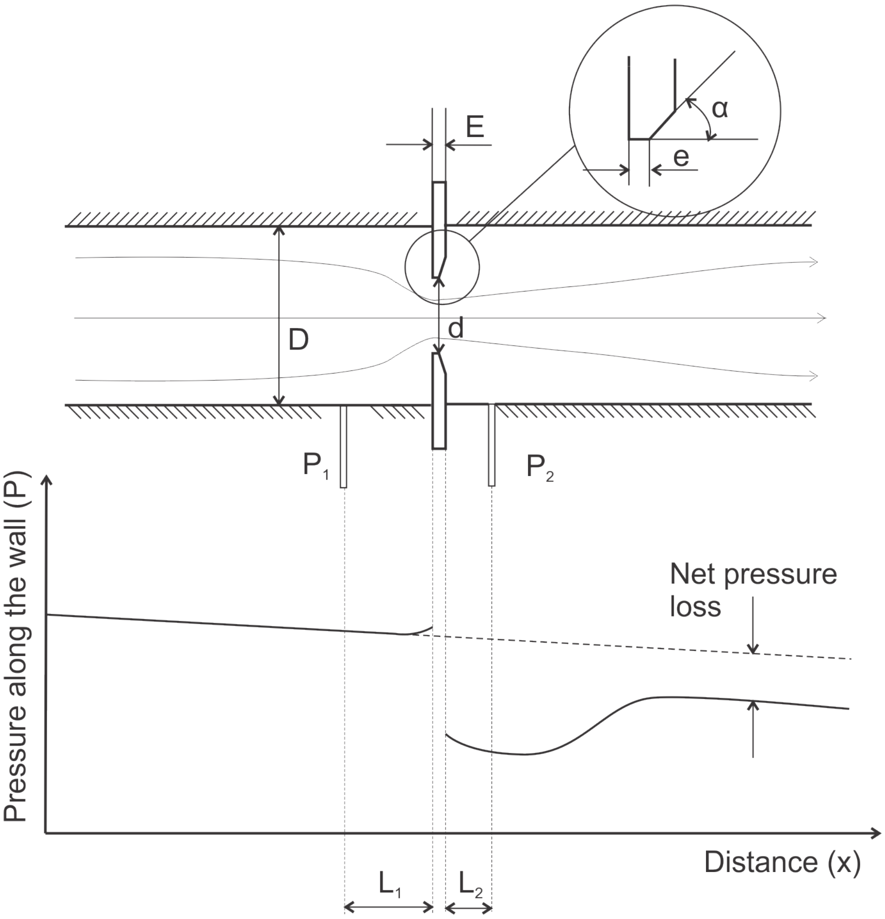

Figure 3.4: Orifice meter with corresponding pressure distribution along the wall, from [14].

for the discharge coefficient and expansion factor in Equation 3.1. This means that orifice meters made according to this standard can be used without having to calibrate it at a known flow rate.

Discharge coefficient

The discharge coefficient contains several factors: C_∞, C_s and tapping terms. The tapping terms are based on the location on the pressure taps. These terms are important because the pressure distribution along the wall of the orifice is not uniform (Figure 3.4). C_∞ is the discharge coefficient using corner tappings for infinite Reynolds number and C_s is the slope term, which gives the increase in discharge coefficient for lower Reynolds numbers. The individual terms will not be treated in detail. A detailed derivation can be found in [14] The resulting equation for the discharge coefficient for $Re_D \geq 5000$ and $D < 71.12$ mm is given by:

$$C = 0.5961 + 0.0261\beta^2 - 0.216\beta^8 + 0.000521(10^6\beta/Re_D)^{0.7} \tag{3.2}$$

$$+(0.0188 + 0.0063a)\beta^{3.5}(10^6/Re_D)^{0.3}$$

$$+(0.043 + 0.080e^{-10L_1} - 0.123e^{-7L_1})(1 - 0.11A)\frac{\beta^4}{1-\beta^4}$$

$$-0.031(M_2' - 0.8M_2'^{1.1})\beta^{1.3} + 0.011(0.75-\beta)\left(2.8 - \frac{D}{25.4}\right)$$

Where β, a and M_2' are defined by:

$$\beta = \frac{d}{D}, \quad a = \left(\frac{19000\beta}{Re_D}\right)^{0.8}, \quad L_2' = \frac{L_2}{D} \quad \text{and} \quad M_2' = \frac{2L_2'}{1-\beta} \tag{3.3}$$

Expansion factor

The equation for the expansion factor is derived from experiment by comparing the performance of the orifice meter when an incompressible fluid like water is used versus the performance of the orifice when a compressible fluid like air is used. The equation for the expansion factor used in ISO 5167-2 is given by:

$$\epsilon_f = 1 - (0.351 + 0.256\beta^4 + 0.93\beta^8)\left\{1 - \left(\frac{p_2}{p_1}\right)^{1/\kappa}\right\} \tag{3.4}$$

Where κ is the isentropic component. The orifice meter used in the experiments can be found in Figure 3.5). The orifice plate is mounted between two pressure chambers. The static pressure in these chambers is measured through static pressure taps (Figure 3.6). The arrows on the side of the orifice meter indicate the direction of the flow. The dimensions of the orifice, as mentioned in Figure 3.4, can be found in Table 3.2.

D		57	mm
d		35	mm
e		1	mm
E		3.2	mm
β	$\frac{d}{D}$	0.614	
α		45	°
L_1		57	mm
L_2		28.5	mm
L_2'	$\frac{L_2}{D}$	0.5	
M_2'	$\frac{2L_2}{1-\beta}$	2.5907	

Table 3.2: Orifice dimensions.

With the dimensions given in Table 3.2, Equation 3.1, 3.2 and 3.4 can be combined to link the pressure drop over the orifice to the flow rate. Since the flow rate

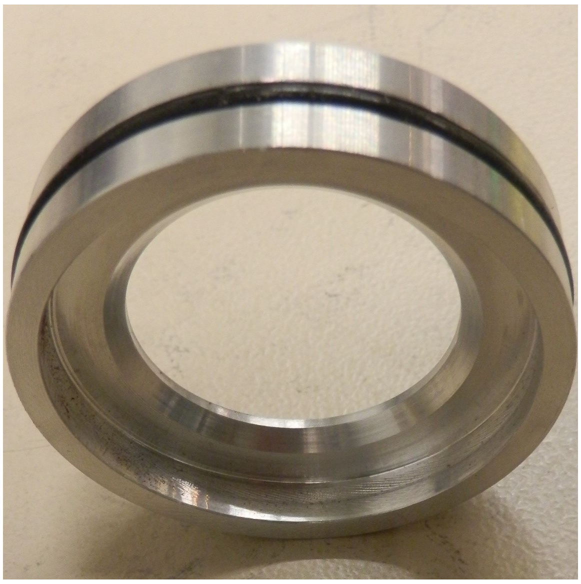

Figure 3.5: Orifice plate made according to ISO 5167-2.

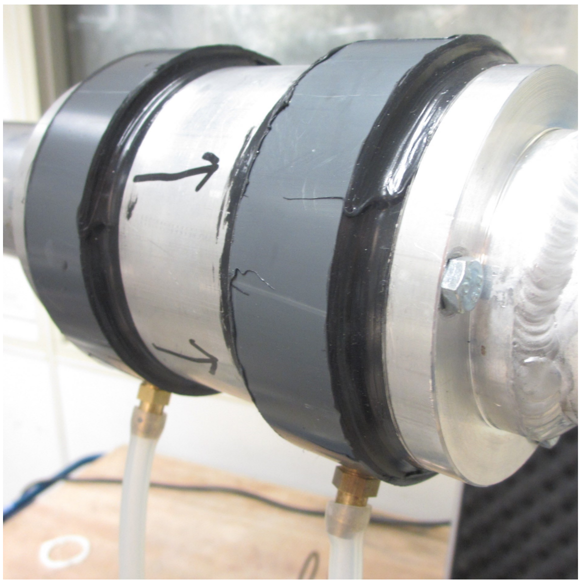

Figure 3.6: Orifice plate mounted in the experimental set-up.

and Reynolds number are both unknown, several iterations will be made based on an estimation of the flow rate. After four iterations, a value for the Reynolds number and the flow rate is obtained with an error of less than 0.001$\%$ with respect to the third iteration.

3.1.3 Pitot tube

A Pitot tube is the most common device for velocity measurements on aircraft and in wind tunnels. A Pitot tube has an open end facing directly towards the flow, measuring the stagnation pressure and pressure taps perpendicular to the flow measuring the static pressure (Figure 3.7).

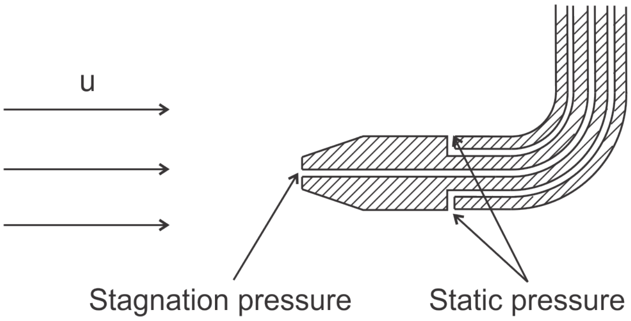

Figure 3.7: Schematic of a Pitot tube inserted in a flow.

The velocity can be determined by calculating the dynamic pressure, which is defined as:

$$q = \frac{1}{2}\rho v^2 = P_0 - P_s \tag{3.5}$$

Where P_0 is the stagnation pressure and P_s is the static pressure. A correction has to be made to the velocity for flow in pipes, since the velocity distribution across the cross-sectional area of the pipe is not uniform. Pitot tubes come in different varieties. The most common Pitot tubes are displayed in Figure 3.7 and measure the fluid velocity in one direction. However, two- or three-dimensional Pitot tubes are also available which have multiple inlets to measure the stagnation pressure. A boundary layer probe [15] was ordered to do boundary layer velocity measurements in the diffusers which will be mentioned in Chapter 3.5 and 3.6. This boundary layer probe has a sensing head diameter of 0.635 mm. The probe could however not be delivered in time to perform these measurements.

3.1.4 Constant Temperature Anemometry

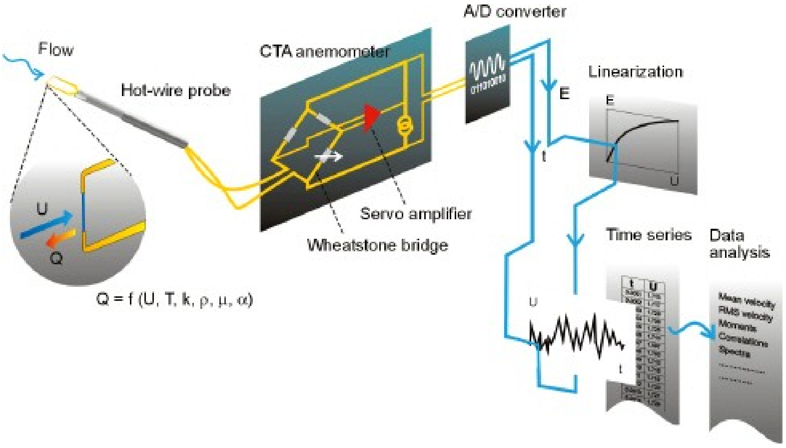

Figure 3.8: Measurement principle for Constant Temperature Anemometry, from [16].

Another measurement technique that can be used to measure fluid velocities is Constant Temperature Anemometry (CTA) (Figure 3.8). CTA is based on the concept of convective heat loss, where an electrically heated probe or hot-wire probe transfers heat to the surrounding fluid. The higher the fluid velocity, the higher the amount of convective heat loss. The probe is connected to a constant temperature anemometer consisting of a Wheatstone bridge and a servo amplifier. The Wheatstone bridge is an electrical circuit with a variable resistance. The servo amplifier keeps the bridge in balance by controlling the current so that the resistance and thus the temperature of the probe are kept constant, regardless of the amount of cooling of the fluid. The voltage over the Wheatstone bridge can be measured and is a direct measure for the fluid velocity. The signal is transferred to an A/D converter which translates the analog signal for data processing. Hot wire probes can come in different varieties. Single wire probes measure the fluid velocity in one-direction, whereas tri-axial wire probes can measure the fluid velocity in three dimensions, providing the possibility to measure turbulence profiles. A calibration has to be performed before each measurement to link the Anemometer voltage to the fluid velocity. A hot-wire probe was also ordered to do velocity measurements, but could also not be deliverd in time.

3.1.5 Static pressure measurement

Static pressure measurements are performed through static pressure taps. The taps have an internal diameter of 0.5 mm. Two types of manometers were used to measure the pressure: a TT series micromanometer (Figure 3.9) and Neotronics micromanometer (Figure 3.10). The manometers measure the difference between the static pressure at the tap location and the ambient pressure in Pascals in case of the TT series micromanometer and in mm$H_2$0 in case of the Neotronics micromanometer.

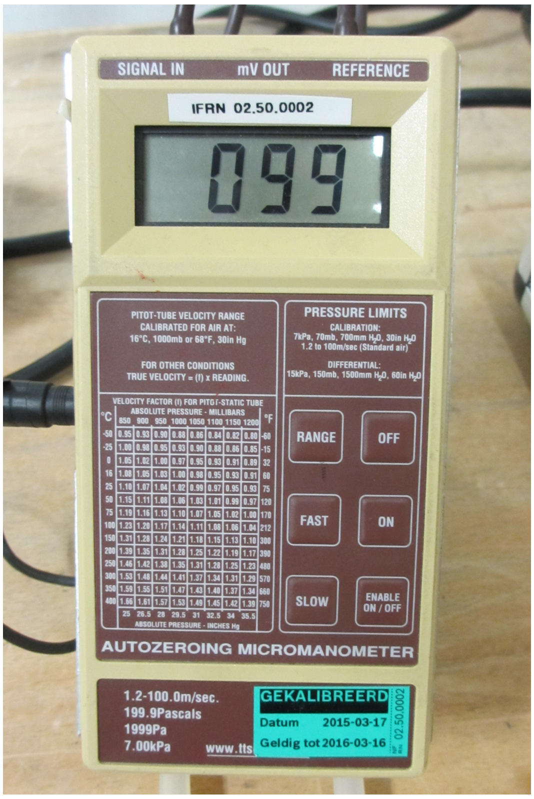

Figure 3.9: TT series micromanometer.

Figure 3.10: Neotronics micromanometer.

3.2 Experiment A: PVC pipe

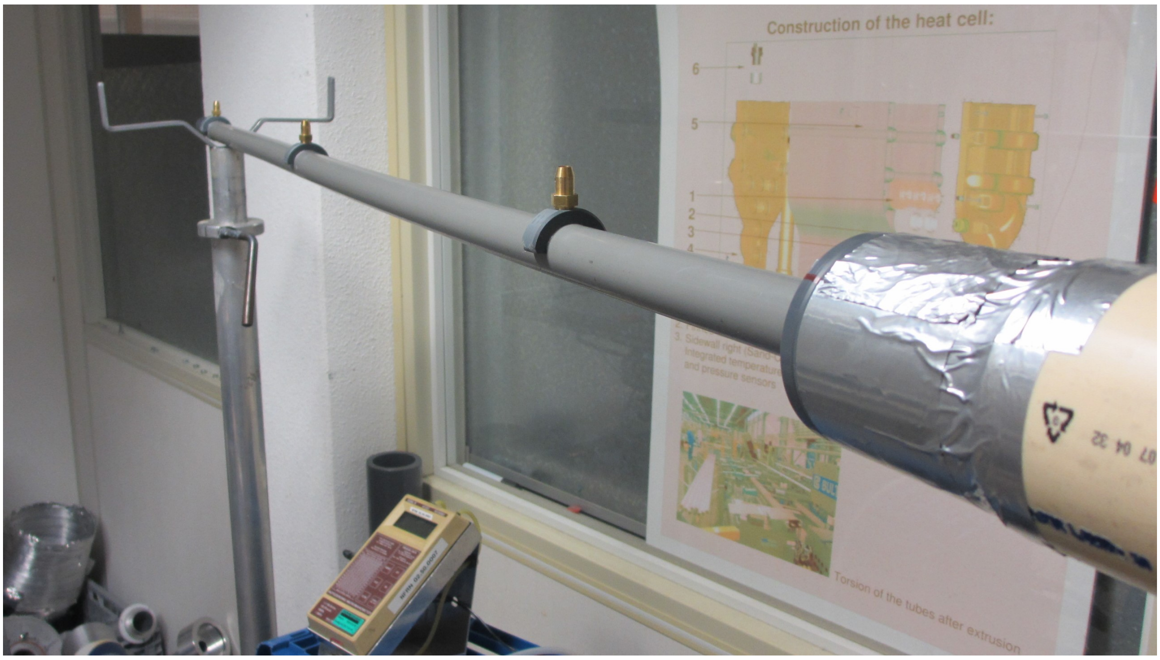

Figure 3.11: PVC pipe with pressure taps connected to the main set-up.

The first step is to measure the pressure drop over a pipe, which can be compared to available experimental data. This will give insight in the precision of the pressure measurement and if enough entry length is present for precise measurements. The test section is mounted to the set-up with the fan and the orifice meter and consists of a PVC tube with an inner diameter of 22.3 mm (Figure 3.11). There are three pressure taps located on the walls of the tube. The first tap is located 10 pipe diameters from the entry of the tube. The second and third tap are located 0.5 m and 1 m downstream of the first tap. The tube is connected to the main set-up by a PVC nozzle with an inlet and outlet diameter of 57 mm and 22.6 mm, respectively. An overview of the dimensions can be found in Figure 3.12.

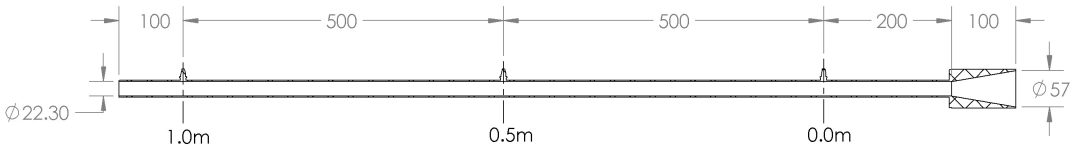

Figure 3.12: PVC pipe test section with corresponding dimensions.

3.3 Experiment B: Copper pipe

Figure 3.13: Copper pipe with pressure taps connected to the main set-up.

For the second measurement, a copper tube with an increased amount of pressure taps is used to get a better view of the pressure profile along the tube. This may also give insight in the required entry length for precise pressure measurements. The copper tube used in the measurements can be seen in Figure 3.13. The inner diameter of the tube is 20 mm. The tube has ten pressure taps with equal spacing of 200 mm. The inlet length before the first pressure tap is 10 pipe diameters, so also 200 mm. The tube is connected to the main set-up by a PVC nozzle with an inlet and outlet diameter of 57 mm and 20 mm, respectively. An overview of the dimensions can be found in Figure 3.14.

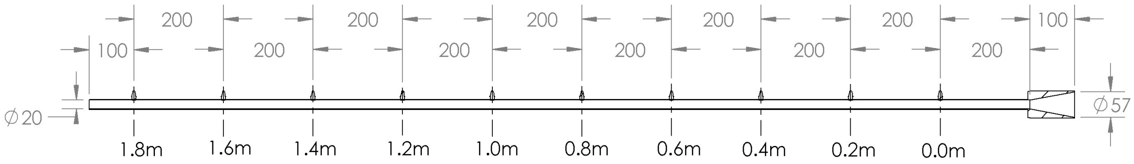

Figure 3.14: Copper pipe test section with corresponding dimensions.

3.4 Experiment C: Copper pipe with grid

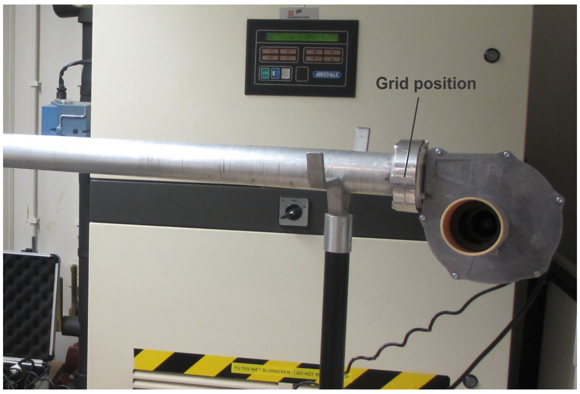

Figure 3.15: Postion of the grid in the experimental set-up.

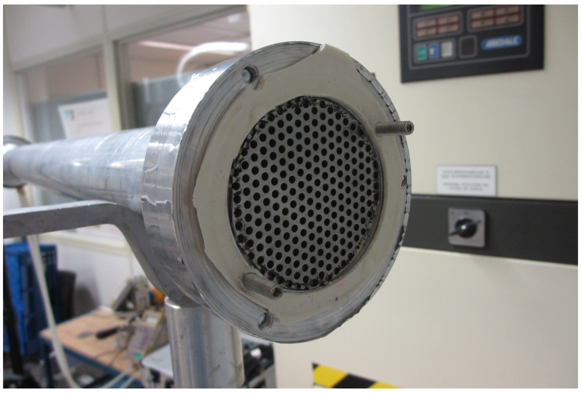

Figure 3.16: Postion of the grid in the experimental set-up.

The goal of this measurement is to see the effect on the pressure drop measurement when a fine and a coarse grid are placed right behind the fan (Figure 3.15 and 3.16). In wind tunnels, a series of screens and honeycombs is used to reduce non-uniformities in the velocity profile and create a homogeneous flow in the test section [17]. Wind tunnel screens are often made of interwoven metal wires which form a square or rectangular mesh. The screens will cause a drop in the static pressure which will make the flow velocity profile more uniform. A screen will also refract the incident flow towards the local normal and reduces the turbulence intensity in the entire flow-field. Screens reduce the longitudinal components of turbulence or mean-velocity variation to a greater extent than the lateral components. These lateral components can be reduced more effectively by a honeycomb. A honeycomb is often placed between a set of screens. The honeycombs and screens are placed in a settling chamber to reduce the amount of pressure loss over each screen and honeycomb. A more detailed explanation on the effect of screens and honeycombs can be found in [18]. An example of an experimental set-up with a settling chamber containing screens and a honeycombs can be found in Figure 3.17. The set-up is powered by a 12 kW radial fan. The flow passes several grids, denoted by LB and DN, and several honeycombs, denoted by GR. Most of the grids and honeycombs are present in the settling chamber, apart from two grids and a honeycomb which are located upstream of the settling chamber. The entry length upstream of the test section could be varied between 3.5 cm and 163.5 cm, wich corresponds to 0.35 to 16.35 entry diameters. The test section consists of a conical diffuser. For a more detailed explanation of the set-up the reader is referred to [8].

Due to the amount of space and the limited output power of the fan, no settling chamber with honeycombs and screens is present in the experimental set-up. In-

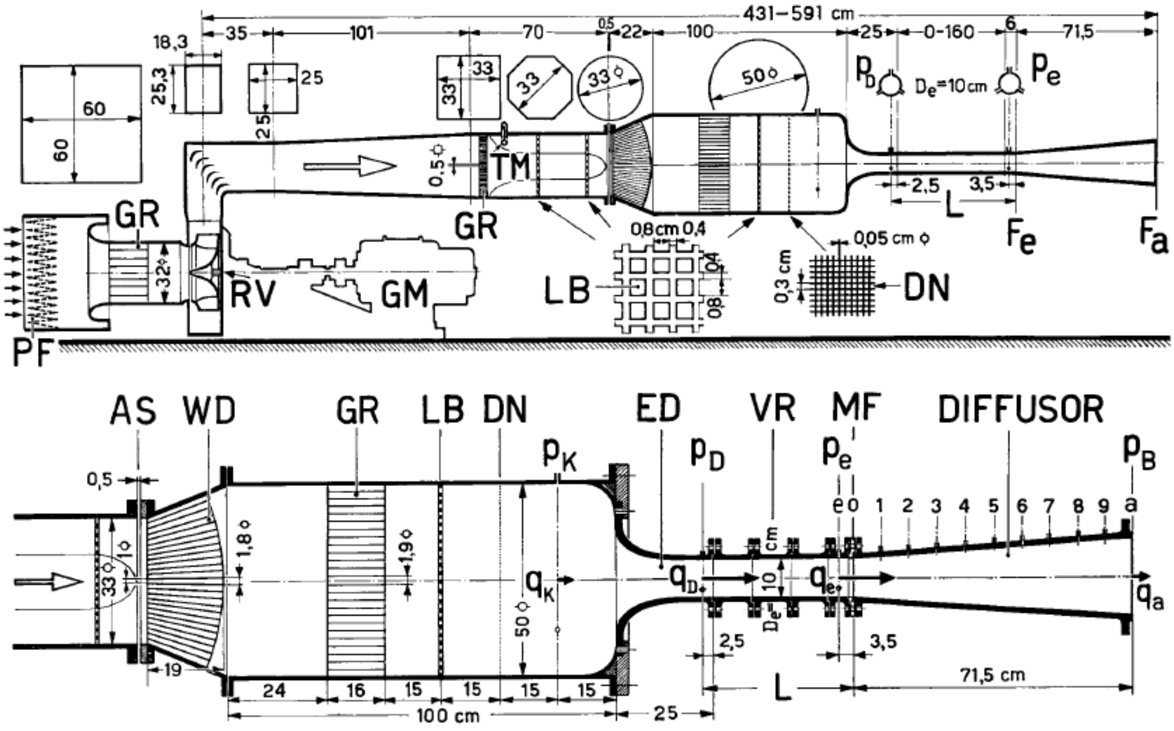

Figure 3.17: Experimental set-up used in the experiments of Sprenger [8].

stead, metal grids are placed right behind the fan to test the effect on the pressure measurement in the test section. The experimental set-up is similar to the set-up described in Chapter 3.3, with the exception of the grids. Both a fine grid and a coarse grid will be tested. The fine grid has a hole diameter of 2 mm, whereas the coarse grid has a hole diameter of 5 mm (Figure 3.18 and 3.19). The measurements with both grids will be compared with measurements without the presence of a grid.

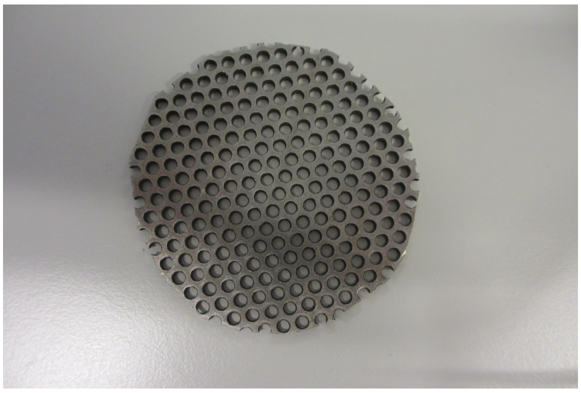

Figure 3.18: Fine grid.

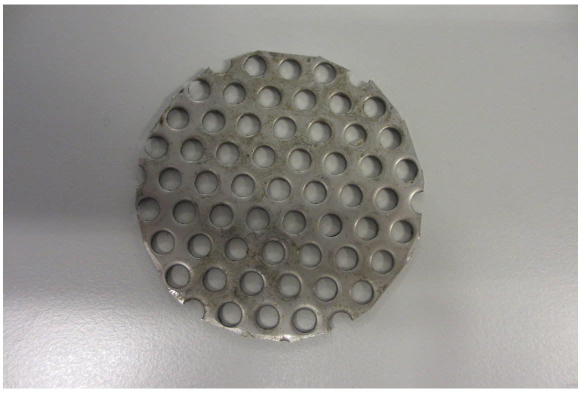

Figure 3.19: Coarse grid.

3.5 Experiment D: Diffuser without gas inlet

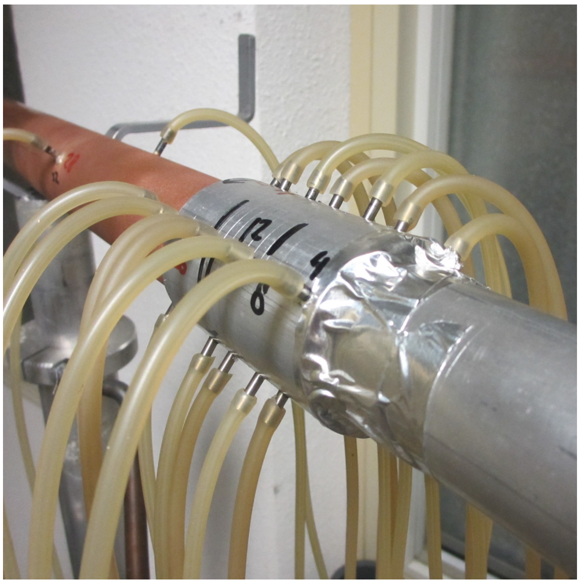

Figure 3.20: Ten degree diffuser mounted in the experimental set-up.

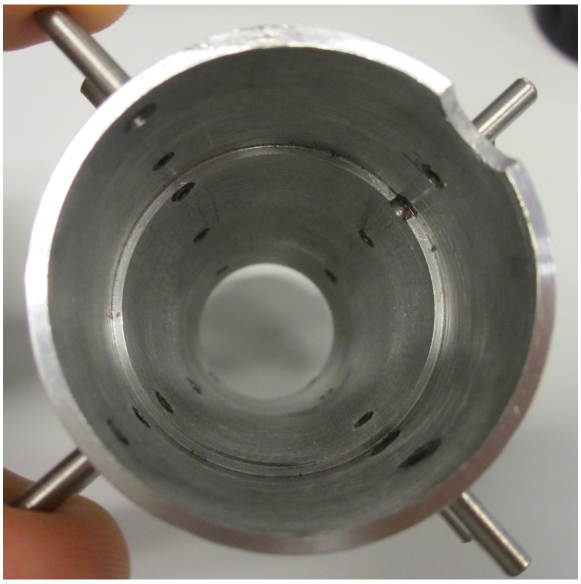

Figure 3.21: Inside of the four degree diffuser with static pressure taps.

In this experiment two conical diffusers with a diverging angle of four and ten degrees degrees will be used. The pressure profile along the diffusers is measured through a range of static pressure taps which have been mounted to the walls of the diffusers. These pressure taps are made of tubes with an external diameter of 3 mm and internal diameter of 1 mm. The axial distance between the taps is small around the entry and exit of the diffusers (2 mm) since these are the locations where the most variations in the pressure are expected. The spacing is slightly larger inside the diffusers (4 mm to 10 mm) to limit the total amount of pressure taps.

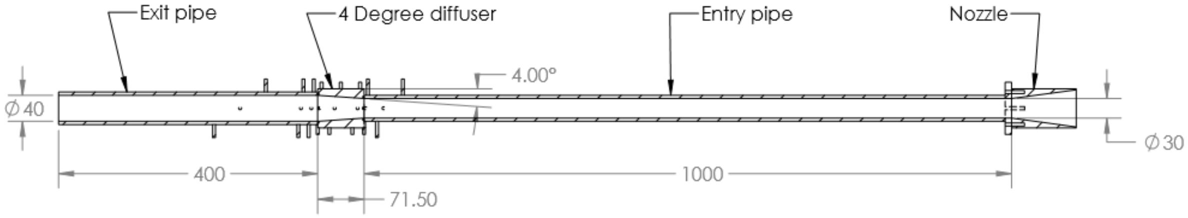

Figure 3.22: Set-up containing a diffuser with an angle of 4 degrees.

A pipe with a diameter of 30 mm and length of 1000 mm is placed upstream of the diffuser entry. This corresponds to an entry length of approximately 33 diameters. This entry length should be sufficient according to the experiments of [3]. However, other experiments mentioned in chapter 2.4 would suggest a larger entry

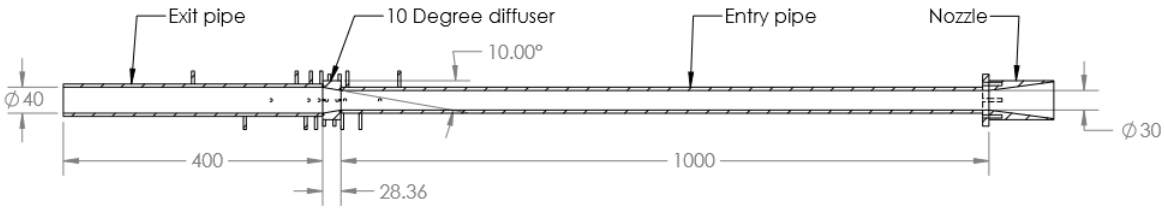

Figure 3.23: Set-up containing a diffuser with an angle of 10 degrees.

length. Due to the available amount of space the entry length is kept at 33 diameters. A larger entry length will also induce a larger amount of pressure loss. Since the power of the fan is limited, this will reduce the maximum possible Reynolds number. Also, an entry length of 33 diameters is most likely to be sufficient for static pressure measurements according to [3]. For detailed measurements on for example turbulence or velocity profiles a larger entry length may be needed. A pipe with a diameter of 40 mm and length of 400 mm is fitted downstream of the diffuser exit, corresponding to an exit length of 10 diameters. Taps are also placed on the entry and exit pipe because the diffuser will also have an influence on the pressure upstream and downstream of the diffuser itself. The test section is connected to the main set-up by a nozzle. The geometry of both set-ups can be found in Figure 3.22 and 3.23. The location of all of the static pressure taps can be found in Figure 3.24 to 3.27. The dimensions of these figures are in mm.

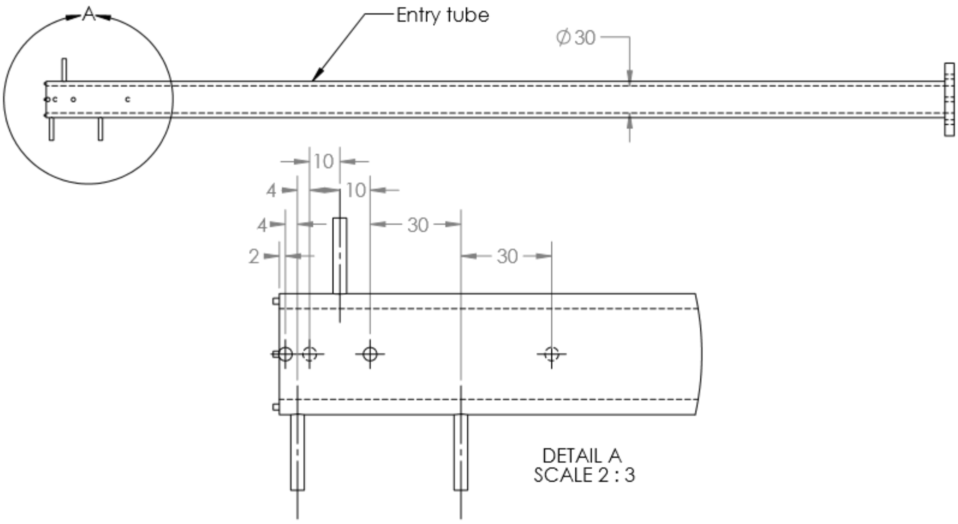

Figure 3.24: Entry pipe with corresponding pressure tap locations.

The geometry of the diffuser with an angle of 4 degrees is based on the experiments of Sprenger [8], which were discussed in Chapter 2.6.

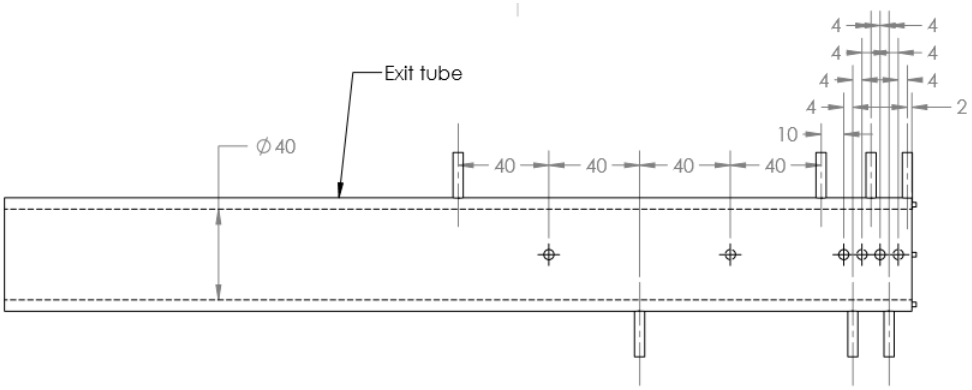

Figure 3.25: Exit pipe with corresponding pressure tap locations.

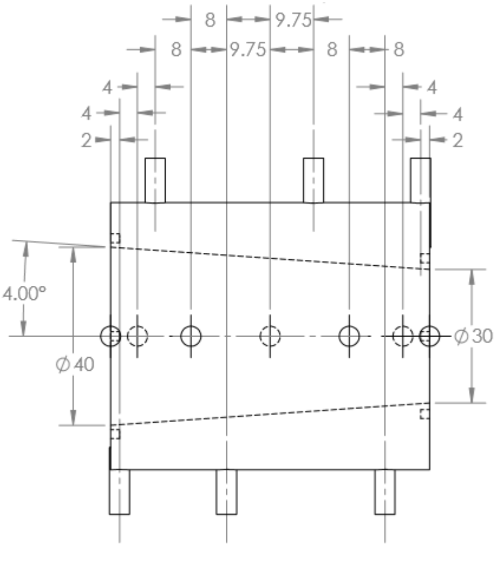

Figure 3.26: 4 Degree diffuser with corresponding pressure tap locations.

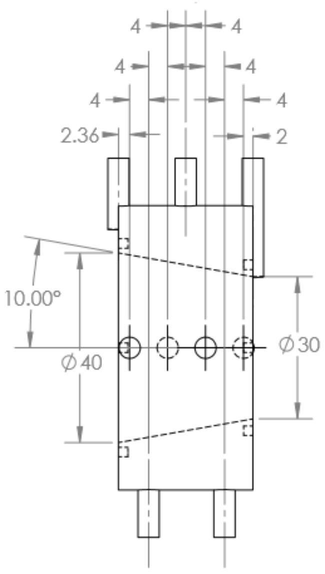

Figure 3.27: 10 Degree diffuser with corresponding pressure tap locations.

3.6 Experiment E: Diffuser with gas inlet

A diffuser with an angle of 4 degrees and 10 degrees with gas inlet will be used in this experiment. The diffusers will have the same geometry as the diffusers mentioned in Chapter 3.5, with the exception of several adjustments:

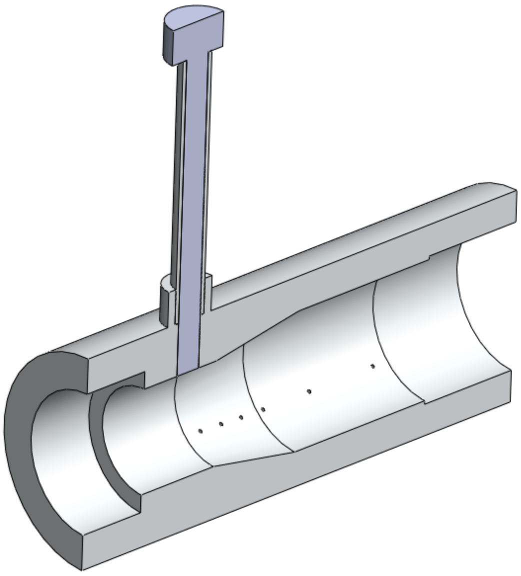

Figure 3.28: Cross-sectional view of the 10 degree diffuser with closed gas inlet.

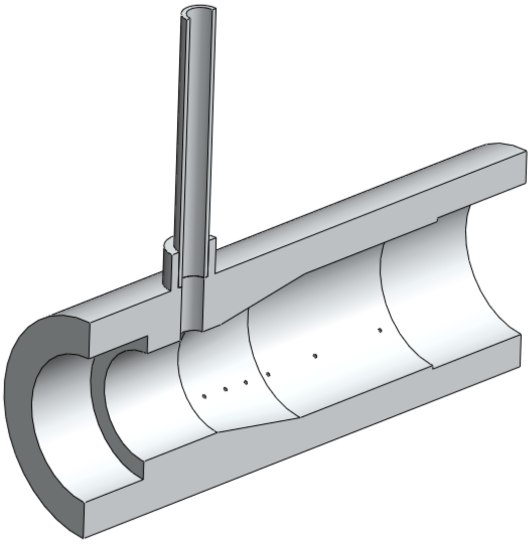

Figure 3.29: Cross-sectional view of the 10 degree diffuser with open gas inlet.

- A gas inlet with a hole diameter of 7.5 mm will be placed 10 mm before the diffuser entry. A pin can be placed inside this hole to block the gas inlet and test the diffuser without a gas inlet (Figure 3.28 and 3.29). This provides the possibility to compare the results with the results obtained from Experiment D.
- A 1 mm hole is drilled through the diffuser wall at each pressure tap location. A 3 mm chamber is drilled on top of the 1 mm holes in which the pressure taps are mounted (Figure 3.30). The holes on the inside of the diffusers are cleared of any burrs. This ensures that the holes on the inside of the diffuser are as smooth as possible.
- Holes that are drilled on the oblique side of the diffuser are drilled perpendicular to the oblique side (Figure 3.31).

The mass flow at the gas inlet is created by the difference between the static pressure before the diffuser entry and the ambient pressure. The flow rate in the gas inlet can be determined based on this pressure difference. The size of the gas inlet

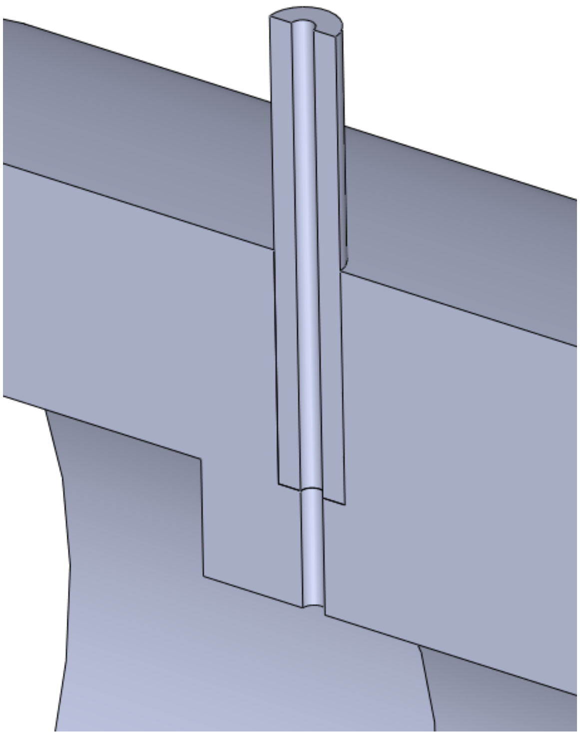

Figure 3.30: Cross-section of a pressure tap on the 10 degree diffuser.

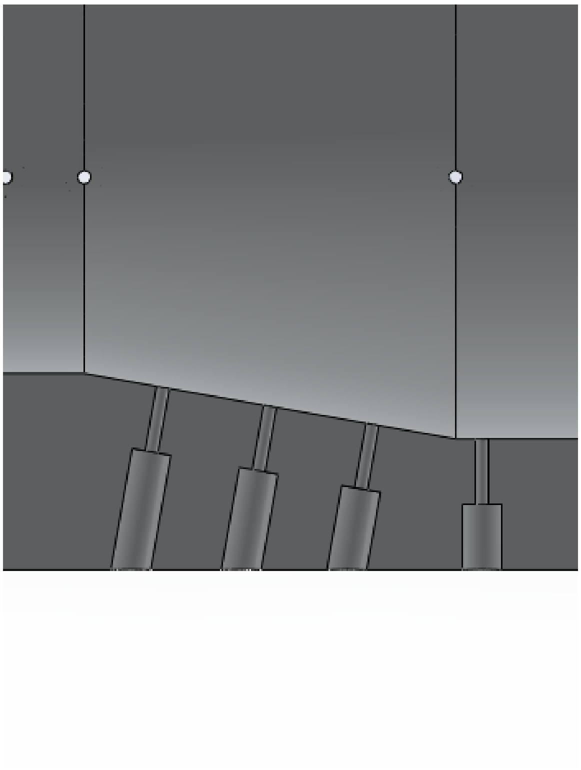

Figure 3.31: Pressure tap holes drilled on the oblique side of the 10 degree diffuser.

is chosen based on the gas to air ratio used in appliances. The mass stoichiometric ratio is the ratio of oxidizer to fuel where all the fuel and oxidizer are used [19]. It is defined as:

$$s = \left(\frac{Y_O}{Y_F}\right)_{st}, \quad \text{with } Y_k = \frac{m_k}{m_{total}} \tag{3.6}$$

Where Y_0 and Y_F are the mass fractions of oxidizer and fuel, respectively. The choice of gas and oxidizer (in this case air) will define the stoichiometric ratio. The equivalence ratio can then be defined as:

$$\phi = s\frac{Y_F}{Y_O} \tag{3.7}$$

Appliances operate at an equivalence ratio lower than one. This implies that more air than needed for stoichiometric combustion is present in the air-gas mixture. This is done for safety reasons, since an equivalence ratio of $s > 1$ will result in incomplete combustion and thus the formation of carbon monoxide. An equivalence ratio which is too low is also unwanted, since it will result in acoustic instability of the burner flame (instable flame). At a certain value of ϕ the flamability limit is reached. At this point the fuel to air ratio is too low for combustion. The equivalence ratio in appliances is typically around 0.8. The combination of the equivalence ratio, appliance output power and type of gas result in values for the mass flow of the gas and air. Choosing an output power of 30kW (which is typical for a regular household), G20 gas and atmospheric operating conditions results in the following mass flow rates of unburnt gas and air:

$$\dot{m}_{gas} = 6.0403 \cdot 10^{-4} \text{ kg/s} \qquad \dot{m}_{air} = 1.2990 \cdot 10^{-2} \text{ kg/s} \tag{3.8}$$

The mass flow of air is generated by the fan and can be monitored with the orifice flow meter. The mass flow of gas is generated by the underpressure which is present before the diffuser entry. A hole is drilled at the location at which the gas is to be injected, on which a tube is mounted. This tube will ensure a better developed entry flow. The inlet length of the tube is chosen to be 10 pipe diameters. No extra flow meter is used to measure the mass flow rate of the gas or the total mass flow rate. Instead, the mass flow is estimated based on the amount of underpressure at the gas inlet location, the hole diameter and the amount of resistance the tube for the gas inlet will generate. Also, the G20 gas is replaced by air for practical reasons. This will result in different behavior of the flow inside the diffuser due to the difference in density, viscosity and amount of mass flow. The goal of the measurements is to validate simulations, which will also be performed with air as a replacement for gas.

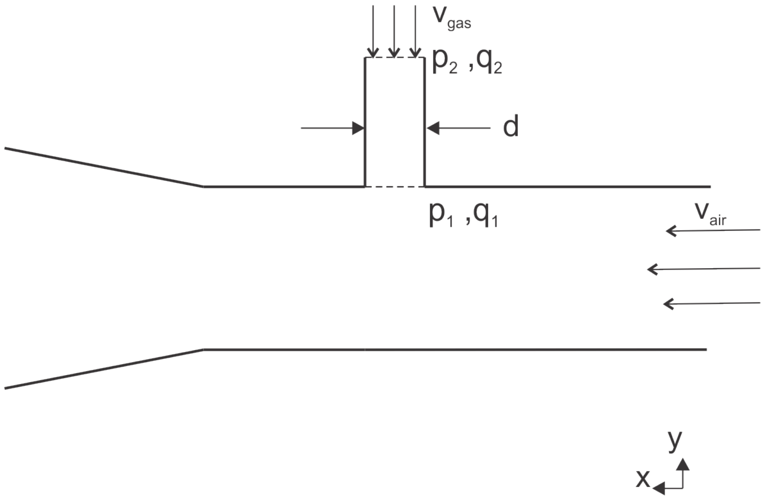

Figure 3.32: Schematic of the diffuser set-up with gas inlet.

The hole diameter needed to achieve a mass flow of $6.0403 \cdot 10^{-4}$ kg/s of air at the inlet can be estimated by analysing the static pressure at the gas inlet location from previous experiments at a flow rate of $1.2990 \cdot 10^{-2}$ kg/s. The location of the gas inlet is chosen to be 1 cm upstream of the diffuser entry. In experiment D, at $Re_D = 40280$ the mass flow rate was $1.117 \cdot 10^{-2}$ kg/s for the 4 degree diffuser. The corresponding static pressure 1 cm upstream of the diffuser entry was found to be

-438 Pa compared to the ambient pressure. The hole diameter can be determined by applying Bernoulli's equation:

$$p_1 + 0.5\rho v_1^2 = p_2 + 0.5\rho v_2^2 \tag{3.9}$$

Where $0.5\rho v^2$ is the dynamic pressure. Figure 3.32 shows that the dynamic pressure at location 1 is zero, since the velocity in the y-direction is zero. At location 2, the static pressure is assumed to be ambient. This results in:

$$p_1 = p_{ambient} + 0.5\rho v_2^2 \tag{3.10}$$

$$p_1 - p_{ambient} = 0.5 \cdot 1.2 * v_2^2 = -438 \tag{3.11}$$

The negative pressure indicates the v_2 operates in negative y-direction.

$$v_2 = \sqrt{\frac{438}{0.6}} \approx 27 \text{ m/s} \tag{3.12}$$

The gas inlet diameter D_g follows from the known mass flow rate:

$$\dot{m} = \frac{0.25\pi d^2 v}{\rho} \tag{3.13}$$

$$D_g = \sqrt{\frac{\dot{m}\rho}{0.25\pi v}} \approx 5.84 \text{ mm} \tag{3.14}$$

Since this calculated diameter does not include the pressure loss that occurs in the pipe, this diameter will have to be larger in reality. An estimation of the pressure loss can be made by assuming a pipe with a diameter of 5.8 mm and length of 58 mm (10 pipe diameters). Applying the Darcy-Weisbach equation gives the amount of pressure loss:

$$\Delta P = f\frac{L}{D_g}\frac{\rho v_{avg}^2}{2} \approx 136.09 \text{ Pa} \tag{3.15}$$

This value can be added to the static pressure used in Equation 3.11 to correct for the pressure loss due to skin friction. Equation 3.12 to 3.14 can be re-evaluated to obtain a new value for the diameter: $D_g = 6.5$ mm.

Detailed drawings of the set-up with both diffusers and the exact location of each static pressure tap can be found in Appendix A and B, respectively. Measurements will be performed at approximately the same Reynolds numbers as in Experiment D.

3.7 Experiment F: Diffuser without gas inlet, extra pressure taps

The results of Experiment D and E showed deviations from the simulations and theory upstream of the diffuser entry. To investigate this behavior further, some extra pressure taps were mounted upstream of the entry of the diffuser. The locations of these taps can be found in Figure 3.33. The location of the first and last pressure tap and the diffuser entry and exit can be found in Figure 3.34 to 3.36, where x = 0 mm is the position of the first pressure tap. The exact position of each pressure tap can be found in Appendix B.

The diffuser of 10 degrees showed no real signs of flow separation, since the theoretical pressure loss (without flow separation) matched the pressure loss of the simulations and measurements. For this reason an extra diffuser was made with an angle of 20 degrees. The expectation is that this diffuser will experience flow separation. This way the accuracy of the simulations where flow separation is present can be tested. Detailed drawings of the 20 degree diffuser can be found in Appendix A.

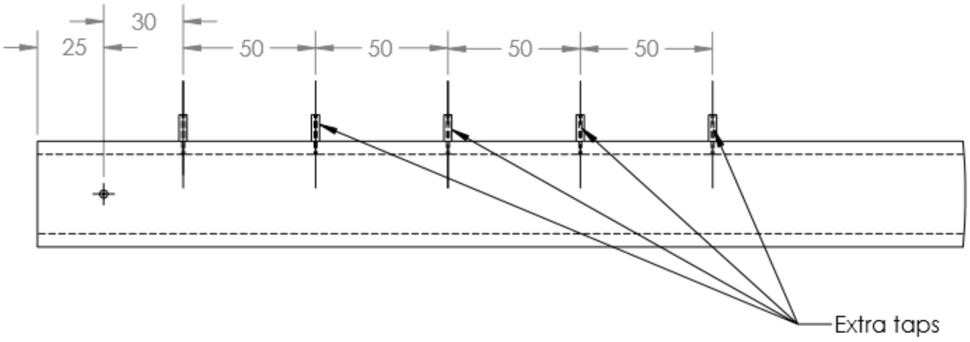

Figure 3.33: Location of the extra pressure taps on the entry tube with inner diameter of 30 mm.

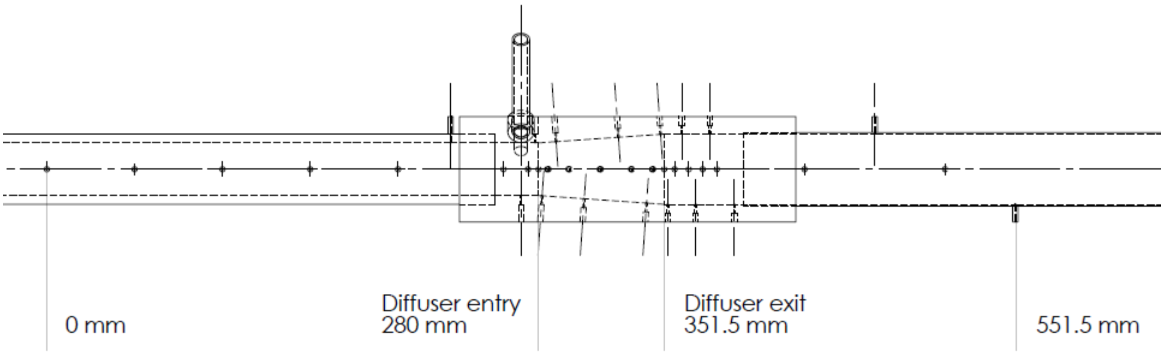

Figure 3.34: Geometry of the test section containing the static pressure taps with 4 degree diffuser.

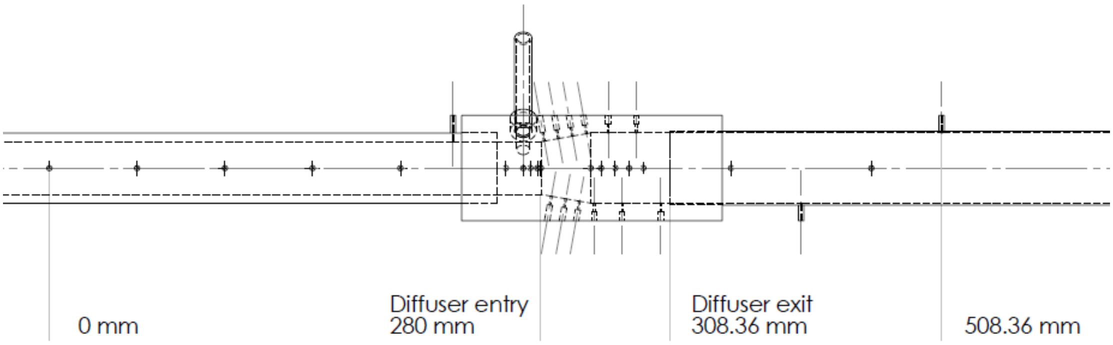

Figure 3.35: Geometry of the test section containing the static pressure taps with 10 degree diffuser.

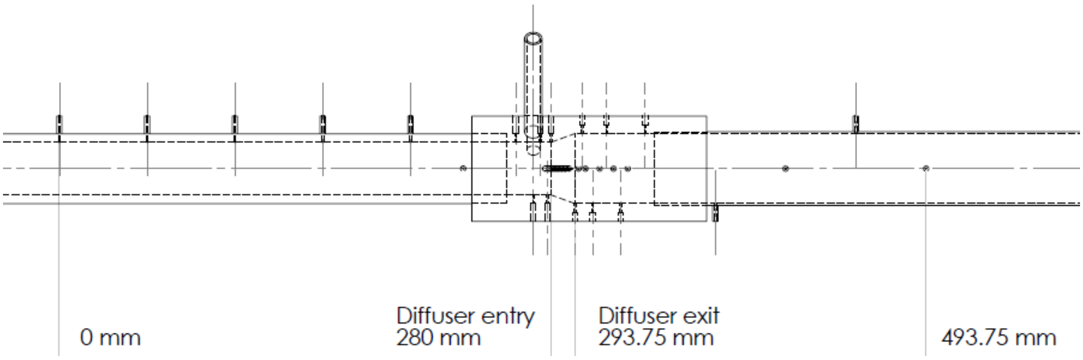

Figure 3.36: Geometry of the test section containing the static pressure taps with 20 degree diffuser.

3.8 Experiment G: WB6 venturi

The next step is to measure an actual venturi which is used in the WB6 project. The venturi has a throat diameter of either 15.0 mm or 15.3 mm and a removable gas injection (Figure 3.37 and 3.38). In this experiment, air is used instead of gas through the gas inlet for practical reasons. The venturi will be tested both with and without gas inlet. The experimental set-up can be seen in Figure 3.39. In contrast to Experiment D to F, air enters the set-up through the venturi and exits the set-up through the fan. The reason for this is that the exit of the venturi has the same diameter as the end of the main set-up and that the gas injection is fitted to the entry of the venturi. A total of seven pressure taps are located on the wall of the venturi. Six more pressure taps are present at the section of tube downstream of the venturi.

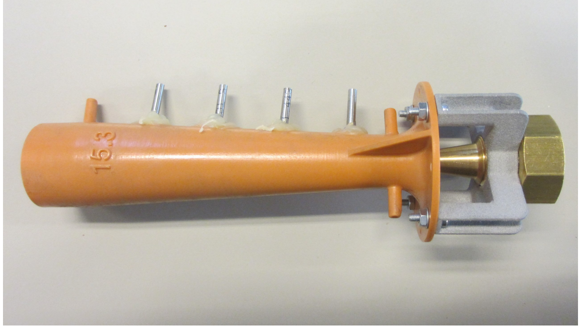

Figure 3.37: 15.3 mm WB6 venturi with gas injection.

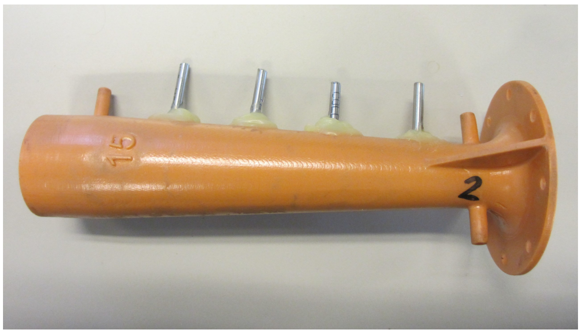

Figure 3.38: 15.0 mm WB6 venturi without gas injection.

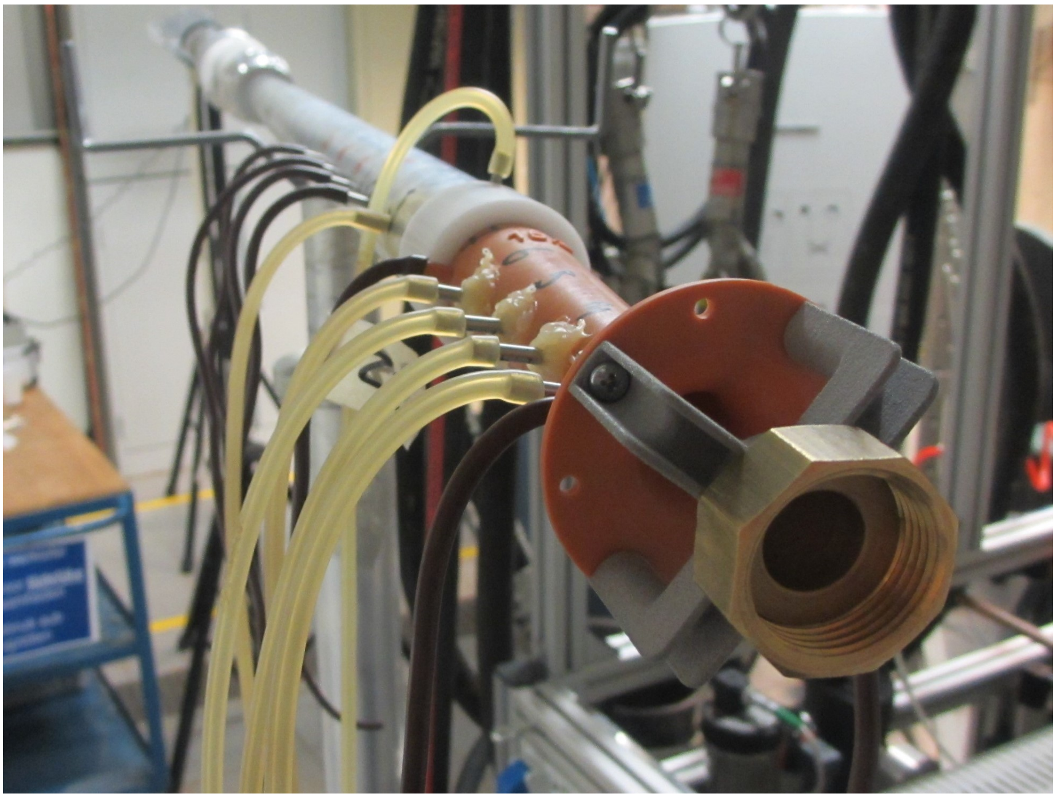

Figure 3.39: Experimental set-up with the WB6 venturi with gas injection.

Chapter 4

Results

The next Chapters will discuss the results of the experiments mentioned in Chapter 3.

4.1 Experiment A: PVC pipe

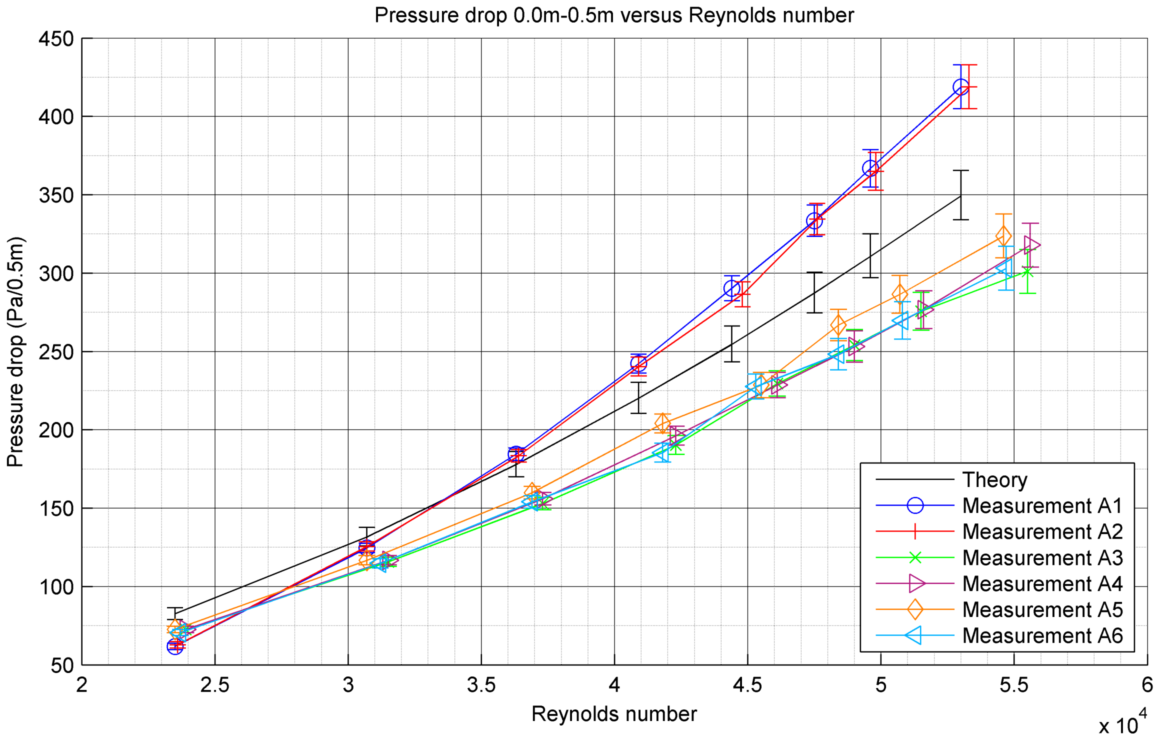

Figure 4.1: Pressure drop over the first section of PVC pipe versus the Reynolds number.

The pressure at different locations on the pipe was measured at different Reynolds numbers. The locations of the static pressure taps can be found in Figure 3.12. Different measurements were performed at fan output powers ranging from 30% to

Measurement	Flow direction
A1	Forward
A2	Forward
A3	Backward
A4	Backward
A5	Backward
A6	Backward
A7	Forward
A8	Forward
A9	Forward

Table 4.1: Configurations during each PVC pipe measurement.

100%, at intervals of 10%. At fan output powers below 30% the mass flow measurement in the orifice meter became inaccurate due to the fact that the fluctuations in the pressure readout were high in comparison with the pressure drop over the orifice meter. Before each measurement the ambient air temperature and pressure were determined to calculate the air density. An overview of the configuration of each measurement can be found in Table 4.1. The fan blows air into the experimental set-up during the first two measurements, which will be referred to as measurements with forward flow. For measurement A3 to A6 the fan and thus the flow direction was reversed. The flow then enters the set-up at the end of the PVC pipe and exits through the fan. This will be referred to as measurements with backward flow. The pressure drop from the first to the second tap and from the second to the third tap are plotted versus the Reynolds number. The results can be found in Figure 4.1 and 4.2. The pressure drop from the first to the last tap versus the Reynolds number can be found in Figure 4.3. The Reynolds number Re_D corresponds to the Reynolds in the test section, where D is the diameter of the PVC tube. The atmospheric conditions during each measurement can be found in Table 4.2. Figure 4.4 to 4.6 show the absolute difference between the theoretical pressure drop and the measured pressure drop plotted versus the Reynolds number.

There is a significant difference between the measured pressure drop and the theoretical pressure drop. Over 1 meter of pipe, the pressure drop of each measurement is not within the error bar range of the theoretical pressure drop. Figure 4.1 and 4.2 show that there is a clear difference between measurement 1 and 2 and measurement 3 to 6, which means the flow direction will have an influence on the measurements. The expectation is that measurement 3 to 6 will give better results between 0.5 m and 1.0 m and measurement 1 and 2 will give better results from 0.0 m to 0.5 m, because the flow will have a greater entry length at these points. However, the opposite is true according to the measurements. Figure 4.4 to 4.6 show

Property	Dynamic viscosity	Specific gas constant	Pressure	Temperature	Density
Symbol	μ	R_s	P	T	ρ
Unit	Pa s	J kg^{-1}K^{-1}	Pa	K	kg m^{-3}
Measurement A1	$1.79 \cdot 10^{-5}$	287	101100	293.15	1.202
Measurement A2	$1.79 \cdot 10^{-5}$	287	101100	293.15	1.202
Measurement A3	$1.79 \cdot 10^{-5}$	287	101800	293.85	1.207
Measurement A4	$1.79 \cdot 10^{-5}$	287	101800	293.85	1.207
Measurement A5	$1.79 \cdot 10^{-5}$	287	101800	293.85	1.207
Measurement A6	$1.79 \cdot 10^{-5}$	287	101800	293.85	1.207

Table 4.2: Atmospheric conditions during experiment A

that the measured pressure drop over 1 meter is more accurate than the measured pressure drop over 0.5 meter. The difference between each measurement is quite large. No clear conclusion can be drawn as to which measurement shows the best results.

During each measurement the problem occurred that the set-up was disturbed each time the manometer was connected to another pressure tap. This caused the set-up to move at connection points, resulting in small gaps through which the airflow could escape. These gaps cause a deviation in the volume flow calculated by the orifice meter. For the next measurement, any connection in the set-up was properly sealed with aluminum tape and a long and flexible plastic tube was connected to each pressure tap, which could be sealed with a plug. A total of three measurements was performed over a range of Reynolds numbers. The results can be seen in Figure 4.7 and 4.8. The configuration during the measurements can be found in Table 4.1. The absolute difference between the theoretical and measured pressure drop can be found in Figure 4.10 to 4.12.

Figure 4.7 to 4.9 show that each measurement gave almost the same values for the static pressure, which means the improvements to the set-up were successful. There is more similarity between the measured pressure drop over the second section of pipe (0.5 m - 1.0 m) and the theoretical pressure drop. Figure 4.10 to 4.12 show that the difference between the theoretical and measured pressure drop is still quite large from 0.0 m to 0.5 m (almost 80 Pa at the highest Reynolds number). This difference is reduced approximately by a factor two for the section of pipe from 0.5 m to 1.0 m. The fact that the measured pressure drop still deviates from the theoretical value could be due to the fact that there is not enough entry length for the flow to develop. There could also be a measurement error in the pressure taps due to defects during manufacturing. These defects could be present in the form of burrs that form after drilling. These burrs can influence the flow and result in different values

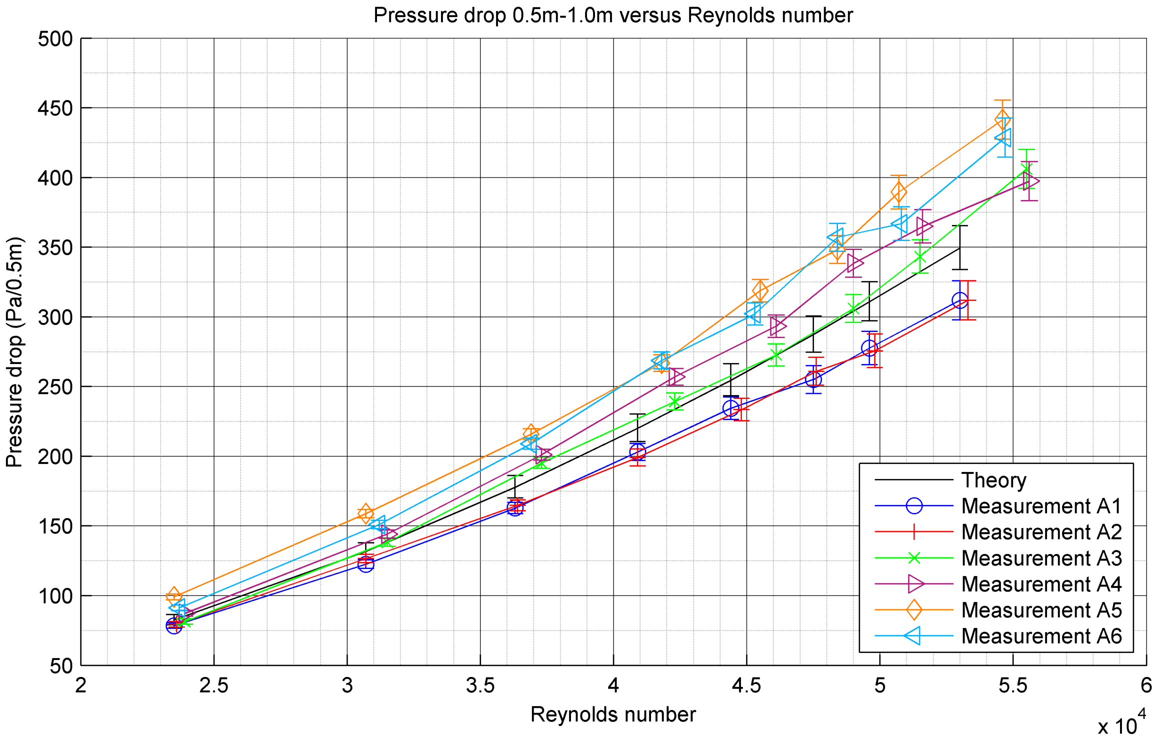

Figure 4.2: Pressure drop over the second section of PVC pipe versus the Reynolds number.

for the static pressure. A measurement with more pressure taps and with a smaller distance between the taps should be performed to investigate this behavior further.

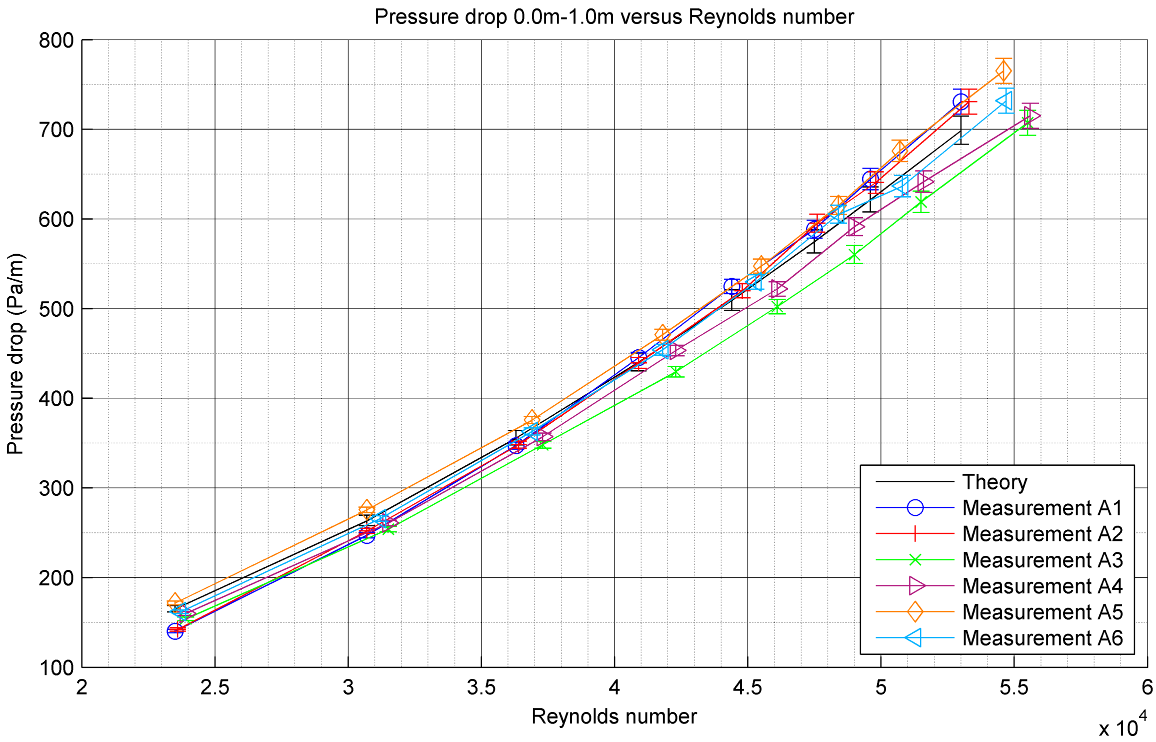

Figure 4.3: Pressure drop over 1 meter of PVC pipe versus the Reynolds number.

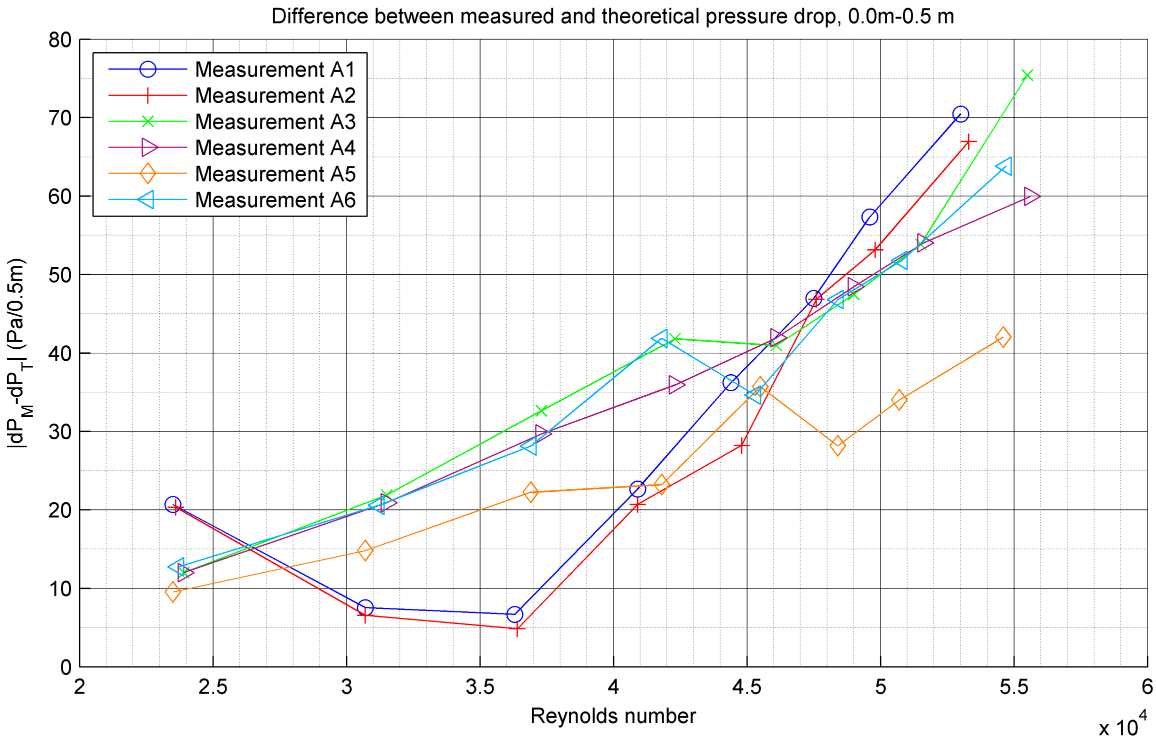

Figure 4.4: Absolute difference between theoretical and measured pressure drop versus the Reynolds number.

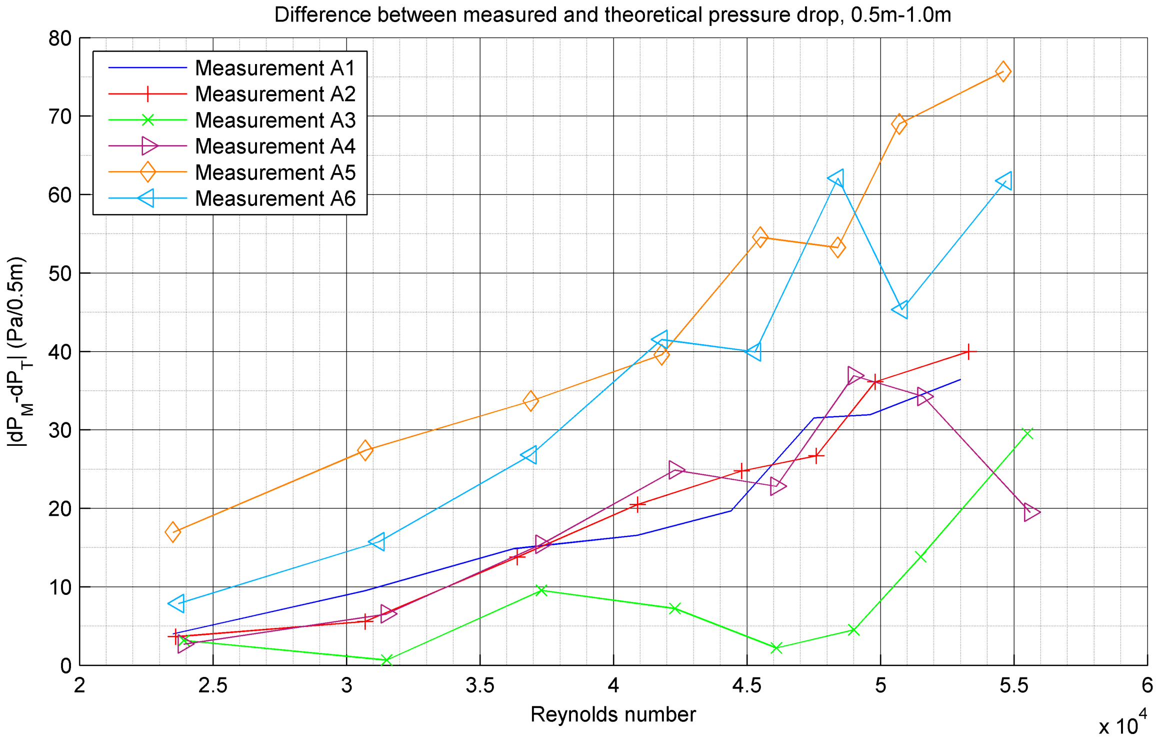

Figure 4.5: Absolute difference between theoretical and measured pressure drop versus the Reynolds number.

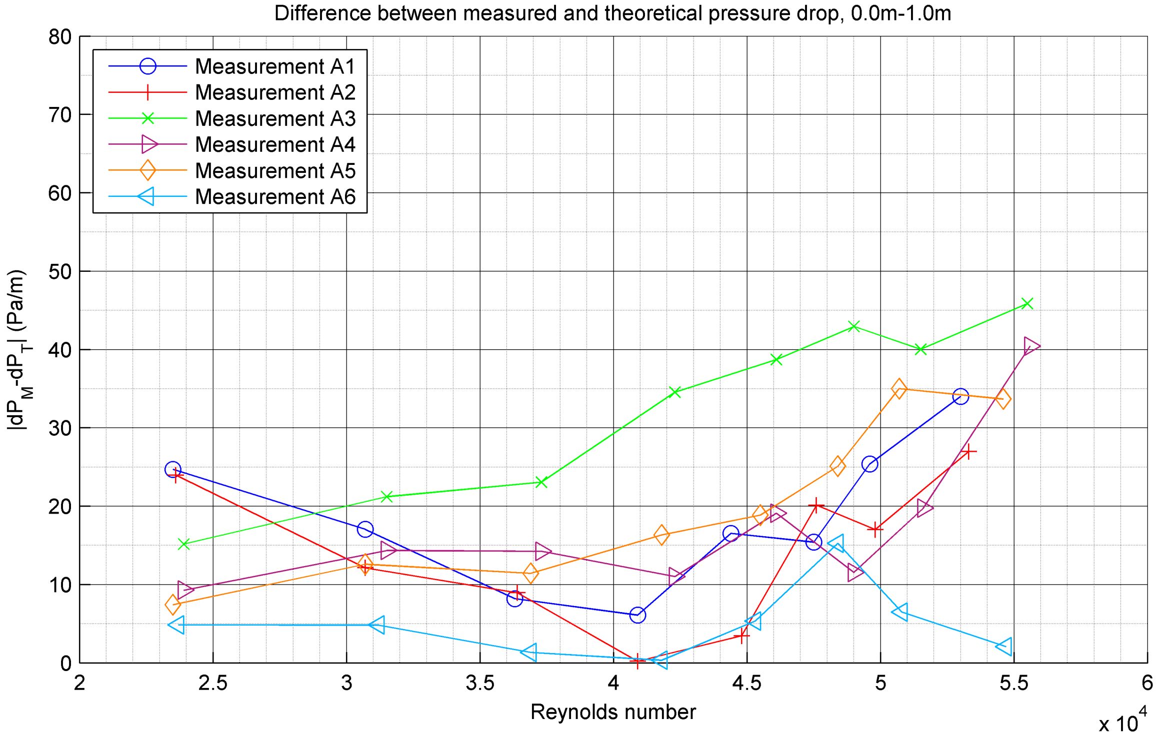

Figure 4.6: Absolute difference between theoretical and measured pressure drop versus the Reynolds number.

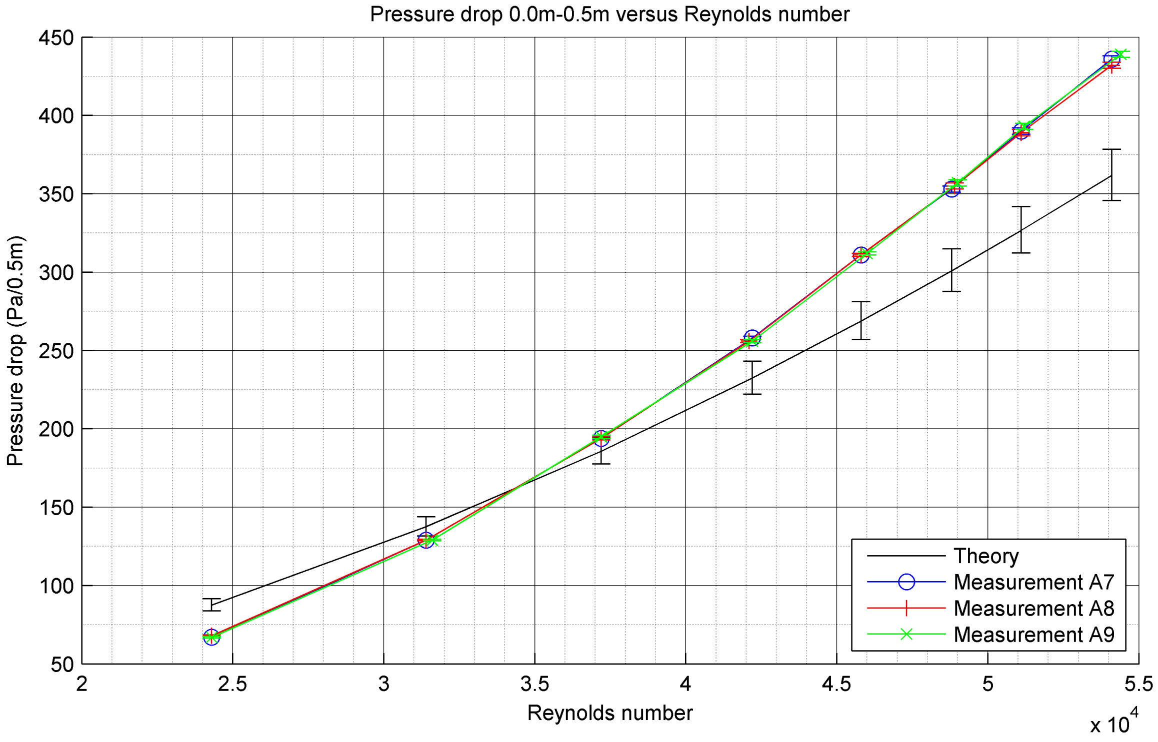

Figure 4.7: Pressure drop over 0.5 meter of PVC pipe with improved set-up versus the Reynolds number. The Reynolds number is determined at the test section.

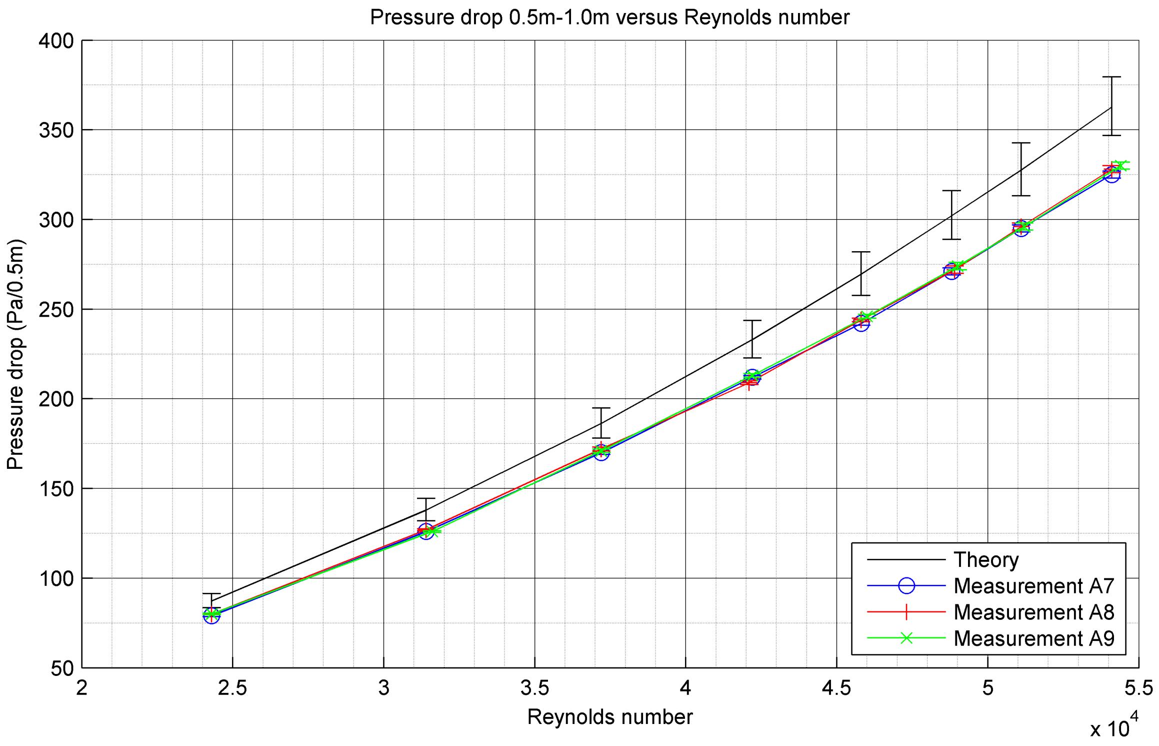

Figure 4.8: Pressure drop over 0.5 meter of PVC pipe with improved set-up versus the Reynolds number. The Reynolds number is determined at the test section.

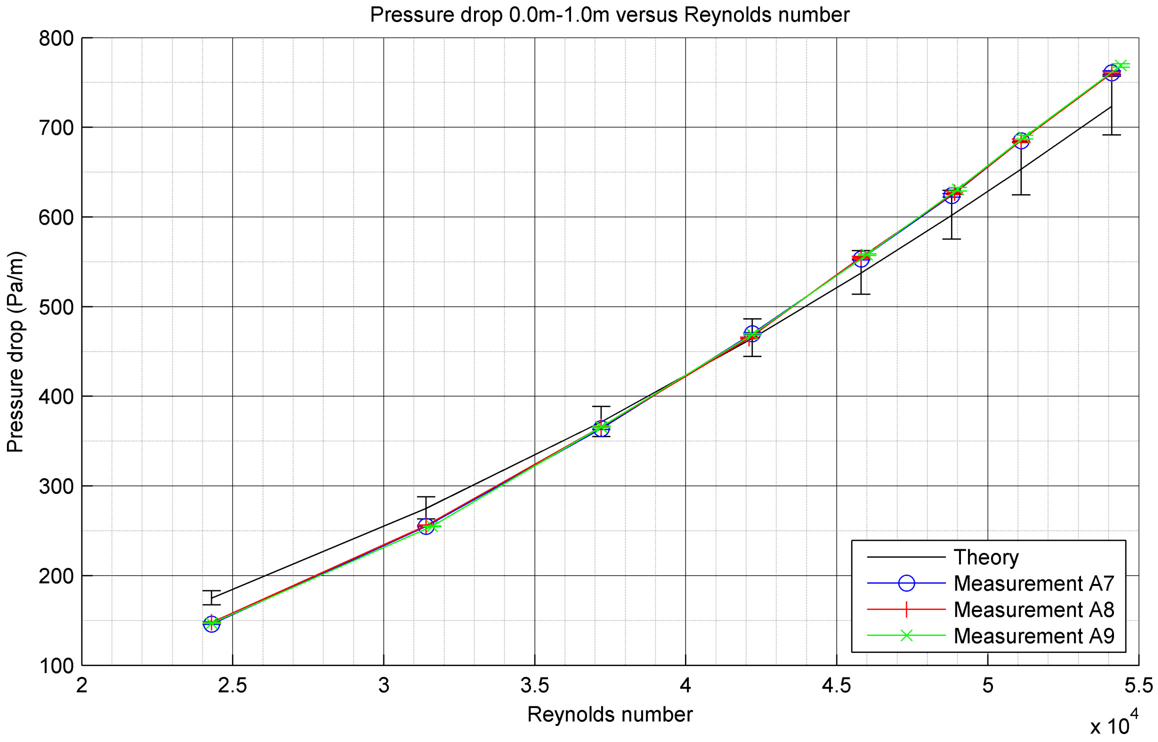

Figure 4.9: Pressure drop over 1 meter of PVC pipe with improved set-up versus the Reynolds number. The Reynolds number is determined at the test section.

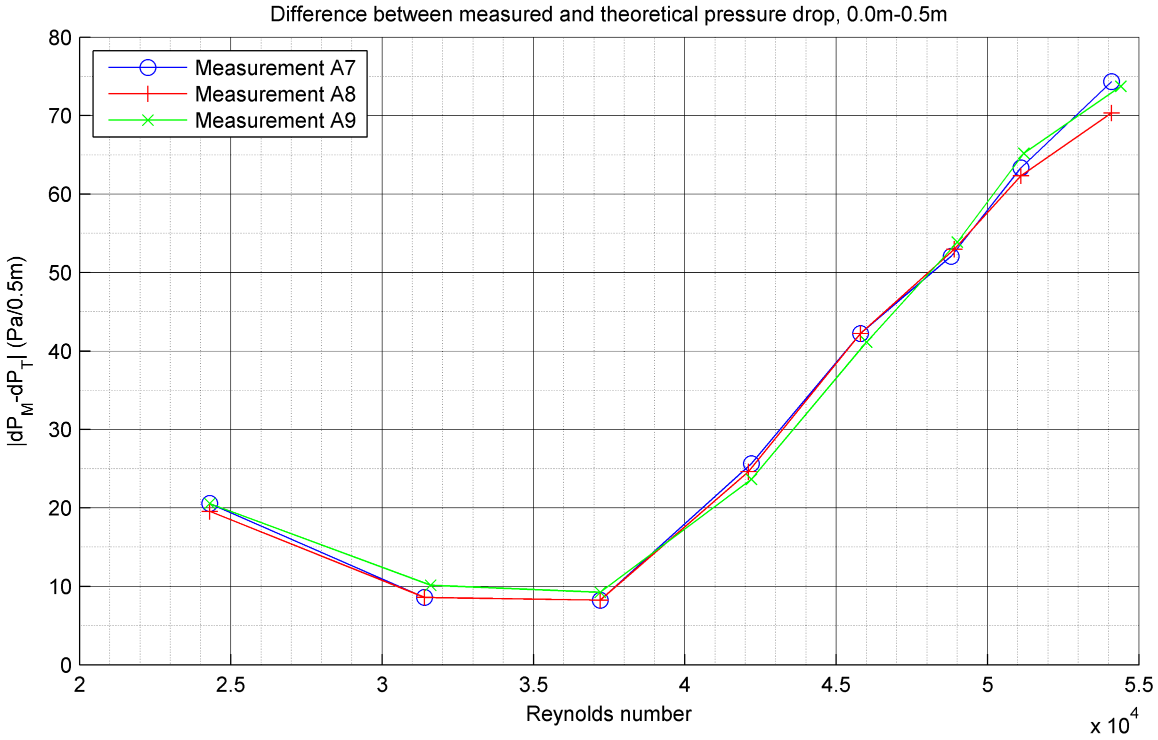

Figure 4.10: Absolute difference between theoretical and measured pressure drop versus the Reynolds number.

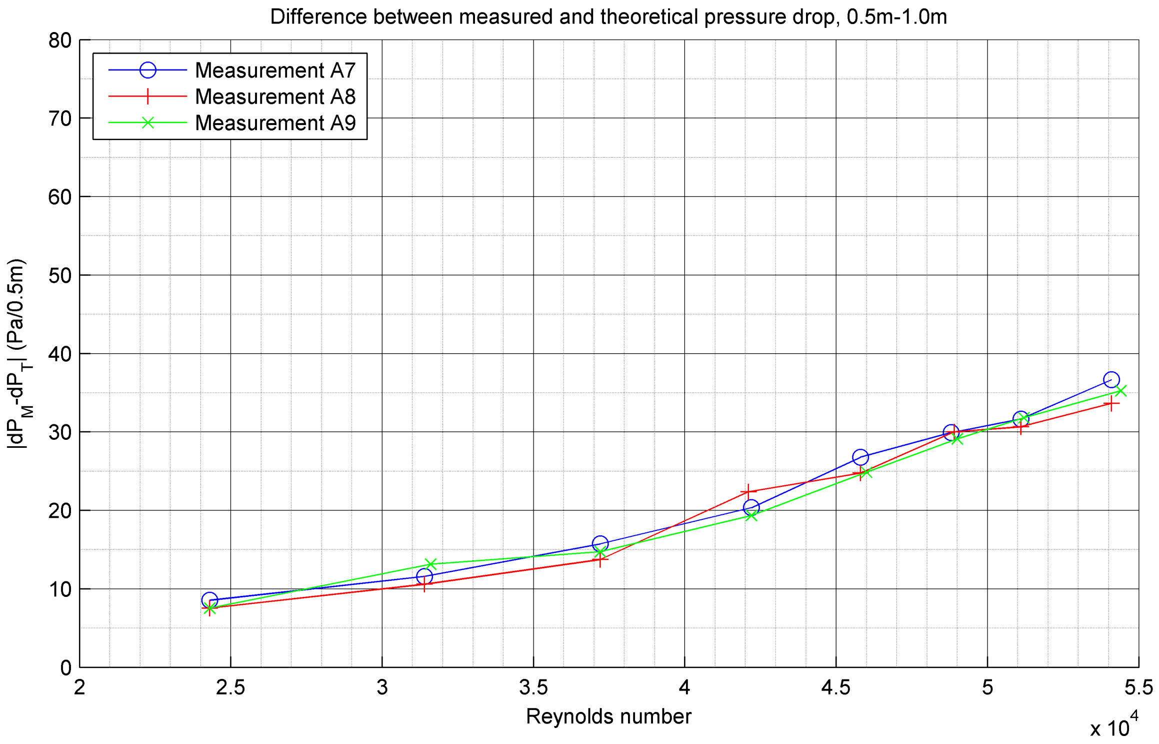

Figure 4.11: Absolute difference between theoretical and measured pressure drop versus the Reynolds number.

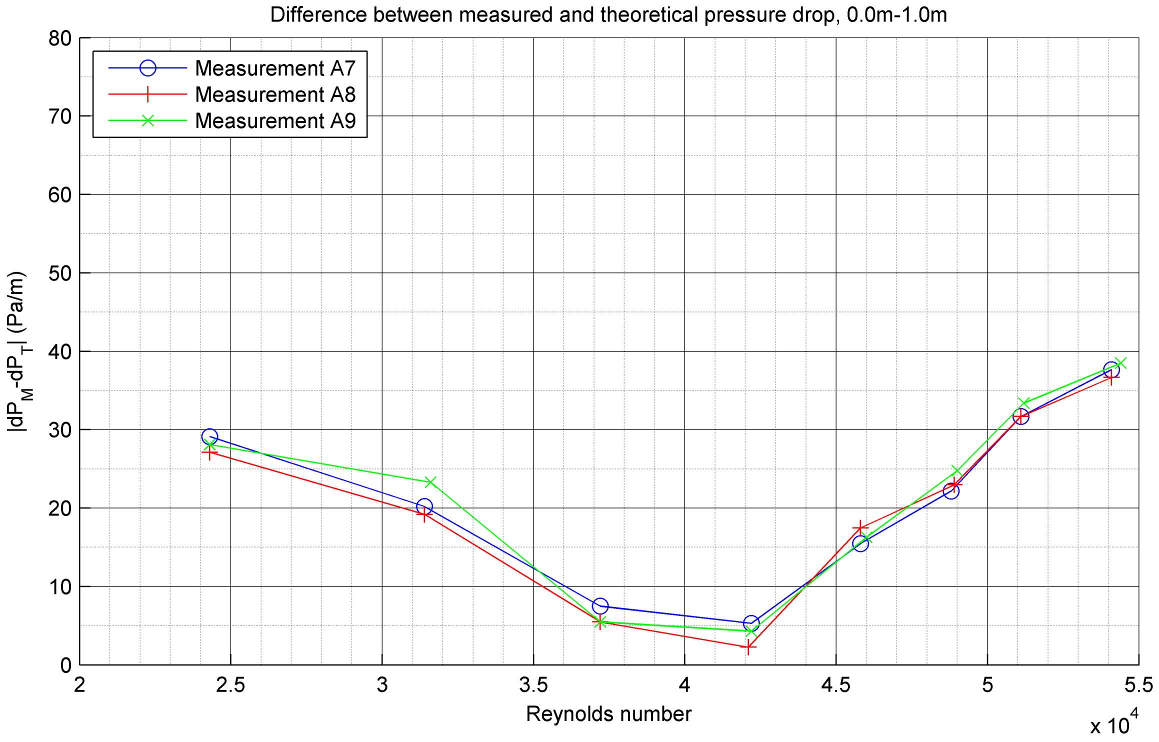

Figure 4.12: Absolute difference between theoretical and measured pressure drop versus the Reynolds number.

4.2 Experiment B: Copper pipe

Measurement	Flow direction	Adjustments
B1	Backward	-
B2	Forward	-
B3	Forward	Tubes are fitted to each pressure tap to prevent any movement of the experimental set-up when the manometer is fitted to another pressure tap
B4	Backward	-
B5	Forward	Any possible gaps in the set-up are made airtight.
B6	Backward	-

Table 4.3: Configurations during each copper pipe measurement.

The second measurement was performed with the copper pipe shown in Figure 3.14. The pressure at different locations on the pipe was measured at the same fan output powers as in Experiment A. A total of six measurements was performed at a range of flowrates. After each measurement several adjustments were made to the set-up. An overview of these adjustments can be found in Table 4.3. The internal diameter of the pipe was determined by measuring the internal diameter of 10 small pieces of pipe (Figure 4.13). The diameter was measured at both ends of each piece of pipe. The results can be found in Table 4.7. The average of these values, D_{avg} = 20.064 mm, is taken as the internal diameter of the pipe.

During measurement B1 and B2, the pressure taps that were not connected to a manometer were sealed with pieces of plastic tubing. The problem with this config-

Property	Dynamic viscosity	Specific gas constant	Pressure	Temperature	Density
Symbol	μ	R_s	P	T	ρ
Unit	Pa s	J kg^{-1}K^{-1}	Pa	K	kg m^{-3}
Measurement B1	$1.79 \cdot 10^{-5}$	287	101800	293.85	1.207
Measurement B2	$1.79 \cdot 10^{-5}$	287	99100	293.65	1.176
Measurement B3	$1.79 \cdot 10^{-5}$	287	100200	293.35	1.190
Measurement B4	$1.79 \cdot 10^{-5}$	287	100200	293.35	1.190
Measurement B5	$1.79 \cdot 10^{-5}$	287	103400	293.55	1.227
Measurement B6	$1.79 \cdot 10^{-5}$	287	103400	293.55	1.227

Table 4.4: Atmospheric conditions during experiment B.

Figure 4.13: Copper pipe samples.

uration is that the set-up was disturbed each time the manometer was connected to another pressure tap, as explained in Experiment A. This effect was again limited by fitting long plastic tubes to each pressure tap that could be closed with a plug. For measurement B5 and B6, any possible gaps in the connections of the set-up were made airtight by applying aluminum tape. Gaps in the set-up can result in pressure drops and errors in the measurement of the volume flow. The measured pressure drop from 0.0 m to 0.8 m and from 0.8 m to 1.6 m can be found in Figure 4.14 and 4.15. For the section from 0.0 m to 0.8 m the entry length is 0.2 m and the exit length 1.1 m. From 0.8 m to 1.6 m the entry length is 1.0 m and the exit length is 0.3 m. The pressure drop from the first to the last tap can be found in Figure 4.16. The pressure drop over each segment of 0.2 m can be found in Figure 4.17 to 4.25. The Reynolds number Re_D corresponds to the Reynolds number in the test section, where D is the diameter of the copper pipe. The atmospheric conditions during each measurement can be found in Table 4.4.

Figure 4.14 to 4.25 show that the measured pressure drop still does not correspond with the theoretical pressure drop. The configurations with forward flow showed the best results (Measurement 2,3 and 5). There is however no improvement in the accuracy of the measurement. Figure 4.17 to 4.25 show that there is a large deviation in the pressure drop over the different sections of 0.2 m. For example, the pressure tap located at 0.4 m showed lower pressures than expected, resulting in a high pressure drop from 0.2 m - 0.4 m and low pressure drop from 0.4 m - 0.6 m. Other sections also showed deviating results in the pressure drop. This means no clear conclusion can be drawn with regard to the entry length needed

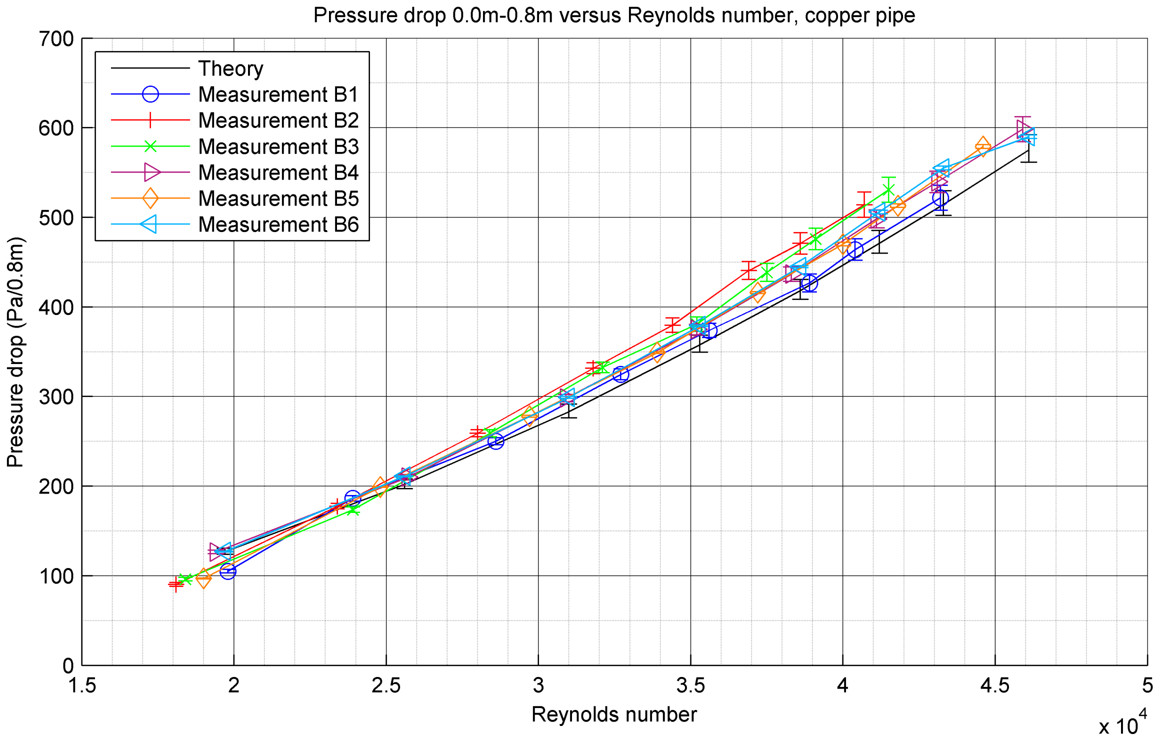

Figure 4.14: Pressure drop from 0.0 m to 0.8 m versus the Reynolds number. The Reynolds number is determined at the test section.

for accurate pressure measurements. The percentage error becomes smaller if the pressure drop is measured over a larger section of pipe (Figure 4.14 to 4.16). The error at each pressure taps is probably due to small defects in the pressure taps or burrs, as explained in Experiment A.

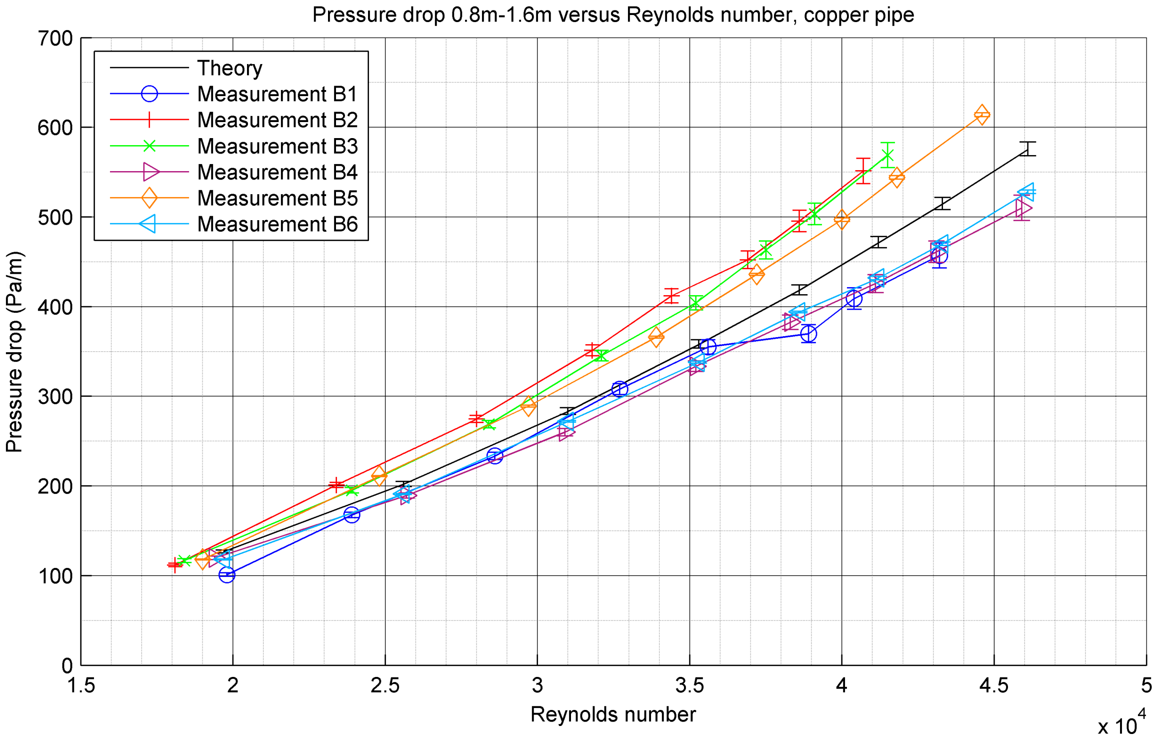

Figure 4.15: Pressure drop from 0.8 m to 1.6 m versus the Reynolds number. The Reynolds number is determined at the test section.

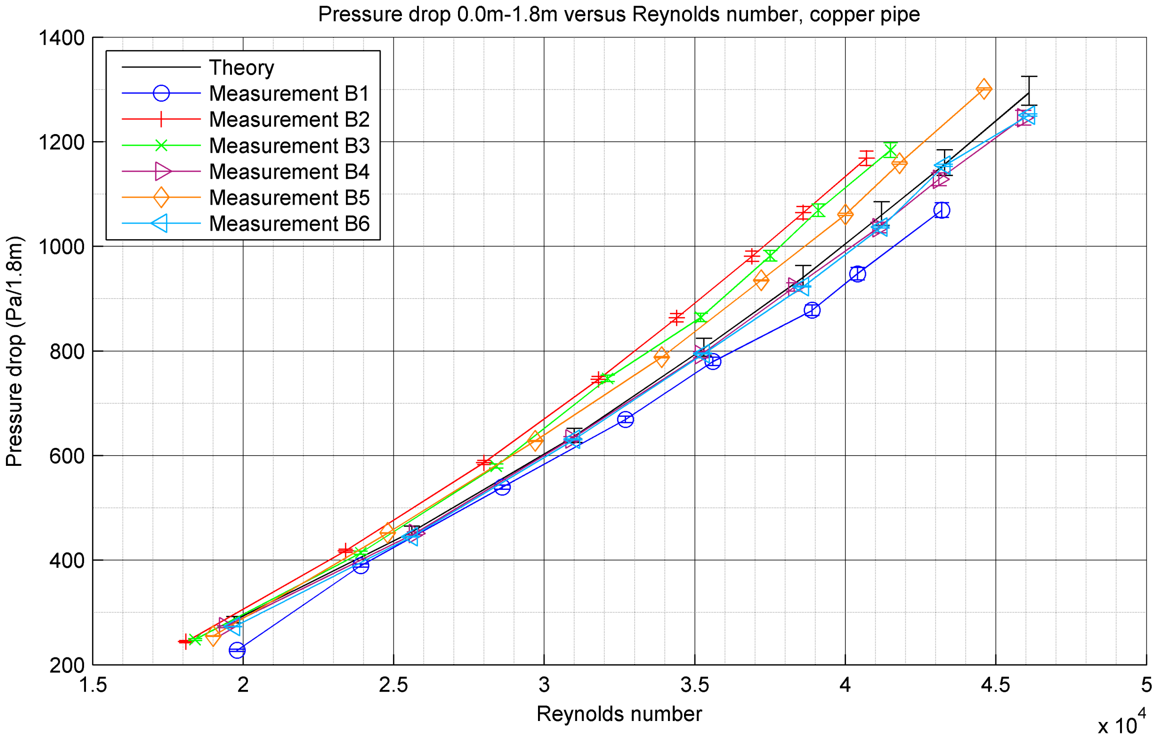

Figure 4.16: Pressure drop over 1.8 meter versus the Reynolds number. The Reynolds number is determined at the test section.

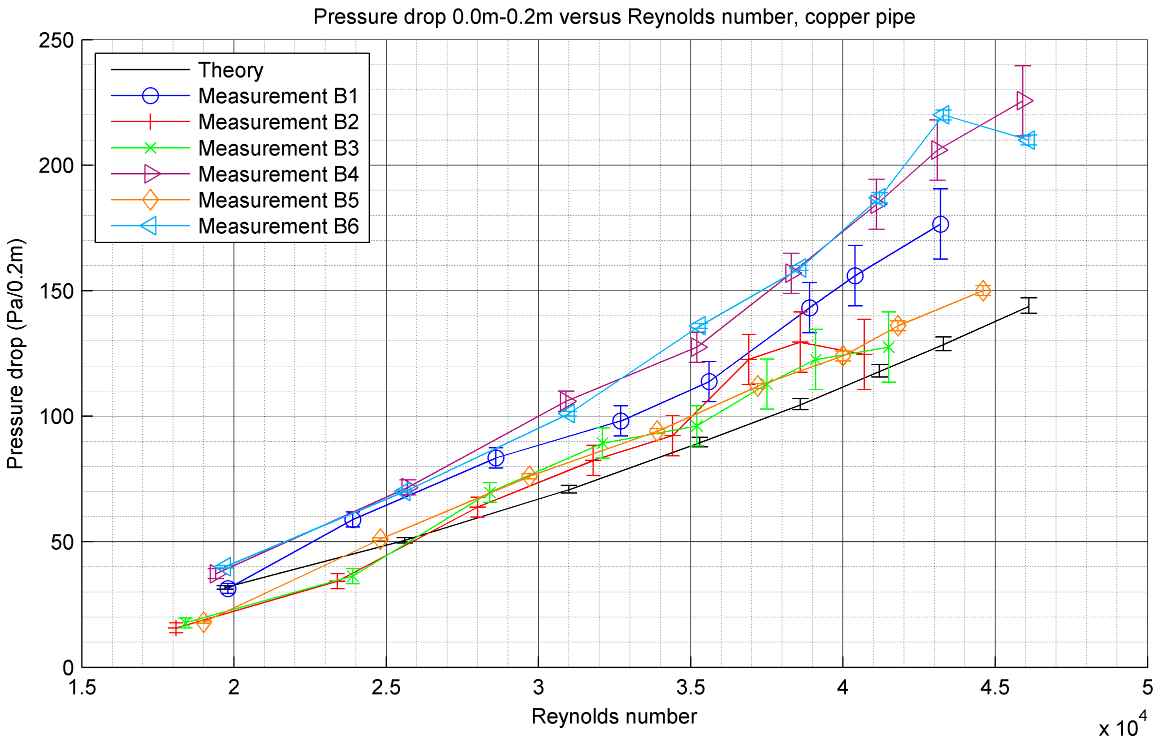

Figure 4.17: Pressure drop from 0.0 m to 0.2 m versus the Reynolds number for the copper pipe.

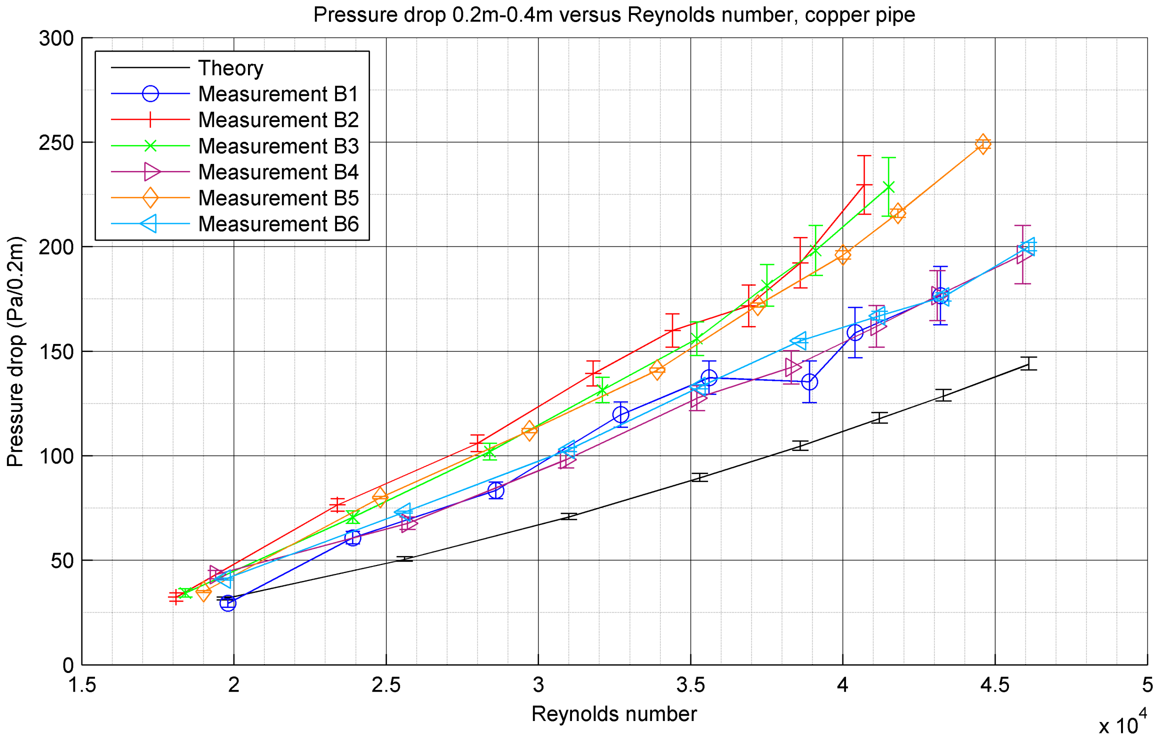

Figure 4.18: Pressure drop from 0.2 m to 0.4 m versus the Reynolds number for the copper pipe.

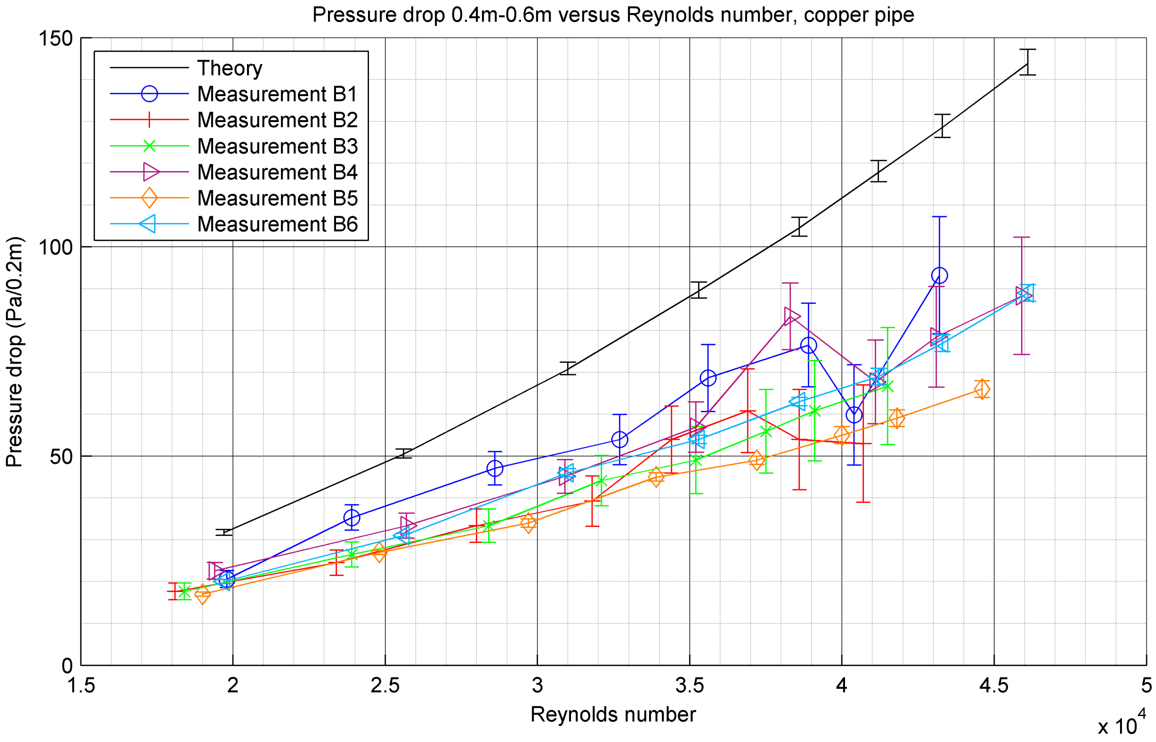

Figure 4.19: Pressure drop from 0.4 m to 0.6 m versus the Reynolds number for the copper pipe.

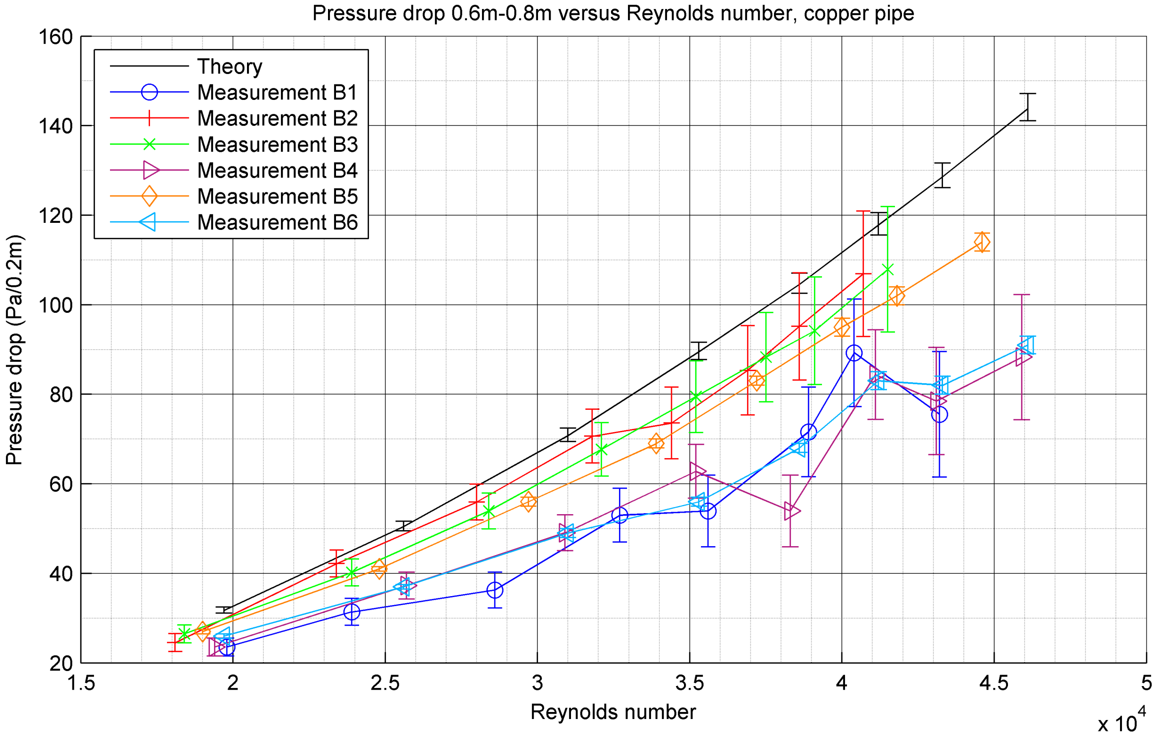

Figure 4.20: Pressure drop from 0.6 m to 0.8 m versus the Reynolds number for the copper pipe.

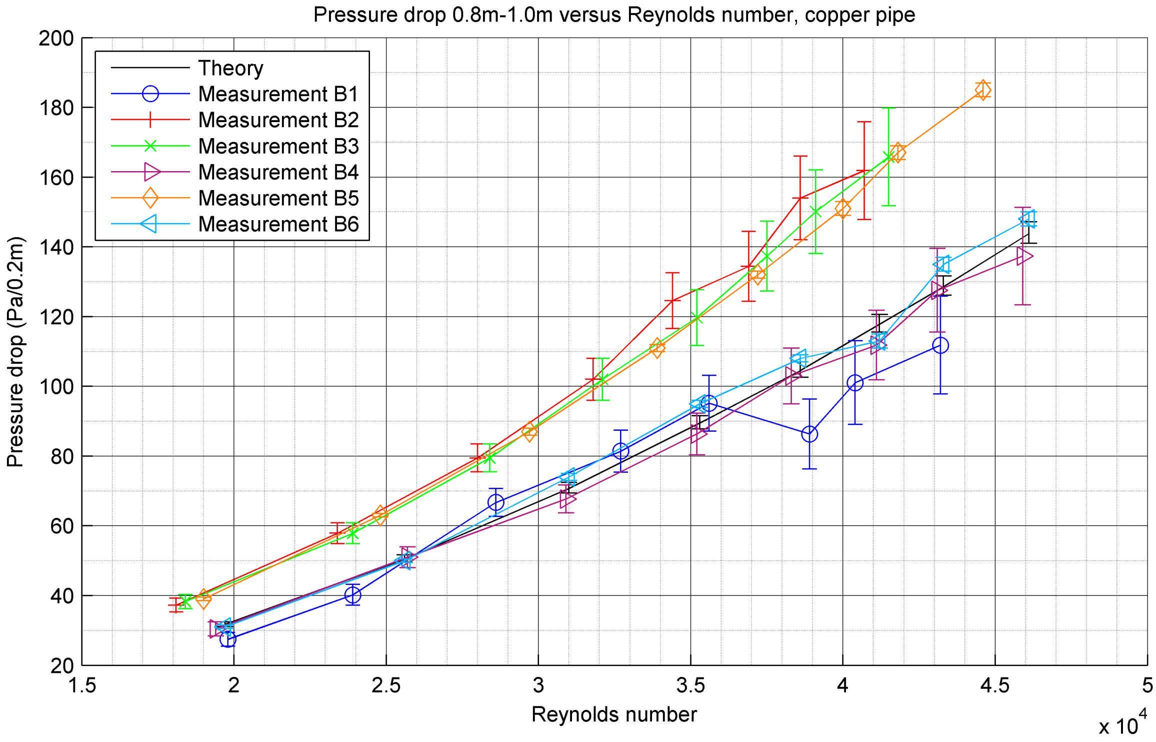

Figure 4.21: Pressure drop from 0.8 m to 1.0 m versus the Reynolds number for the copper pipe.

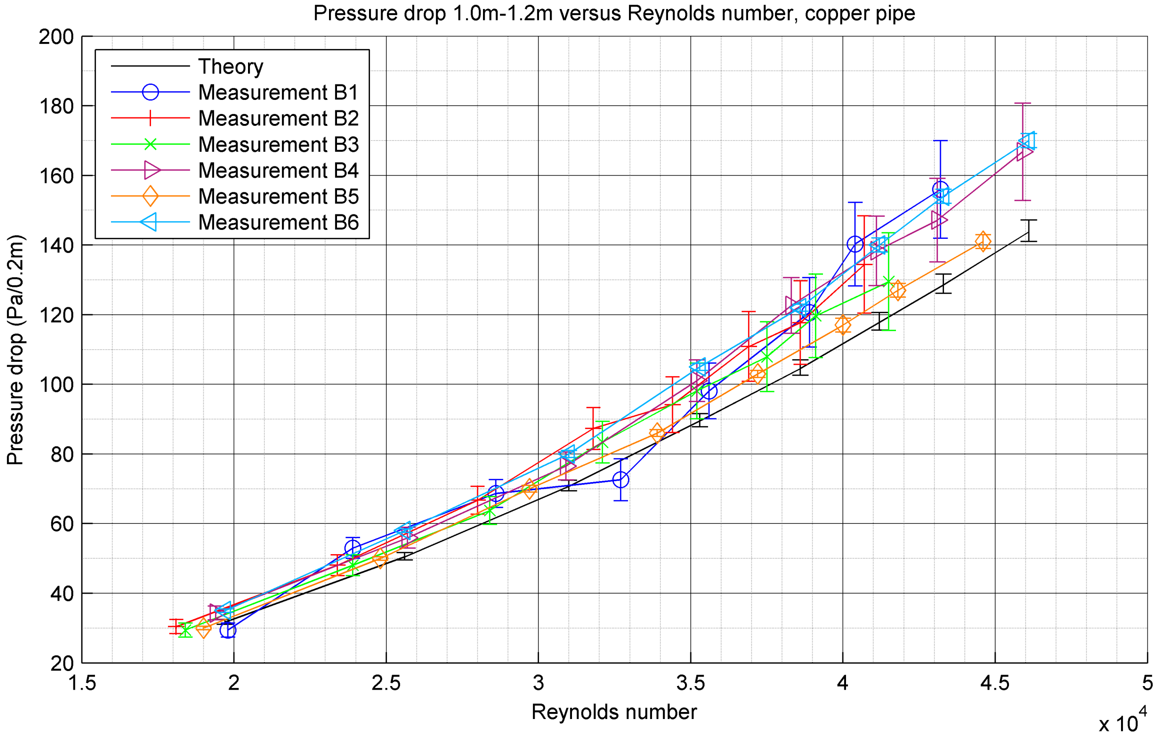

Figure 4.22: Pressure drop from 1.0 m to 1.2 m versus the Reynolds number for the copper pipe.

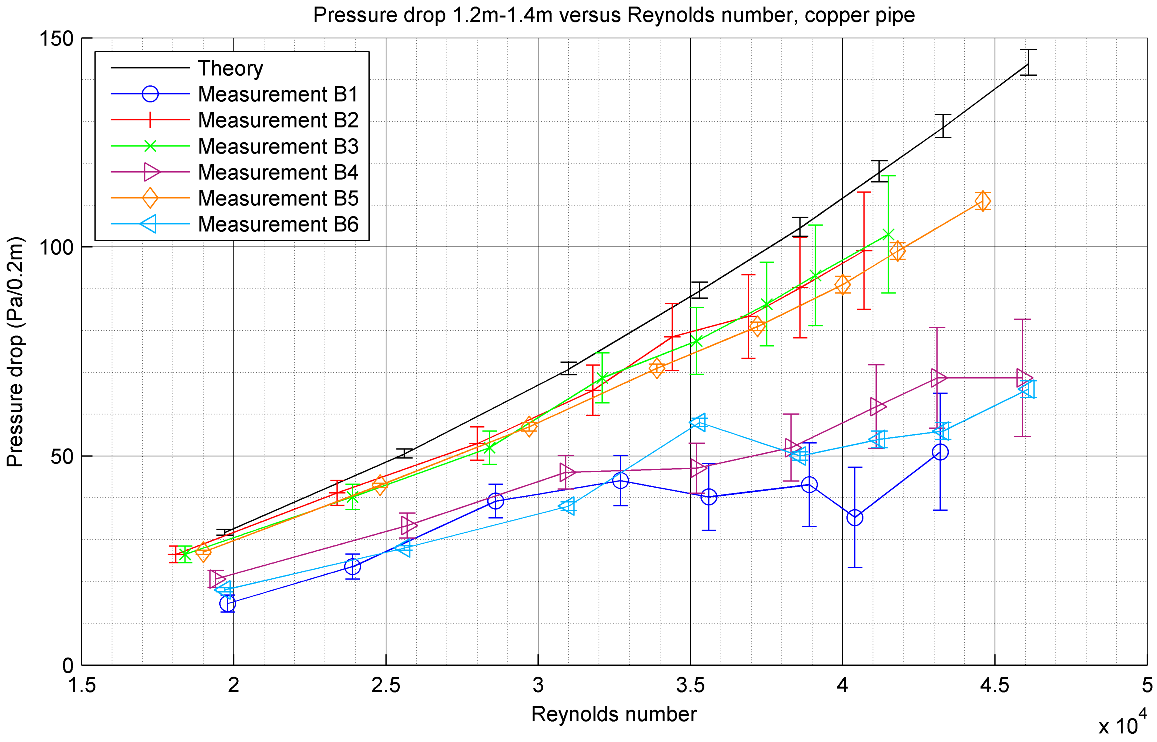

Figure 4.23: Pressure drop from 1.2 m to 1.4 m versus the Reynolds number for the copper pipe.

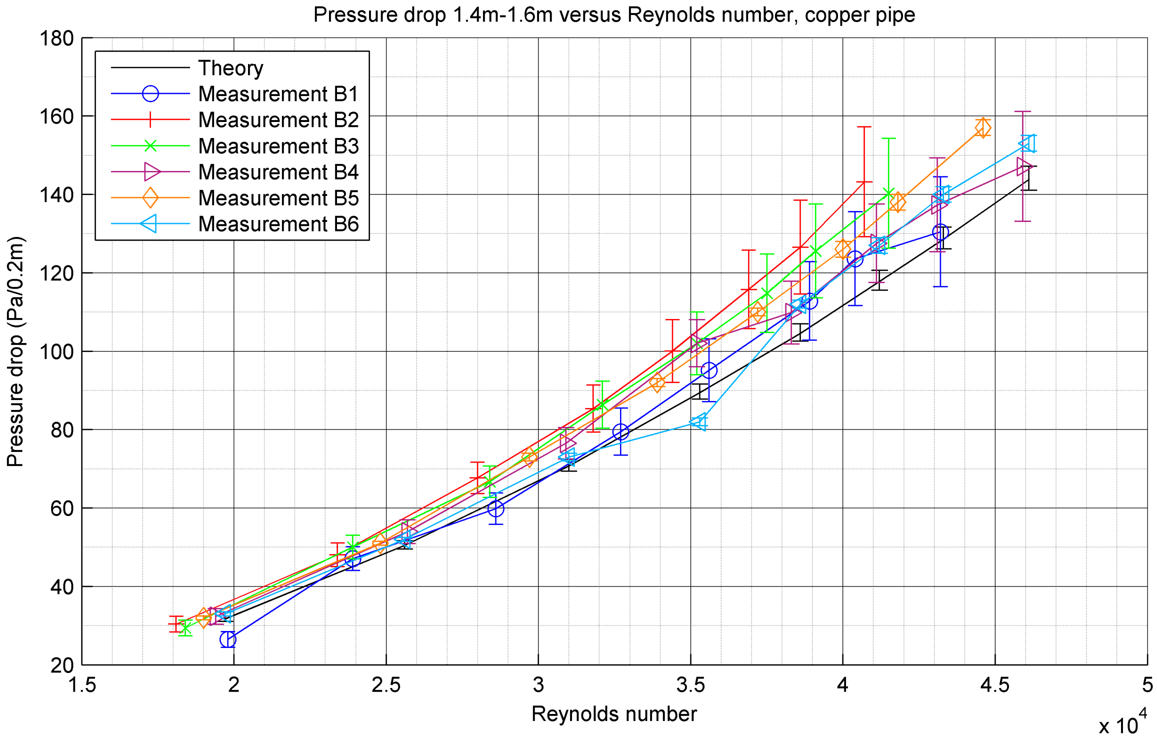

Figure 4.24: Pressure drop from 1.4 m to 1.6 m versus the Reynolds number for the copper pipe.

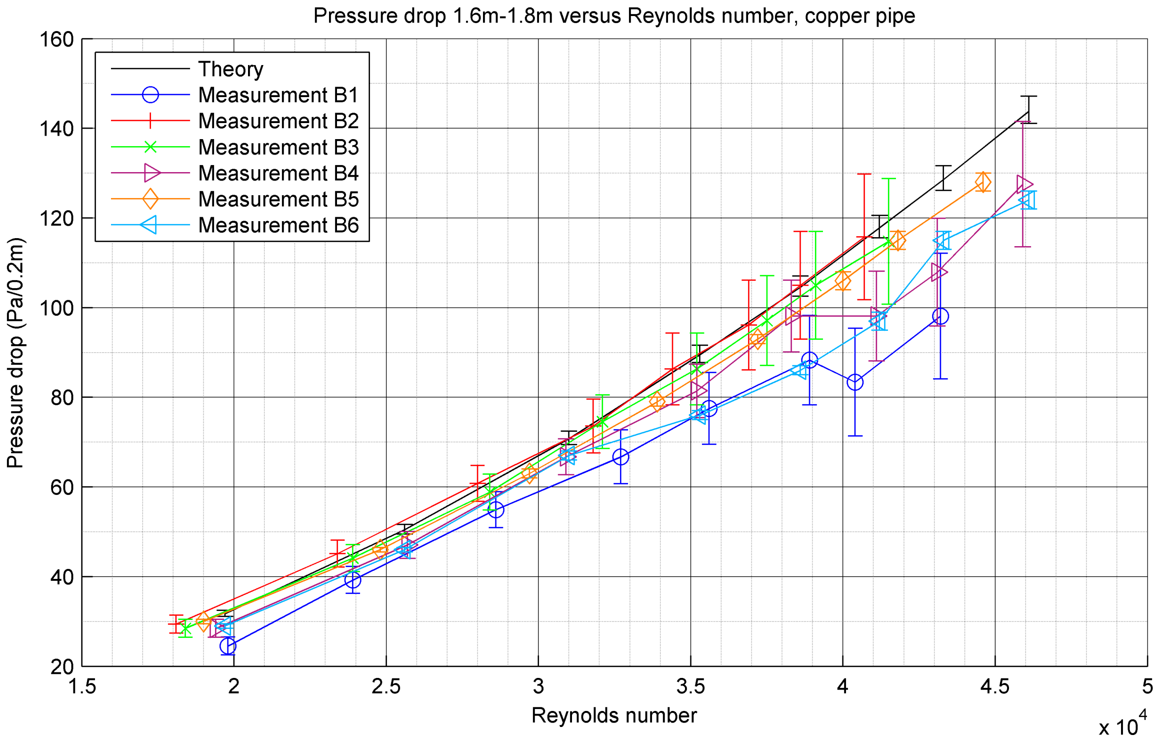

Figure 4.25: Pressure drop from 1.6 m to 1.8 m versus the Reynolds number for the copper pipe.

4.3 Experiment C: Copper pipe with grid

The measurement procedure in this experiment was similar to the procedure in Chapter 4.2. The flow direction will be forward since this configuration showed the best results in Experiment B. The pressure drop from 0.0 m to 0.8 m and from 0.8 m to 1.6 m can be found in Figure 4.26 and 4.27. The pressure drop over the entire pipe can be found in Figure 4.28. The pressure drop over each section of 0.2 m can be found in Figure 4.29 to 4.37. The atmospheric conditions during each measurement can be found in Table 4.6. The configuration during each measurement can be found in Table 4.5.

Measurement	Flow direction	Grid type
C1	Forward	Fine grid
C2	Forward	Coarse grid
C3	Forward	No grid

Table 4.5: Configurations during Experiment C.

Property	Dynamic viscosity	Specific gas constant	Pressure	Temperature	Density
Symbol	μ	R_s	P	T	ρ
Unit	Pa s	J kg^{-1}K^{-1}	Pa	K	kg m^{-3}
Measurement C1	$1.79 \cdot 10^{-5}$	287	100400	293.25	1.193
Measurement C2	$1.79 \cdot 10^{-5}$	287	100400	293.25	1.193
Measurement C3	$1.79 \cdot 10^{-5}$	287	100400	293.25	1.193

Table 4.6: Atmospheric conditions during experiment C.

Figure 4.26 to 4.37 show that the grids do not have a noticeable effect on the accuracy of the pressure measurement. The grids do have an effect on the maximum Reynolds number at full fan power, which is reduced. The reduction is the greatest for the coarse grid. This reduction is due to the fact that the grids will induce an amount of pressure loss, since the flow is partially blocked. There is an improvement in overall accuracy compared to Experiment B. This may be due to the fact that the set-up is more airtight than in Experiment B. Figure 4.26 and 4.27 show that there is a difference in pressure drop between the first and second section of pipe. At low Reynolds numbers, the first section (0.0 m to 0.8 m) shows lower values for the pressure drop, whereas the second section (0.8 m to 1.6 m) shows higher values for the pressure drop at high Reynolds numbers. This means the pressure

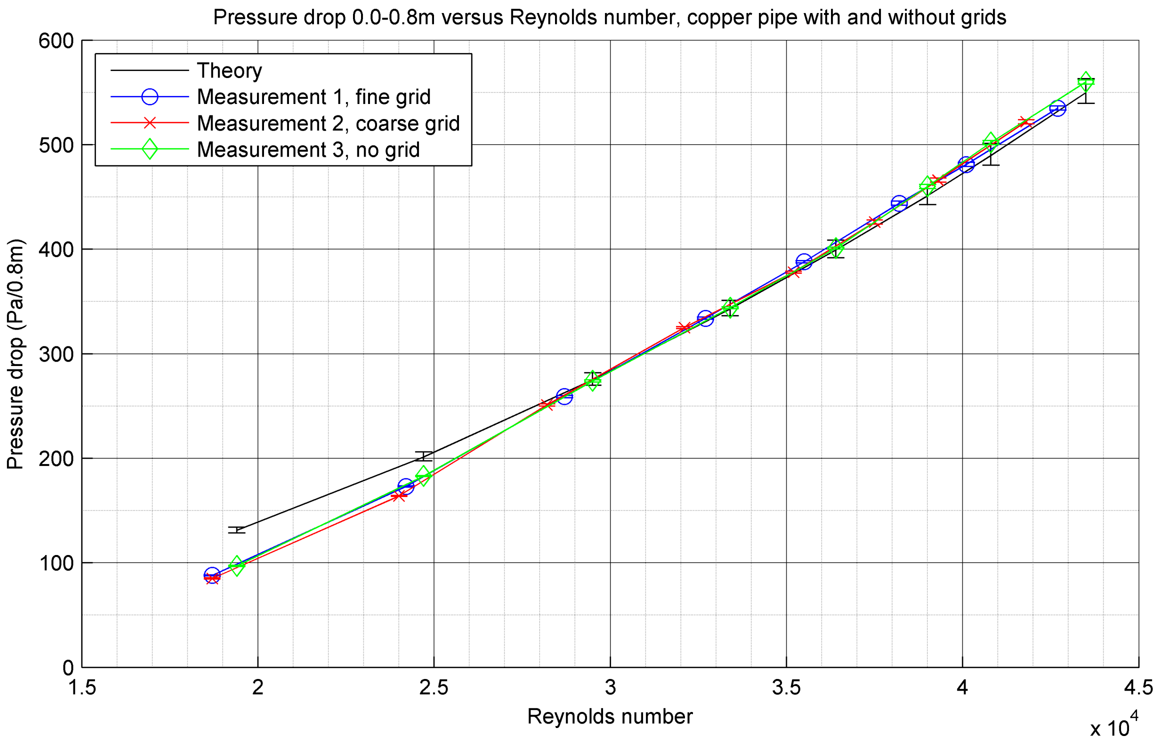

Figure 4.26: Pressure drop from 0.0 m to 0.8 m of versus the Reynolds number, copper pipe with and without grids. The Reynolds number is determined at the test section.

measurements do not show a significant effect on the entry length needed for precise pressure measurements. For the section (0.0 m to 0.8 m) the entry length is 10 diameters. For the second section of pipe (0.8 m to 1.6 m), the entry length is 50 diameters. Figure 4.29 to 4.37 show that there is still a large variation in the pressure drop per section of 0.2 m.

The reason that the effect of the grids cannot be noticed may be due to the fact that more screens and a honeycomb are needed in the presence of a settling chamber to effectively create a homogeneous flow in the test section. One grid may not be enough to achieve a noticeable improvement as it is located far away from the test section. Detailed velocity analyses should be performed to properly investigate the effect of the grid.

4.3.1 Error estimation

The errorbars in Figure 4.1 to 4.37 represent errors due to different factors. The internal diameter of the PVC pipe and copper pipe were 22.3 mm and 20.06 mm, respectively. However, measurement with a caliper showed small deviations in the internal diameter. The errorbars on the theoretical pressure drop represent a deviation of ± 0.2 mm in the internal diameter of the PVC pipe. Other factors, like the

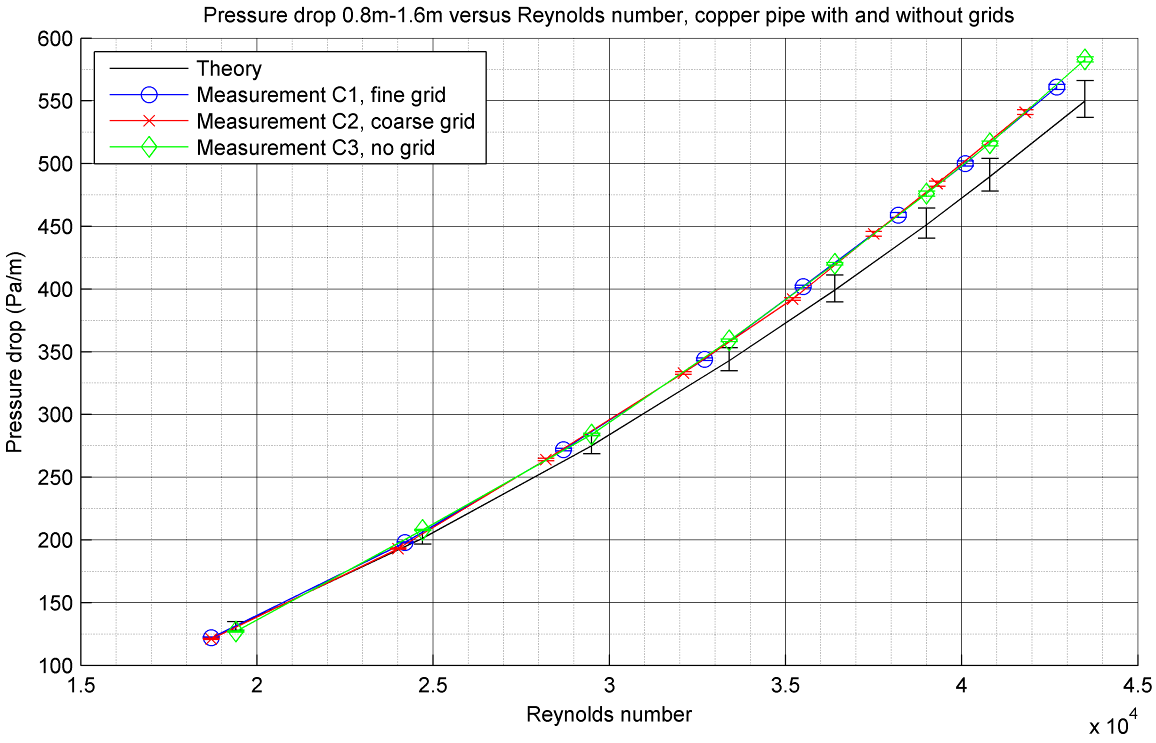

Figure 4.27: Pressure drop from 0.8 m to 1.6 m of versus the Reynolds number, copper pipe with and without grids. The Reynolds number is determined at the test section.

roughness height ϵ are not taken into account in the errobars because they are hard to quantify. The error in the internal diameter of the copper pipe was determined by taking the minimum and maximum found in Table 4.7, and subtracting them from the average value of 20.06 mm. This results in an error of -0.094 mm and +0.076 mm. These errors have an effect on the theoretical pressure drop, but also on the flow rate and the Reynolds number. The error in the Reynolds number is small however, less than 1 percent at most. The errors in the pressure readout are mainly due to fluctuations in the pressure displayed by the manometers. The TT series micromanometer had a readout error ranging between 0.5 Pa and 2.0 Pa, depending on the Reynolds number. The error in the readout of the Neotronics micromanometer ranged between 0.2 and 1 mmH_20. Multiplying by a factor 9.81 gives the pressure in Pascals. This results in an error of approximately 2 to 10 Pa. The resolution of the manometers is negligible in comparison with the error in the readout (± 0.05 Pa). The error in the readout of the orifice meter appeared to be lower: approximately 1 Pa. This corresponds to an error in the flow rate of approximately 1 percent. The error in the orifice meter itself is due to possible disturbances in the flow and tolerances in the dimensions. It is hard to give a value to the error in the orifice meter as these quantities are hard to determine. An overview of the different parameters and corresponding error margins is given in Table 4.8.

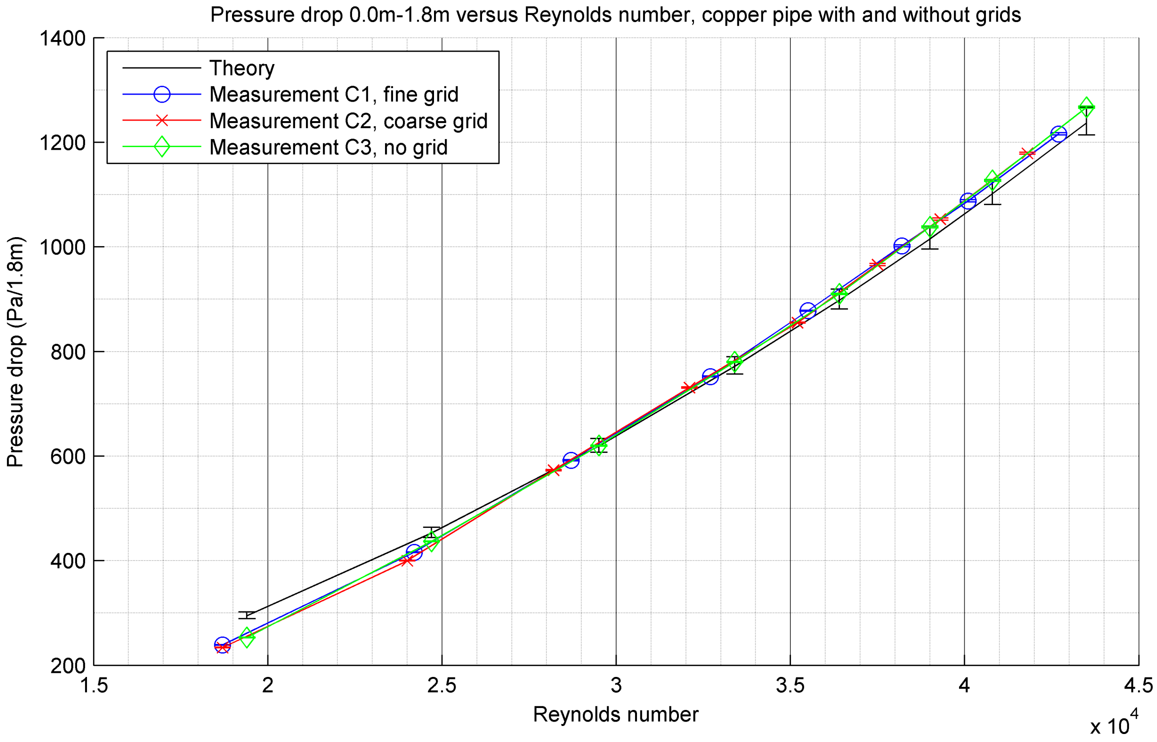

Figure 4.28: Pressure drop over 1.8 meter versus the Reynolds number, copper pipe with and without grids. The Reynolds number is determined at the test section.

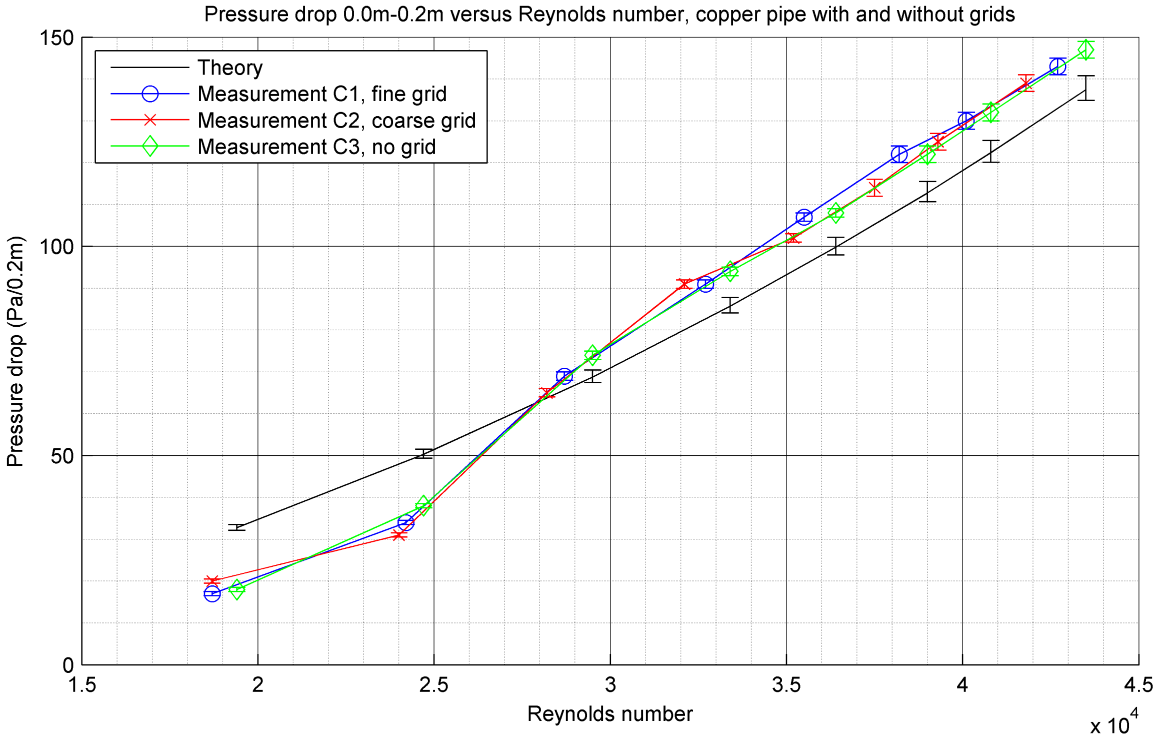

Figure 4.29: Pressure drop from 0.0 m to 0.2 m versus the Reynolds number for the copper pipe with and without grids.

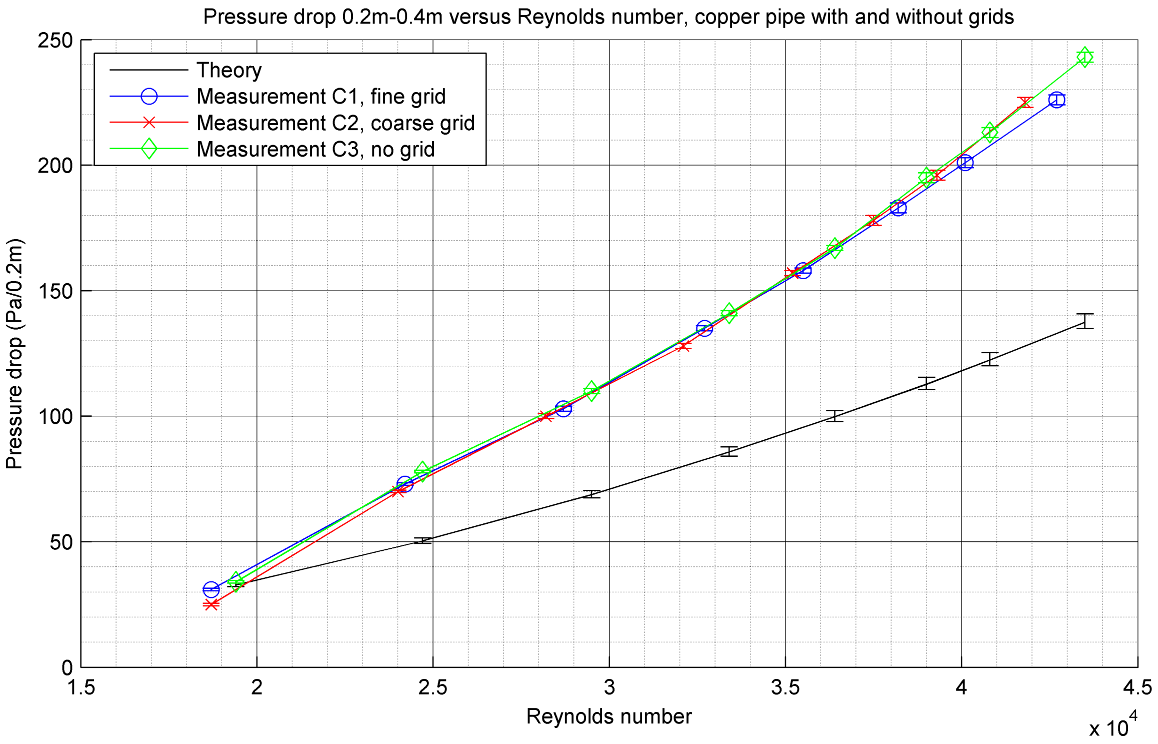

Figure 4.30: Pressure drop from 0.2 m to 0.4 m versus the Reynolds number for the copper pipe with and without grids.

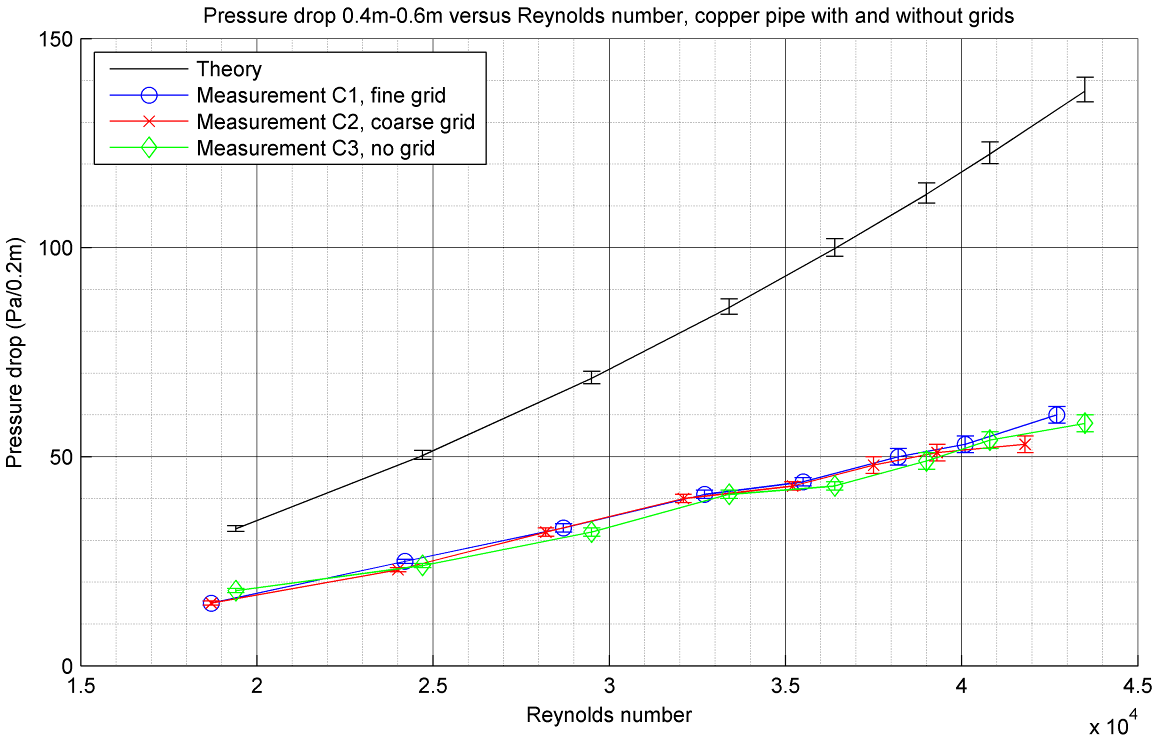

Figure 4.31: Pressure drop from 0.4 m to 0.6 m versus the Reynolds number for the copper pipe with and without grids.

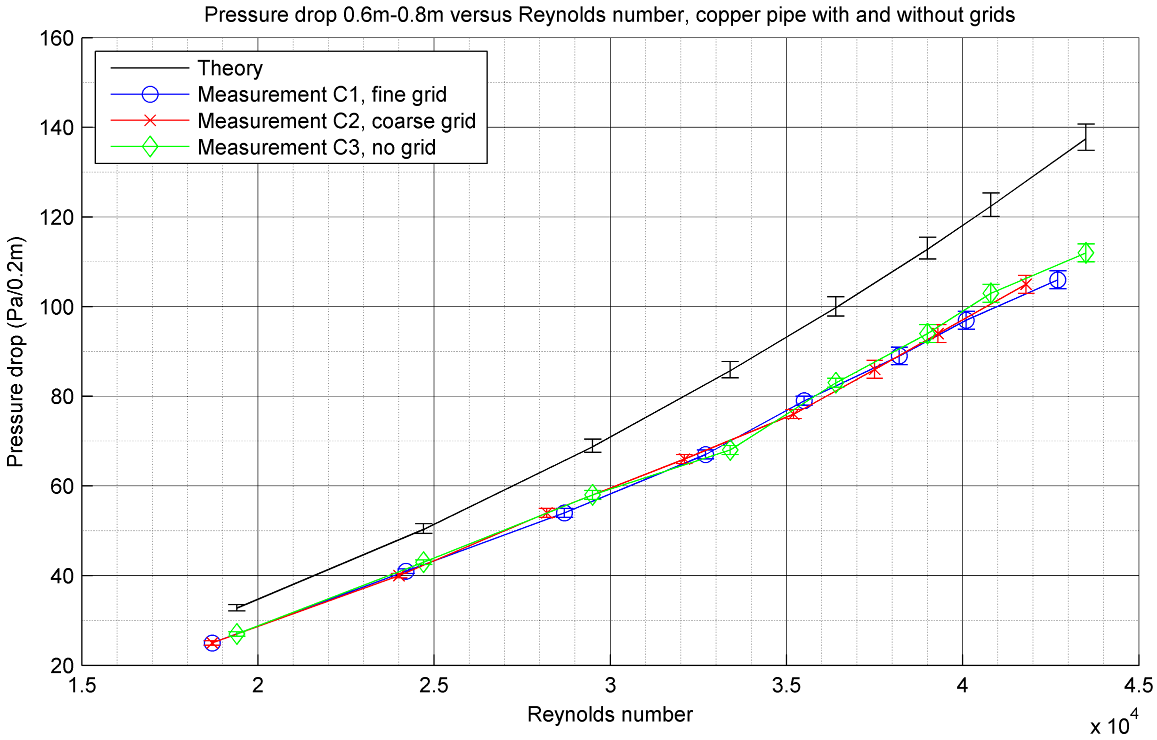

Figure 4.32: Pressure drop from 0.6 m to 0.8 m versus the Reynolds number for the copper pipe with and without grids.

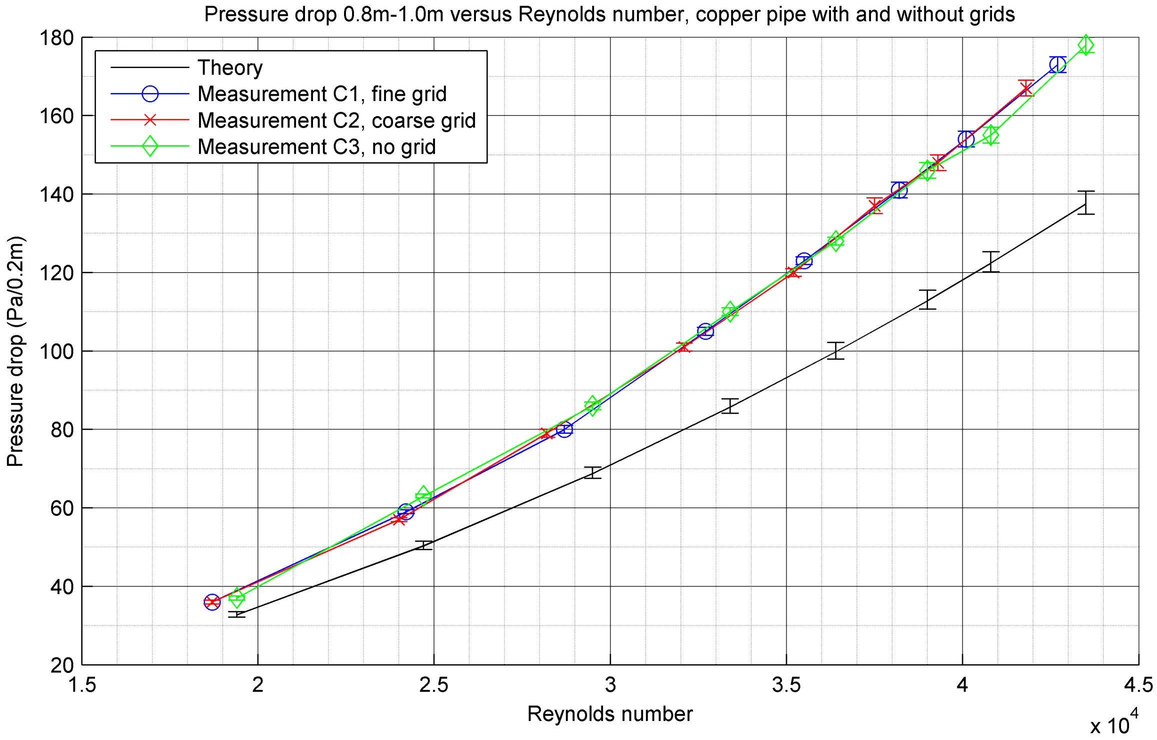

Figure 4.33: Pressure drop from 0.8 m to 1.0 m versus the Reynolds number for the copper pipe with and without grids.

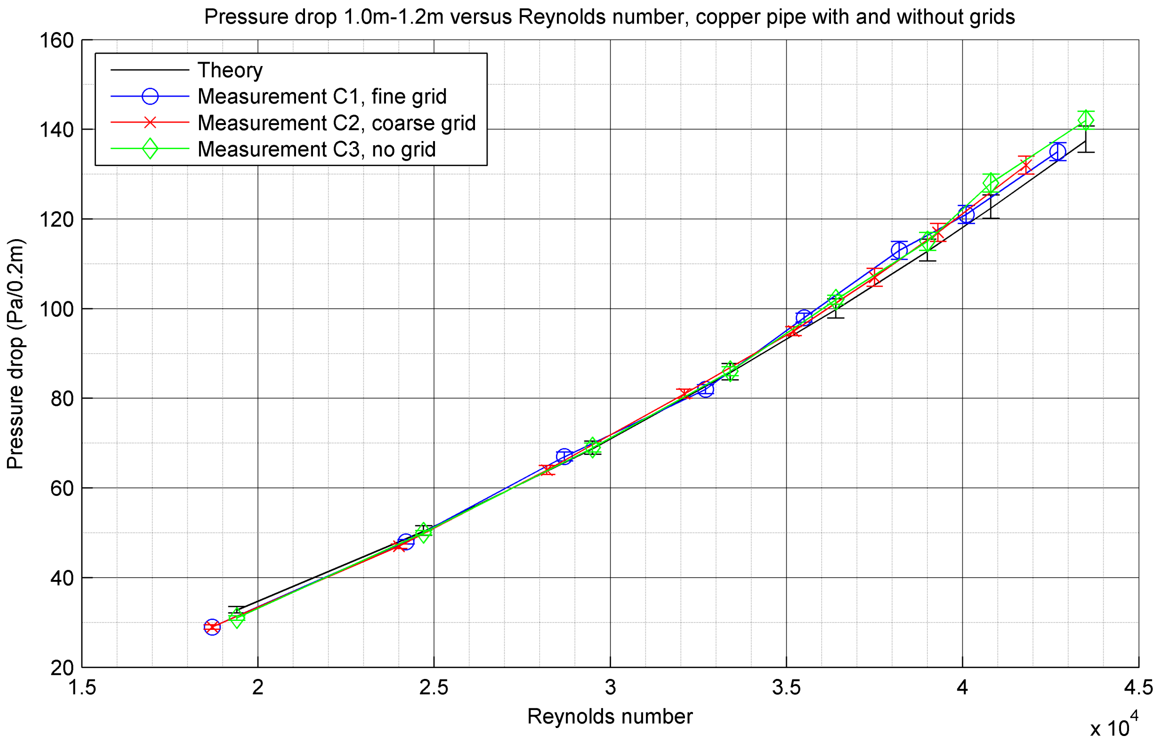

Figure 4.34: Pressure drop from 1.0 m to 1.2 m versus the Reynolds number for the copper pipe with and without grids.

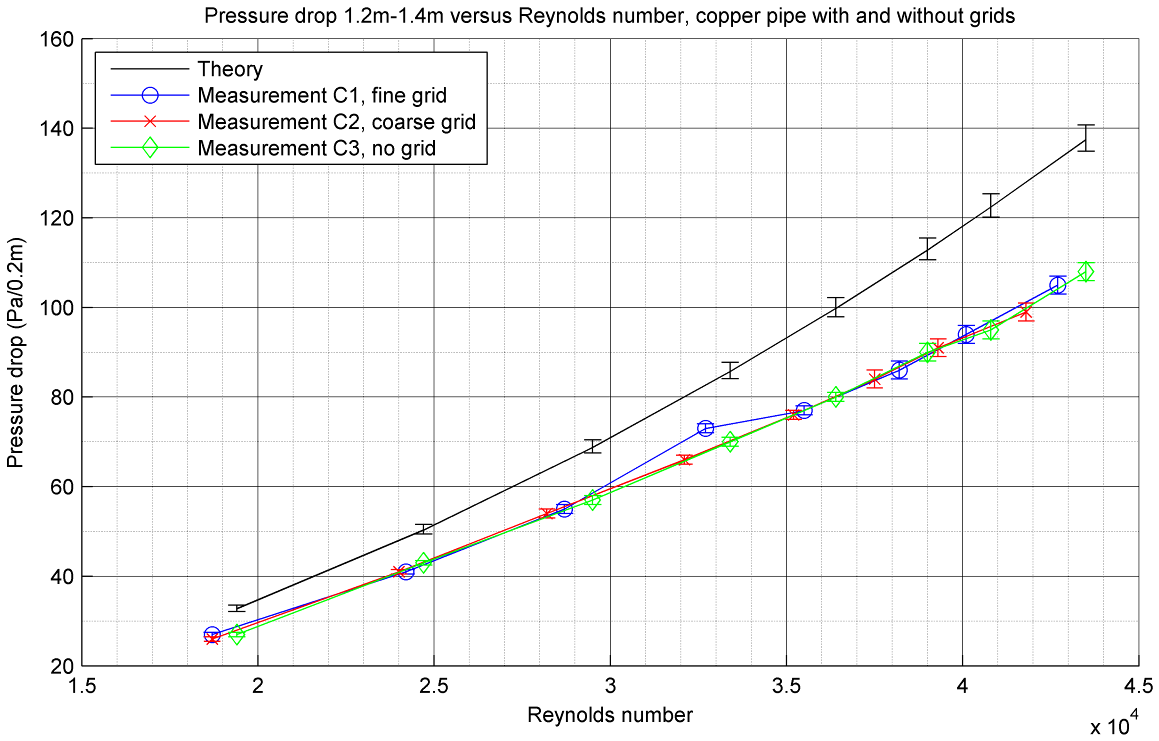

Figure 4.35: Pressure drop from 1.2 m to 1.4 m versus the Reynolds number for the copper pipe with and without grids.

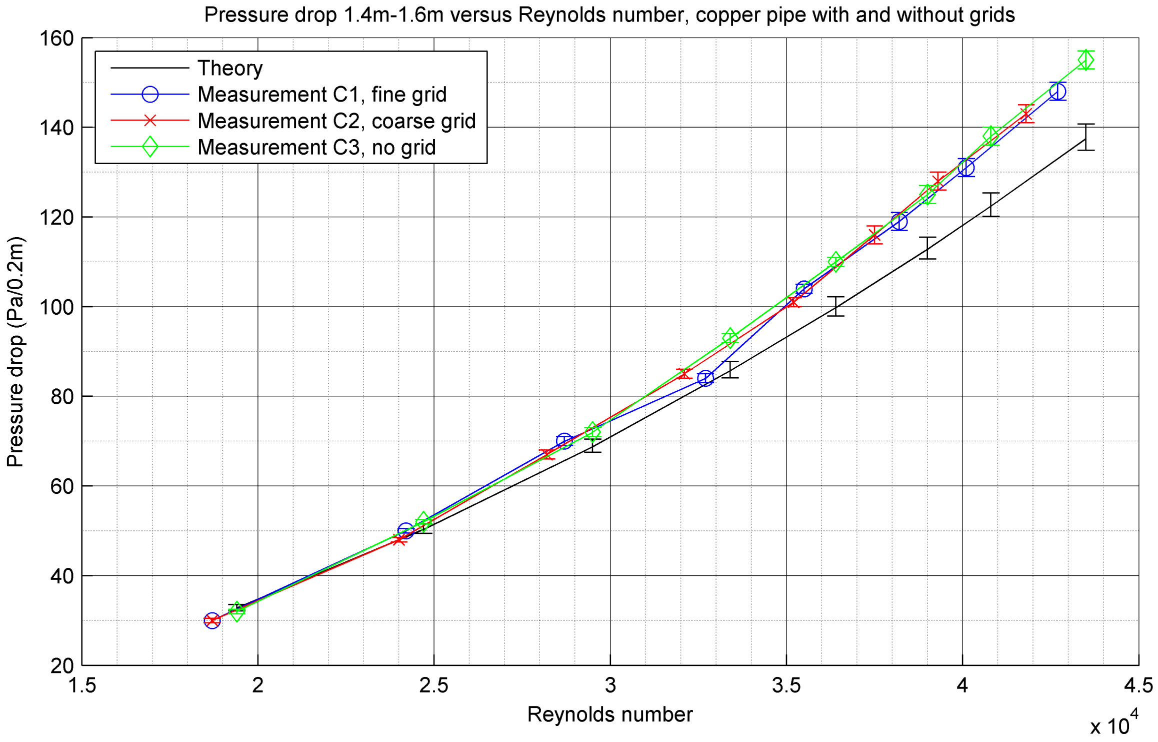

Figure 4.36: Pressure drop from 1.4 m to 1.6 m versus the Reynolds number for the copper pipe with and without grids.

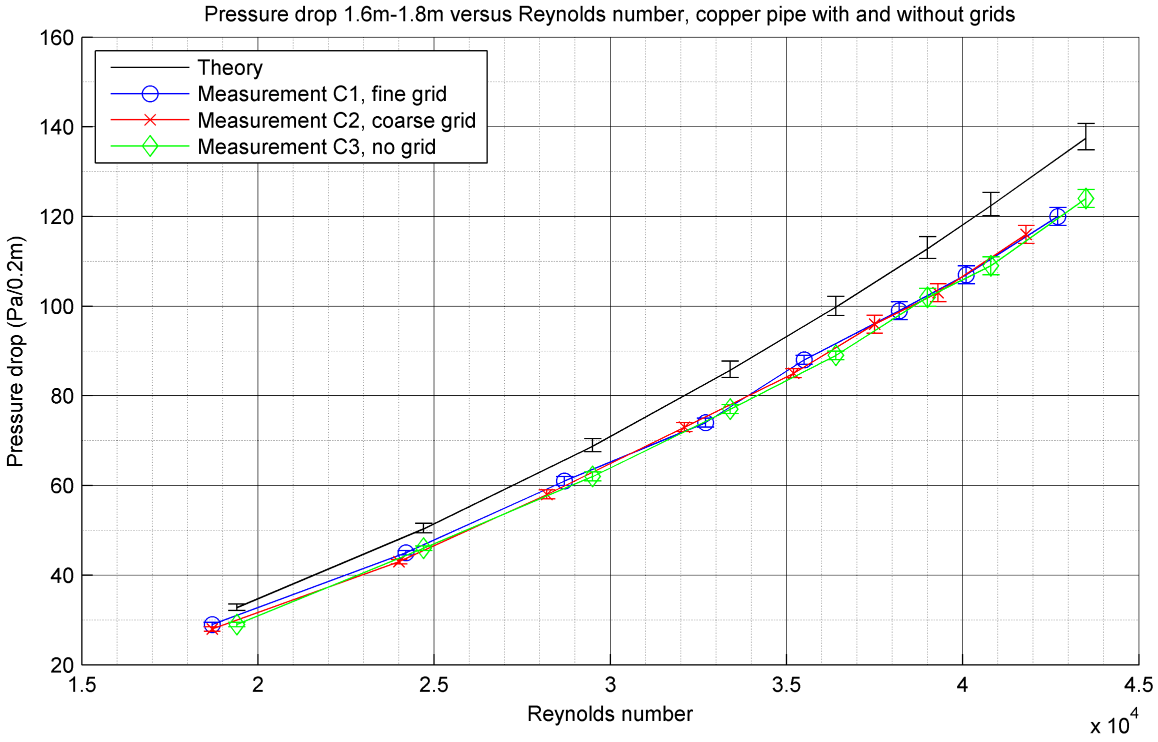

Figure 4.37: Pressure drop from 1.6 m to 1.8 m versus the Reynolds number for the copper pipe with and without grids.

Tube number	1	2	3	4	5
Diameter 1 (mm)	20.02	20.06	20.05	20.07	20.14
Diameter 2 (mm)	20.05	20.0	20.04	19.97	20.13
Tube number	6	7	8	9	10
Diameter 1 (mm)	20.09	20.12	20.04	20.01	20.12
Diameter 2 (mm)	20.05	20.11	20.09	20.04	20.08

Table 4.7: Internal diameter of the copper tube. Diameters 1 and 2 correspond to diameters at both ends of the tubes.

Error source	Parameter	Approximate error
PVC pipe dimension	Variation in diameter	±0.2 mm
	Theoretical pressure drop	Depending on flow rate, ranging from 20 to 90 Pa
	Reynolds number	<1 percent
Copper pipe dimensions	Variation in diameter	+0.076 mm, -0.094 mm
	Theoretical pressure drop	Depending on flow rate, ranging from 3 to 16 Pa/m
	Reynolds number	<1 percent
Pressure taps	Pressure	Unknown
Orifice meter	Internal error	Unknown
	Readout error	± 1 Pa
Manometers	Resolution	± 0.05 Pa
	Readout error	Depending on flow rate, ranging from 0.5 to 10 Pa

Table 4.8: Overview of the possible errors in the experimental set-up. PVC pipe dimensions correspond to experiment A, Copper pipe dimensions correspond to experiment B and C.

4.4 Experiment D, E and F, no injection

The static pressure in the diffusers without air injection was measured at three different Reynolds numbers for all three experiments. The Reynolds numbers (Re_D) are determined at the entry of the diffuser, which has a diameter of $D = 30$ mm. One Reynolds number should be approximately 55000 to be able to compare the measurement to the experiments of Sprenger [8]. The resulting pressure distributions are compared to the theoretical pressure distributions and simulations. Chapter 4.4.1 to 4.4.3 will show the results for the 4, 10 and 20 degree diffusers. The theoretical pressure distribution includes the pressure increase in the diffuser according to Bernoulli's equation and pressure losses due to skin friction, where the pressure is assumed to be atmospheric at the exit of the set-up. Pressure losses due to possible flow separation are not taken into account. The corresponding geometries of the test sections containing the 4, 10 and 20 degree diffuser can be found in Figure 4.38, 4.48 and 4.58. The atmospheric conditions during each measurement can be found in Table 4.9.

Simulations were performed in ANSYS Fluent using a standard $k - \epsilon$ turbulence model with enhanced wall treatment and axisymmetric geometry [20]. In addition, simulations on the 20 degree diffusers at the lowest Reynolds number were also performed using a realisable $k - \epsilon$ model and Reynolds stress model. The reason for this is that the standard $k - \epsilon$ model did not show the same amount of pressure drop as in the measurements. The meshes and resulting pressure and velocity distributions in the diffuser can be found in Chapter 4.4.1 to 4.4.3.

Property	Dynamic viscosity	Specific gas constant	Pressure	Temperature	Density
Symbol	μ	R_s	P	T	ρ
Unit	Pa s	J kg^{-1}K^{-1}	Pa	K	kg m^{-3}
Experiment D 4° NI	$1.79 \cdot 10^{-5}$	287	101200	293.55	1.201
Experiment D 10° NI	$1.79 \cdot 10^{-5}$	287	101900	293.25	1.211
Experiment E 4° NI	$1.79 \cdot 10^{-5}$	287	102200	293.25	1.214
Experiment E 10° NI	$1.79 \cdot 10^{-5}$	287	101900	293.85	1.208
Experiment F 4° NI	$1.79 \cdot 10^{-5}$	287	102200	293.25	1.214
Experiment F 10° NI	$1.79 \cdot 10^{-5}$	287	101100	293.25	1.201
Experiment F 20° NI	$1.79 \cdot 10^{-5}$	287	100500	293.55	1.193

Table 4.9: Atmospheric conditions during experiment D, E and F without air injection (denoted by NI).

4.4.1 4 Degree diffuser

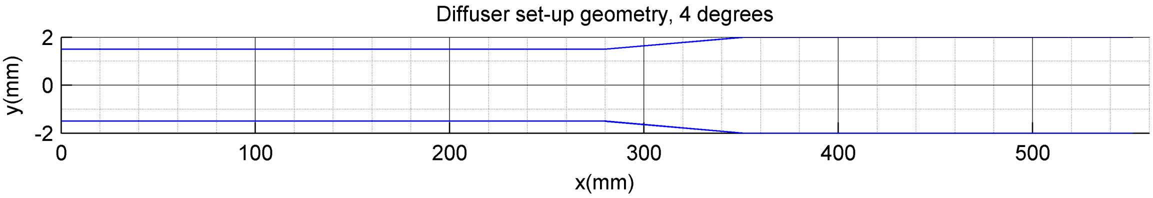

Figure 4.38: Geometry of the test section with the 4 degree diffuser.

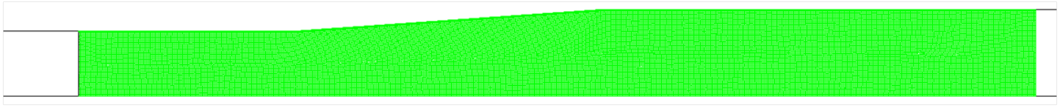

Figure 4.39: Mesh for the simulation of the 4 degree diffuser.

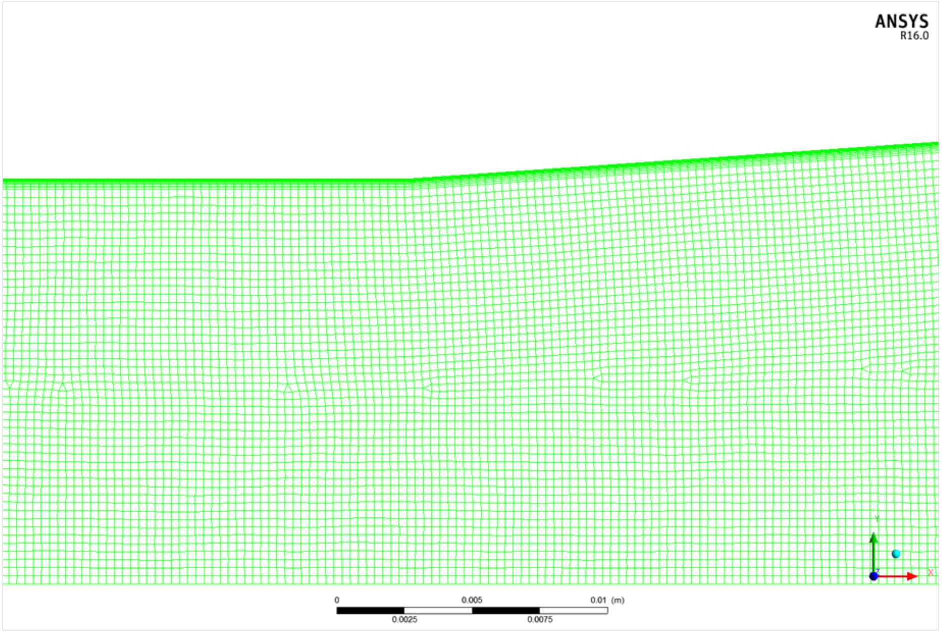

Figure 4.40: Mesh for the simulation of the 4 degree diffuser, zoomed in around the diffuser entry.

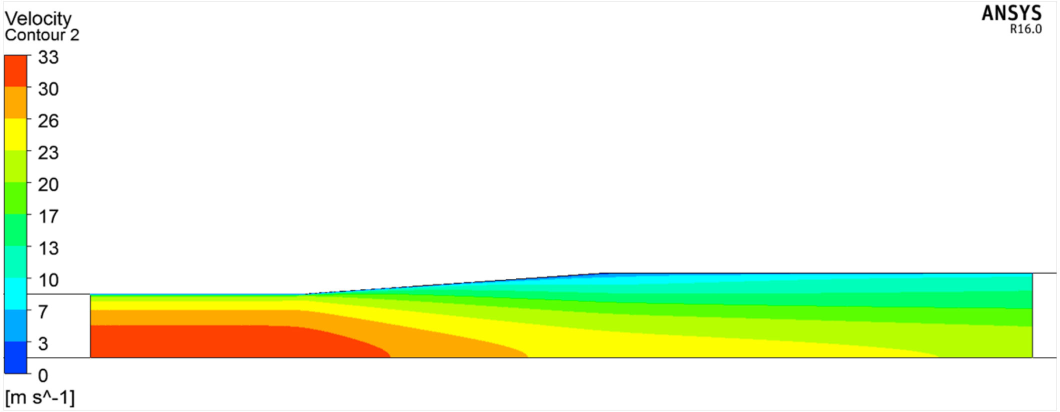

Figure 4.41: Velocity distribution in the 4 degree diffuser, Re_D = 52980.

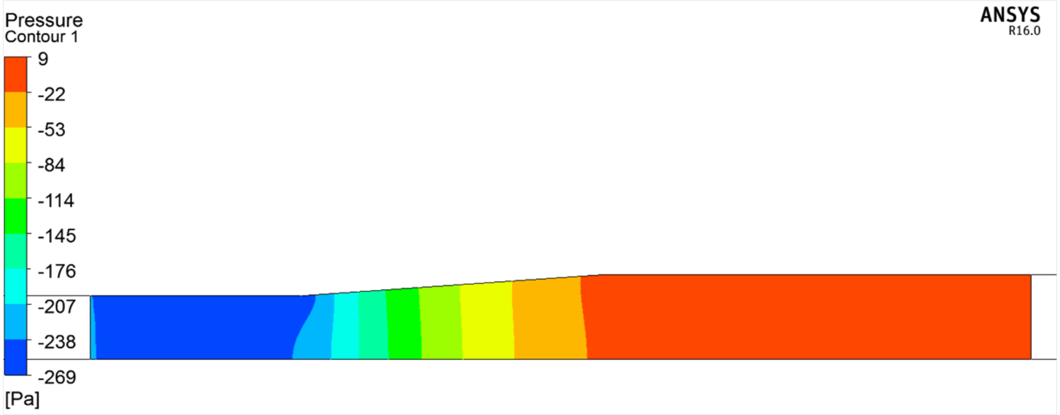

Figure 4.42: Static pressure distribution in the 4 degree diffuser, Re_D = 52980.

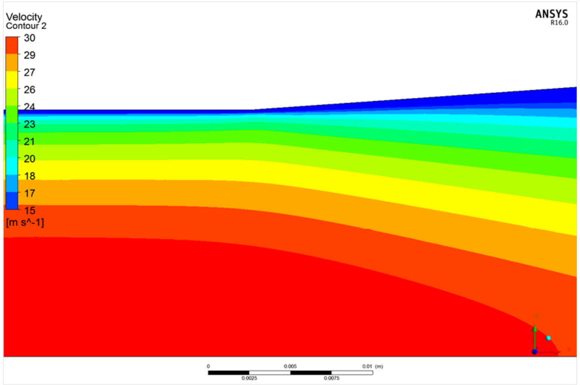

Figure 4.43: Velocity distribution in the 4 degree diffuser, zoomed in around the diffuser entry, Re_D = 52980.

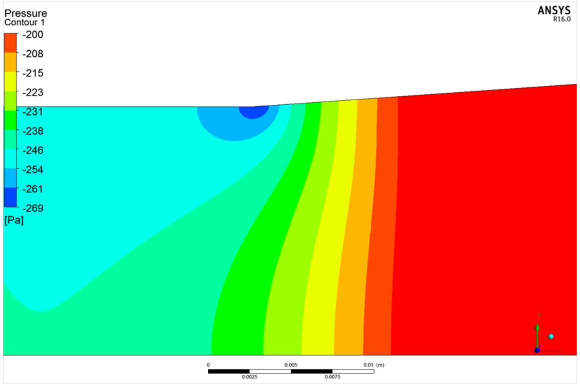

Figure 4.44: Static pressure distribution in the 4 degree diffuser, zoomed in around the diffuser entry, Re_D = 52980.

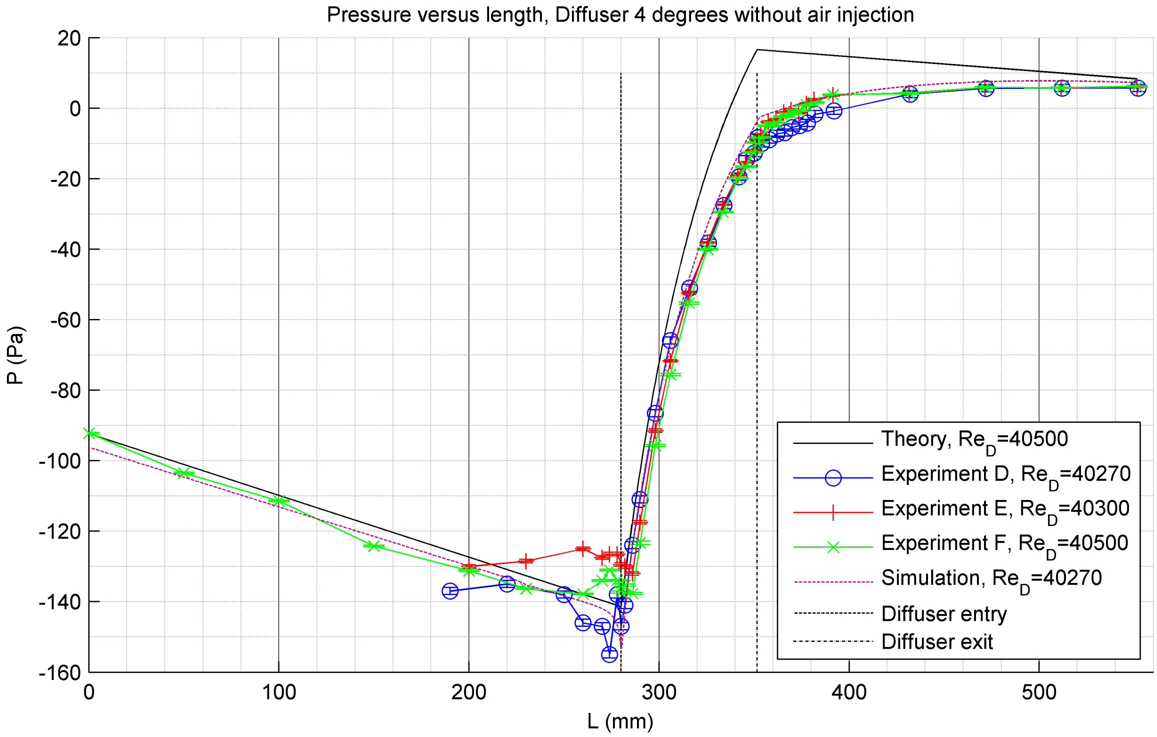

Figure 4.45: Static pressure versus length, 4 degree diffuser. Re_D corresponds to the Reynolds number at the diffuser entry.

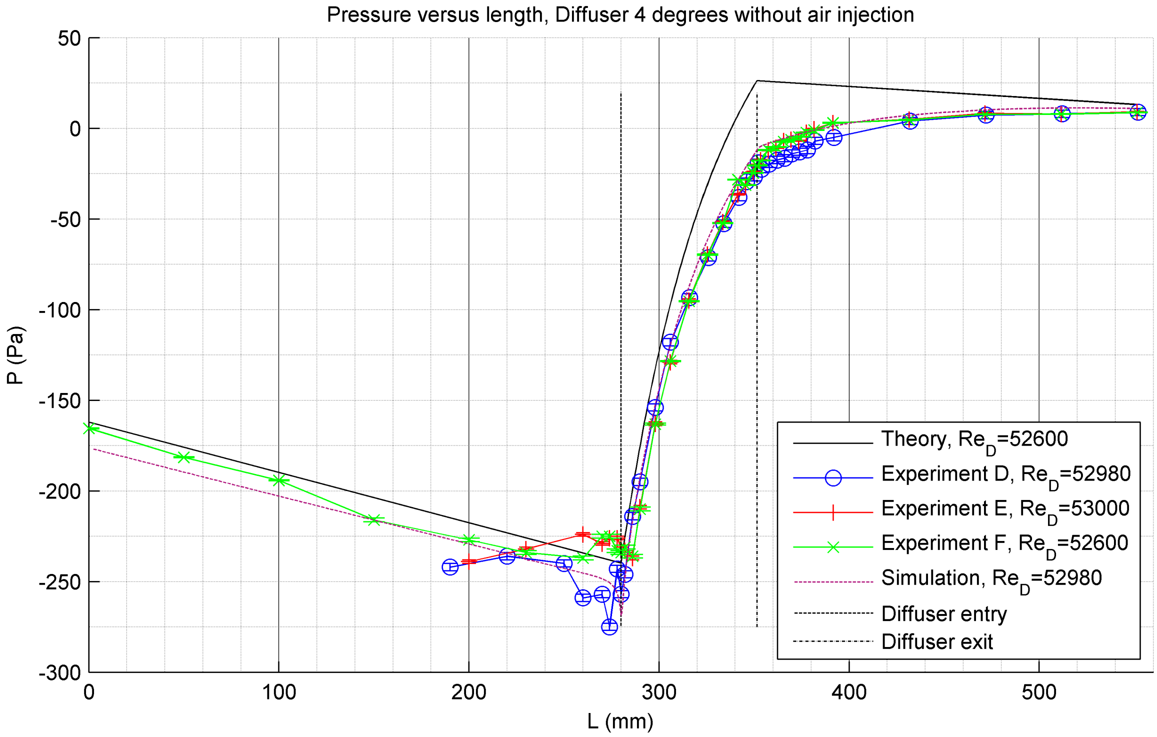

Figure 4.46: Static pressure versus length, 4 degree diffuser. Re_D corresponds to the Reynolds number at the diffuser entry.

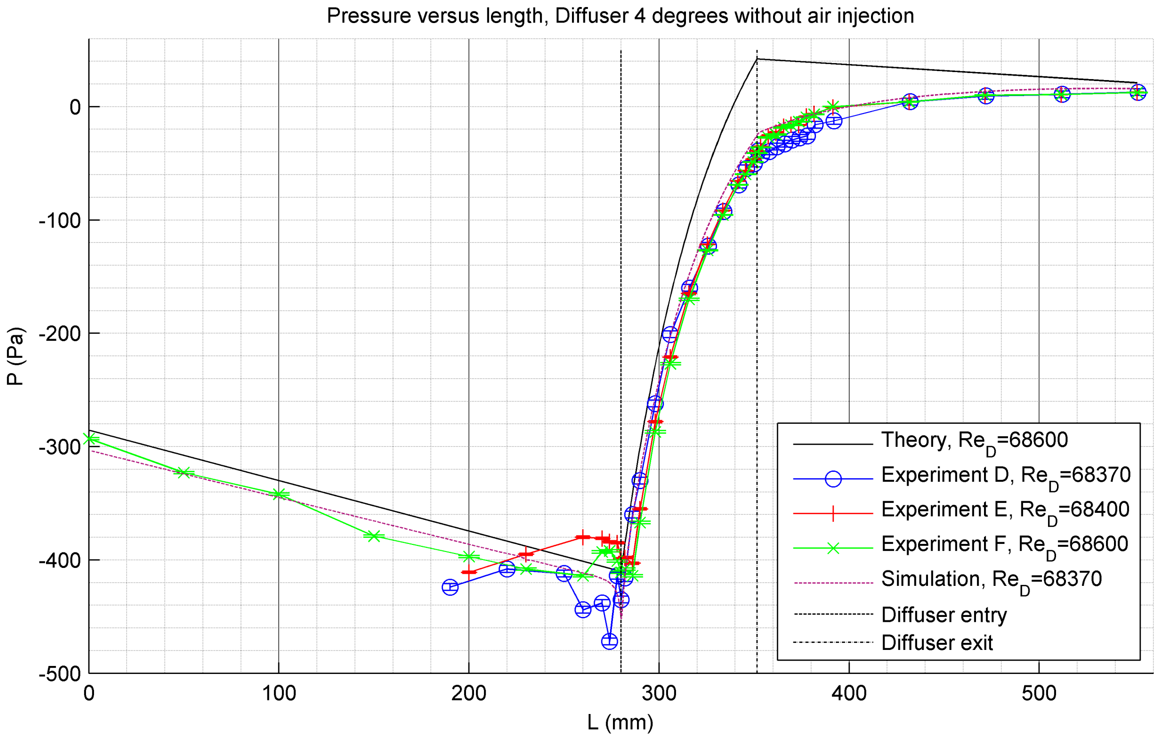

Figure 4.47: Static pressure versus length, 4 degree diffuser. Re_D corresponds to the Reynolds number at the diffuser entry.

4.4.2 10 Degree diffuser

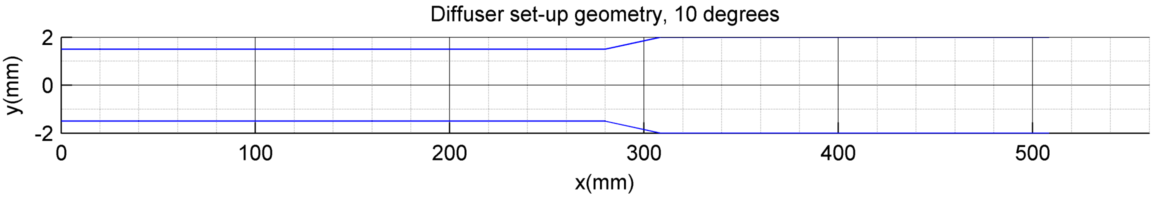

Figure 4.48: Geometry of the test section with the 10 degree diffuser.

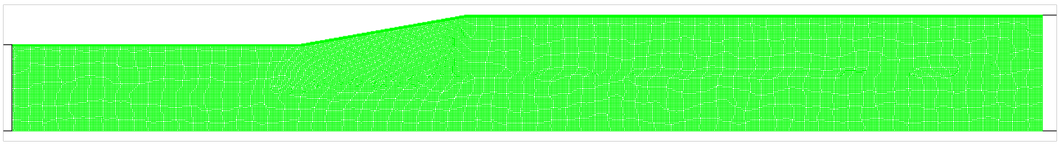

Figure 4.49: Mesh for the simulation of the 10 degree diffuser.

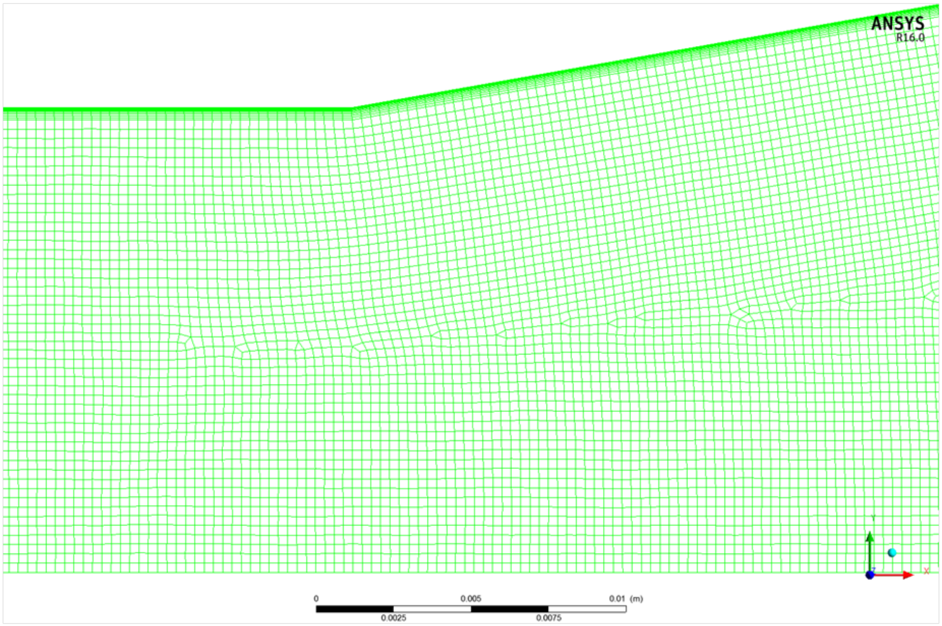

Figure 4.50: Mesh for the simulation of the 10 degree diffuser, zoomed in around the diffuser entry.

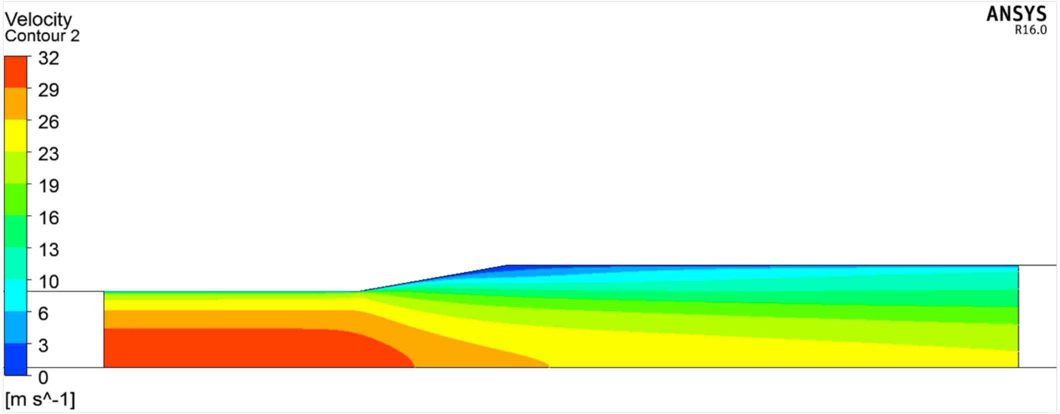

Figure 4.51: Velocity distribution in the 10 degree diffuser, Re_D = 52230.

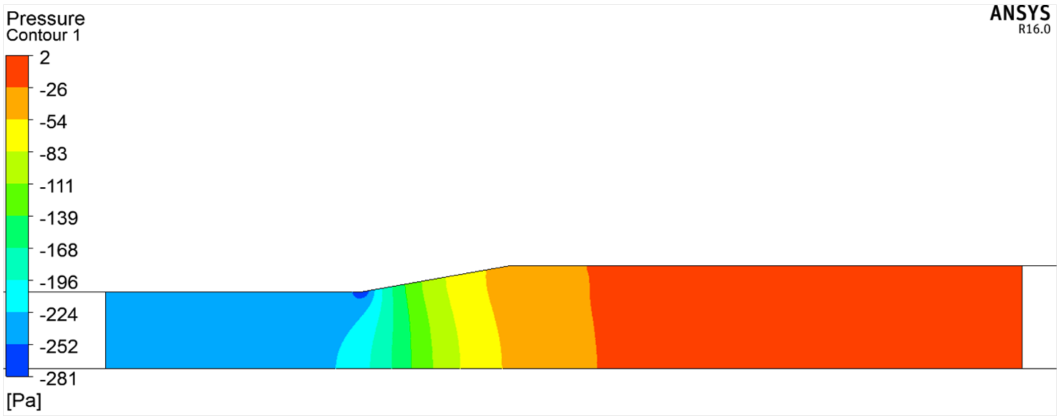

Figure 4.52: Static pressure distribution in the 10 degree diffuser, Re_D = 52230.

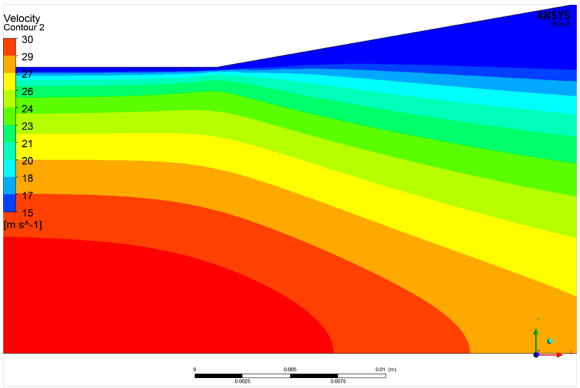

Figure 4.53: Velocity distribution in the 10 degree diffuser, zoomed in around the diffuser entry, Re_D = 52230.

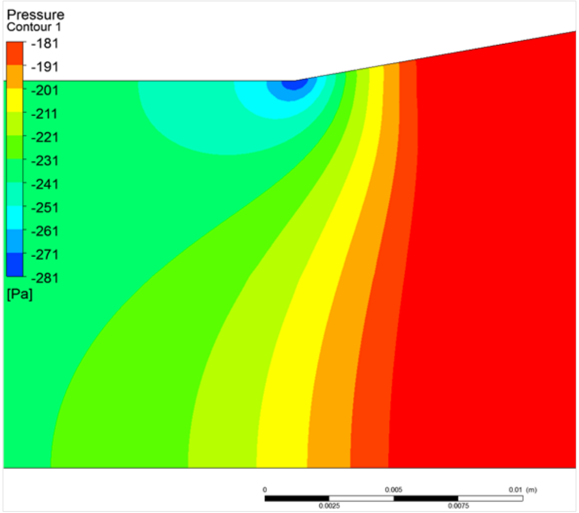

Figure 4.54: Static pressure distribution in the 10 degree diffuser, zoomed in around the diffuser entry, Re_D = 52230.

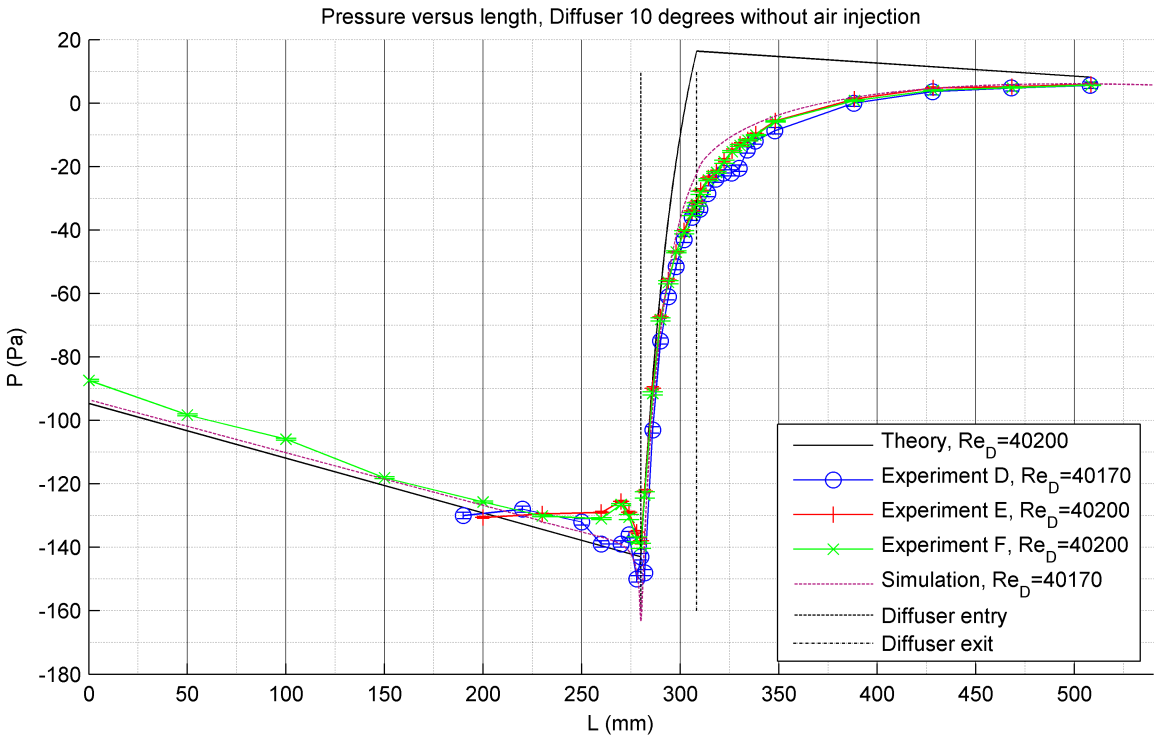

Figure 4.55: Static pressure versus length, 10 degree diffuser. Re_D corresponds to the Reynolds number at the diffuser entry.

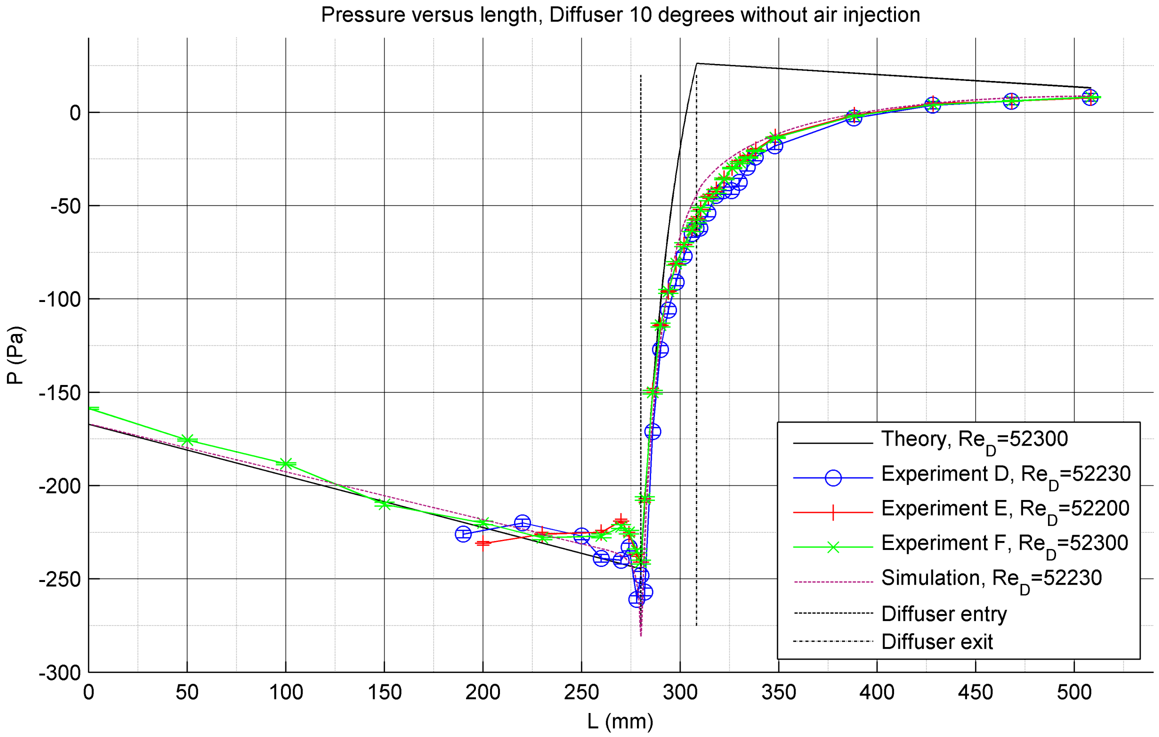

Figure 4.56: Static pressure versus length, 10 degree diffuser. Re_D corresponds to the Reynolds number at the diffuser entry.

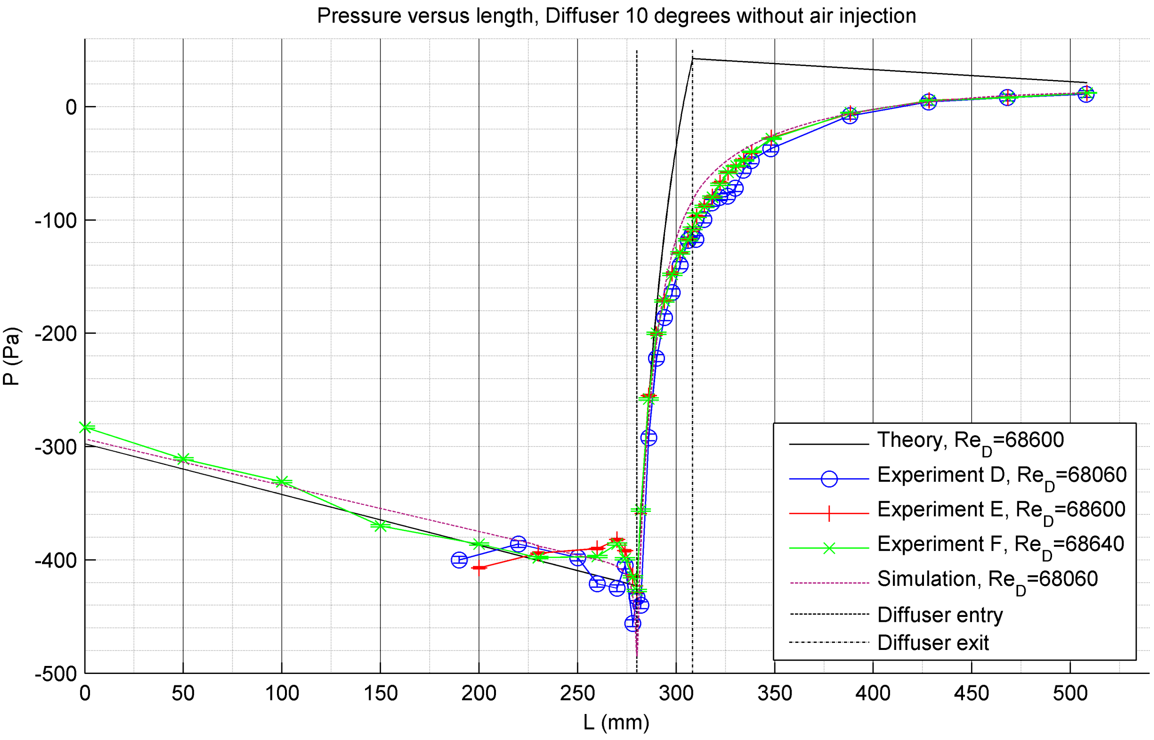

Figure 4.57: Static pressure versus length, 10 degree diffuser. Re_D corresponds to the Reynolds number at the diffuser entry.

4.4.3 20 Degree diffuser

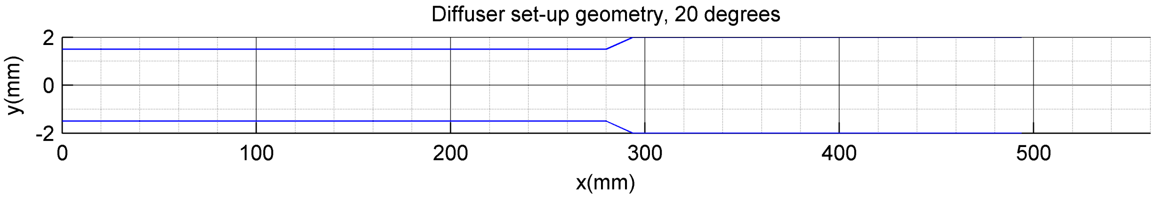

Figure 4.58: Geometry of the test section with the 20 degree diffuser.

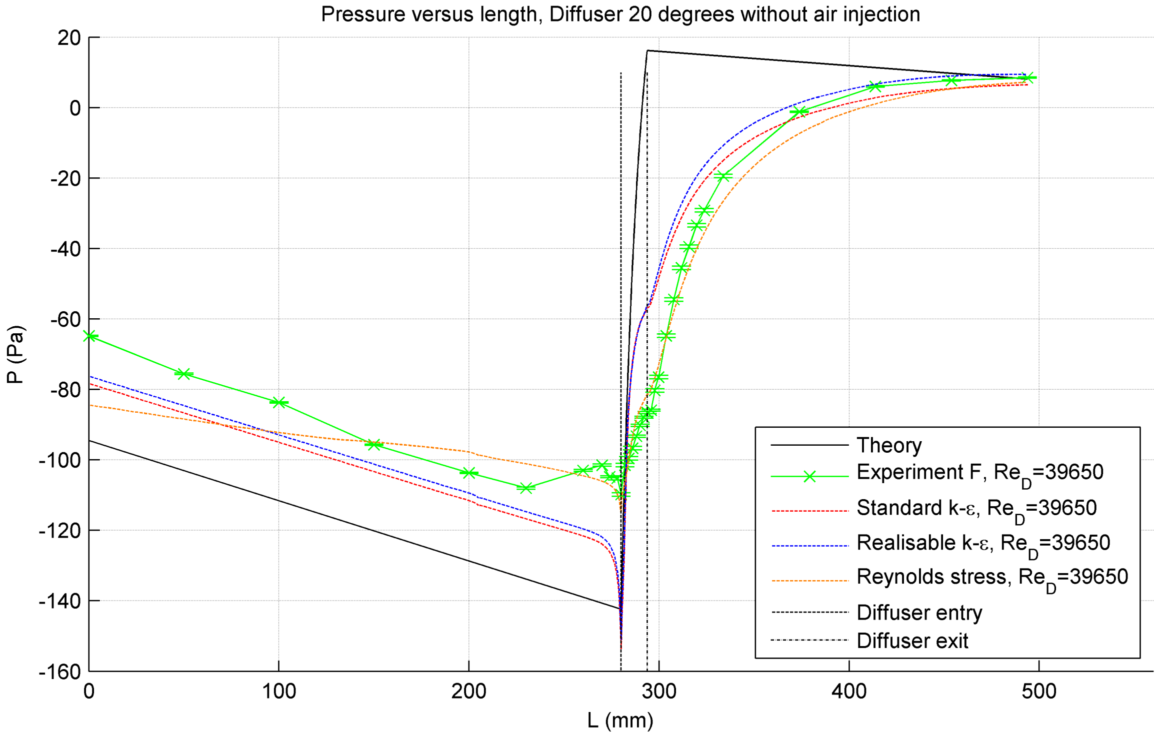

Figure 4.59: Static pressure versus length, 20 degree diffuser. Re$_D$ corresponds to the Reynolds number at the diffuser entry.

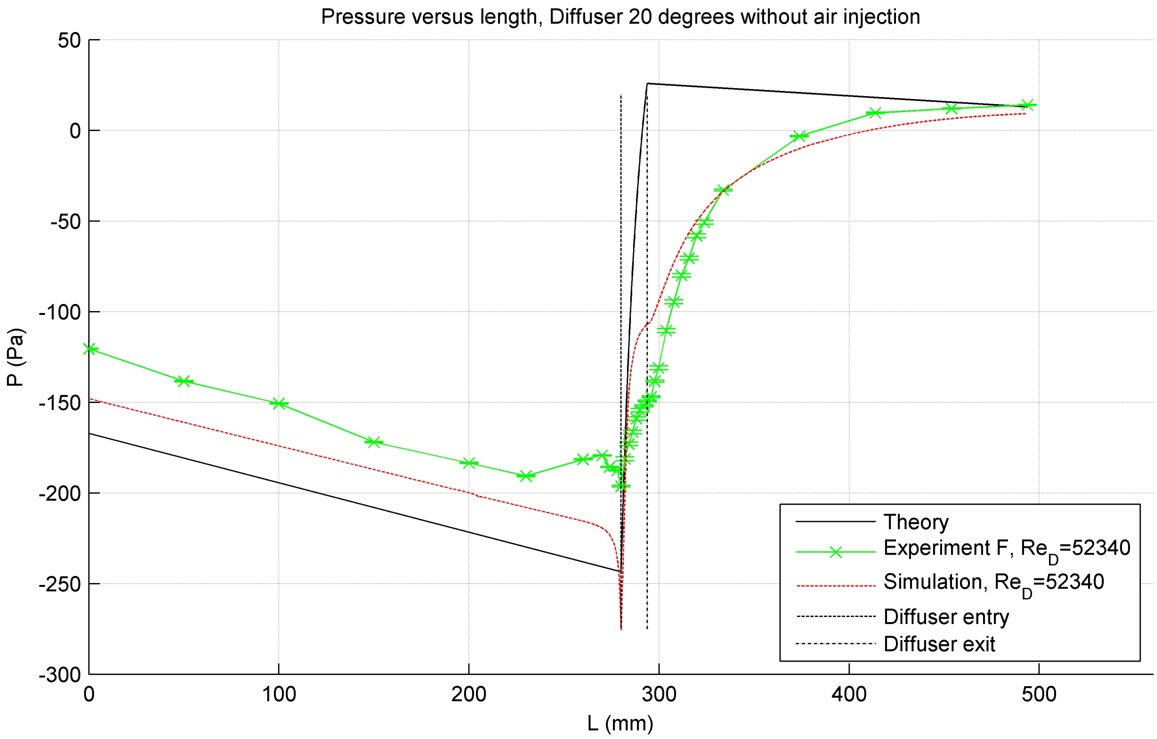

Figure 4.60: Static pressure versus length, 20 degree diffuser. Re_D corresponds to the Reynolds number at the diffuser entry.

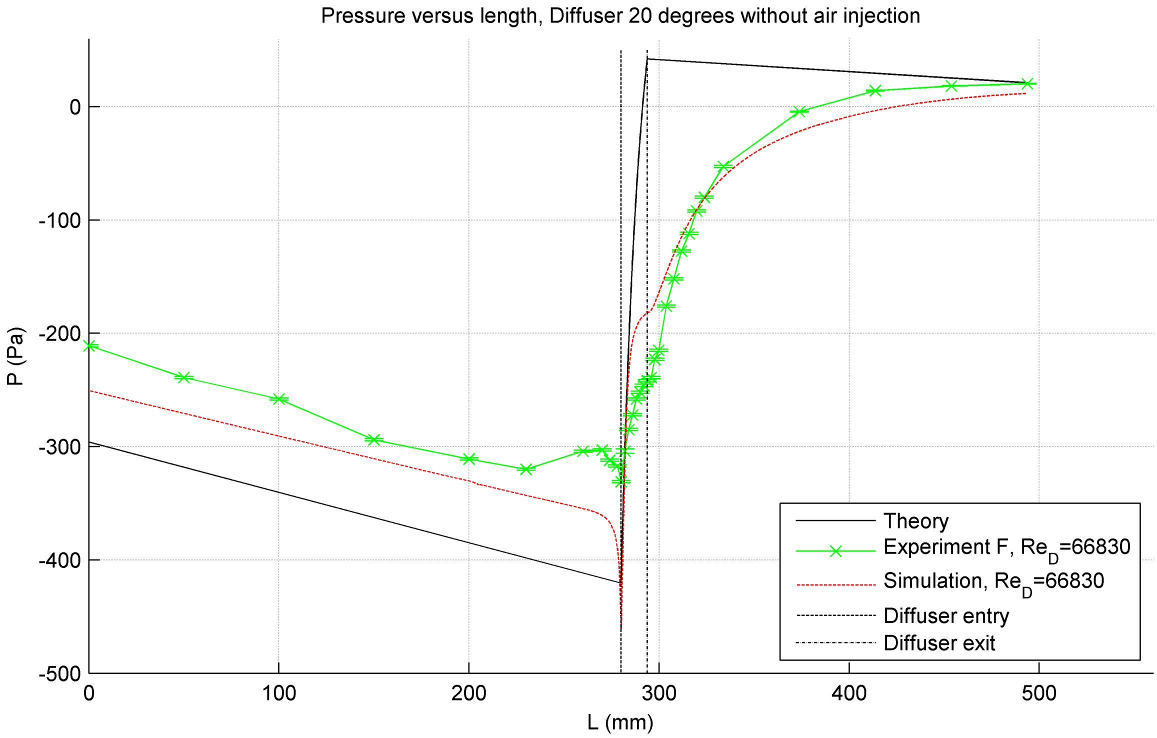

Figure 4.61: Static pressure versus length, 20 degree diffuser. Re_D corresponds to the Reynolds number at the diffuser entry.

4.4.4 Discussion

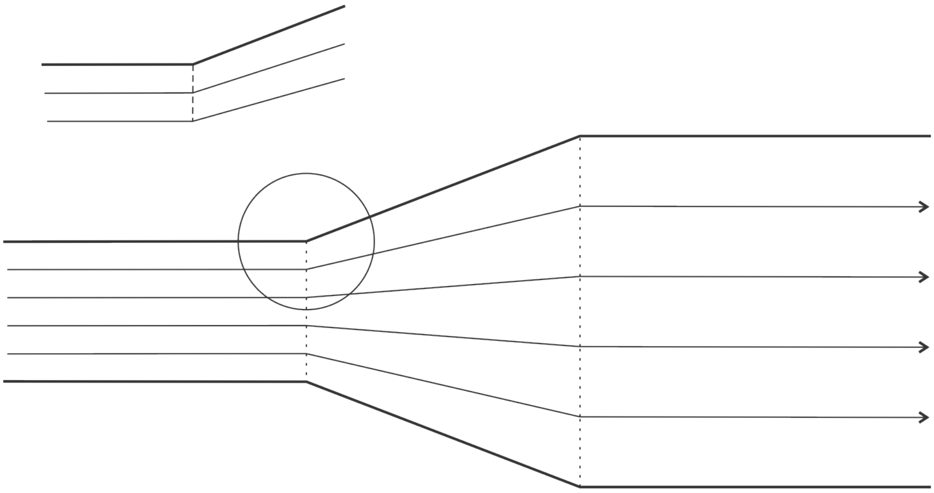

Figure 4.62: Streamlines in a diffuser without viscous effects.

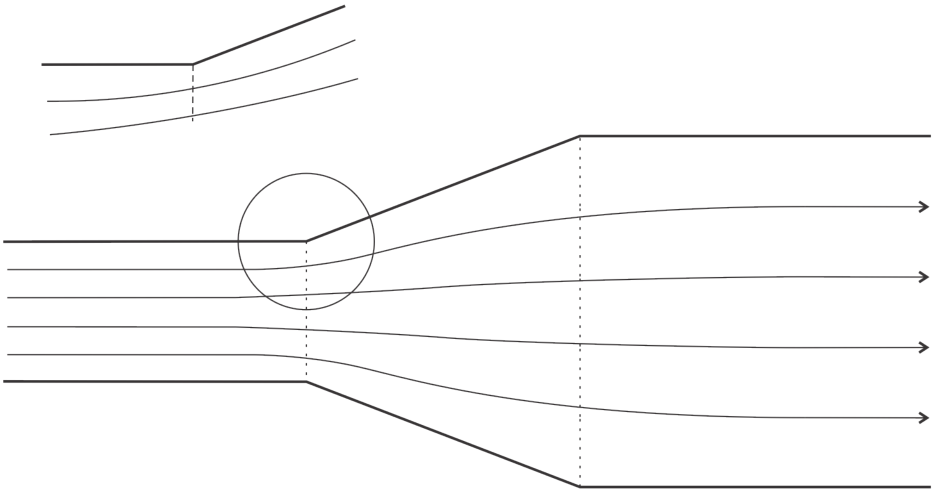

Figure 4.63: Streamlines in a diffuser with viscous effects.

Figure 4.45 to 4.57 show good similarity between the measured pressure and the simulations. A few mm before the flow enters the diffuser there is a decrease in pressure (Figure 4.64). This effect is noticed by simulations and measurements, but not by theory. The reason for this can be explained by looking at Figure 4.62 and 4.63. The theoretical pressure increase in the diffuser according to Bernoulli and the continuity equation is an ideal case where viscosity is neglected. The angle in the streamlines at the diffuser entry and exit is sharp. However, in reality the streamlines are more smooth due to viscous effects. When the flow passes a sharp edge the streamlines will lie closer together close to the corner to overcome the sudden increase in pressure the corner induces. This means the pressure will decrease locally around the entry before it increases in the diffuser itself. This effect can also be noticed in Figure 4.43, 4.44, 4.53 and 4.54.

The pressure increase in the diffuser itself is also different in theory than it is in measurements and simulations. The reason for this behavior can be explained by looking at the velocity profiles along the cross-section of the diffuser (Figure 4.41 and 4.51). When the flow enters the diffuser the bulk flow wants to follow a straight path and does not evenly spread in the diffuser. This will cause the velocity to be lower at the wall of the diffuser than it would be in the ideal case where the velocity profile across the diffuser is fully developed. It will take a certain length of pipe for the velocity profile to be fully developed again. This effect becomes easier to notice when the diverging angle of the diffuser becomes larger, as can be seen in the resulting pressure distribution for the 4, 10 and 20 degree diffuser.

The pressure drop in the 20 degree diffuser shows larger values for the pressure drop in experiment than the theory and simulations predicted. This is due to the presence of flow separation. The realisable $k - \epsilon$ shows slightly more pressure drop than the standard $k - \epsilon$ model. The Reynolds stress model shows even more pressure drop. However, the pressure distribution in the tube before the diffuser entry deviates from the theoretical and measured pressure distribution.

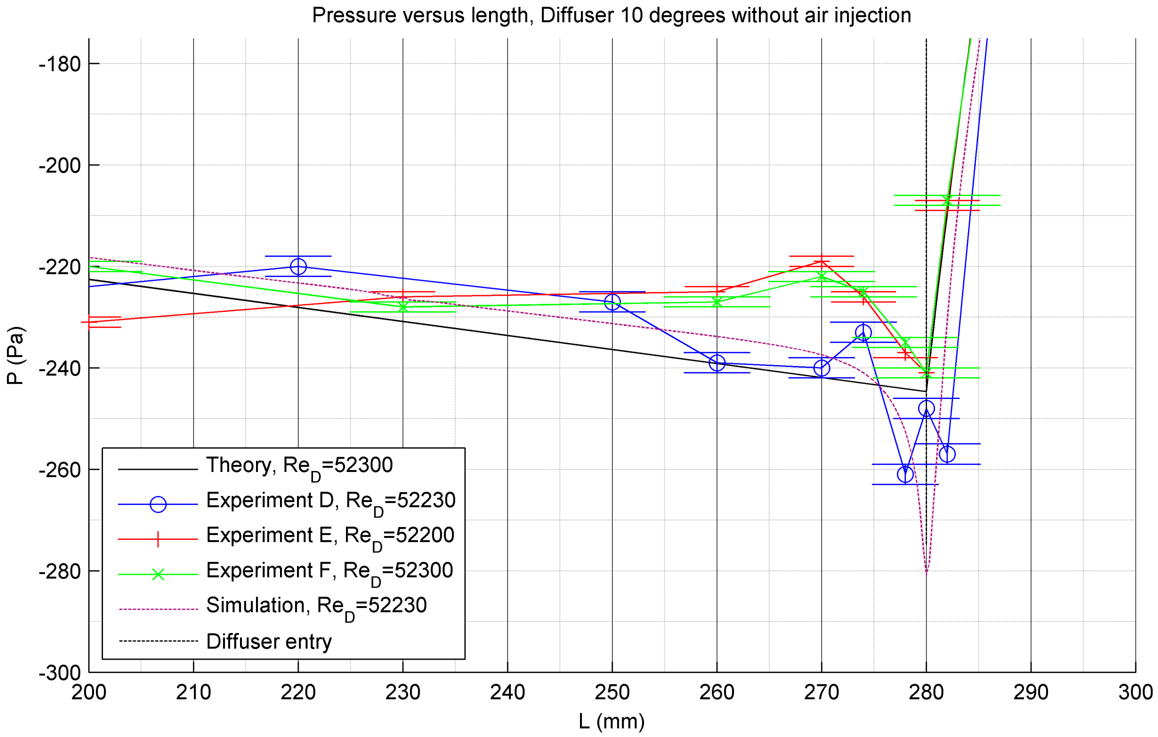

Figure 4.64: Pressure versus length, 10 degree diffuser zoomed in around the entry of the diffuser. Re_D corresponds to the Reynolds number at the diffuser entry.

Experiment E and F showed a slight increase in pressure upstream of the diffuser entry before the drop in pressure at the diffuser entry (Figure 4.64). This was not the case for experiment D. The reason for this behavior is probably due to slight differences in the geometry of both diffusers. Measurements with a caliper showed that the diameter of the entry tube was approximately 29.7 mm, whereas the diameter of the diffuser entry of Experiment E and F was approximately 30.0 mm. The transition from pipe to diffuser is located at a distance of 255 mm. This transition in diameters explains the slight increase in pressure. This also means that the pressure from 0 mm to 230 mm in the plots of the pressure in the 4, 10 and 20 degree diffuser will be slightly higher if the entry tube has a diameter of exactly 30 mm. This also means the difference between the simulations and measurements will be slightly higher. The extra amount of pressure loss can be accredited to the fact that the inside of the diffuser is not smooth. The extra amount of roughness height ϵ will result in more pressure loss due to skin friction.

To compare the results of the 4 degree diffuser with the diffuser from the experiments of Sprenger [8] and the 10 degree diffuser, the pressure and position in the diffuser can be written in a dimensionless form as described in Chapter 2.2. The position in the diffuser can be written in dimensionless form by dividing the diffuser diameter at location x by the diffuser diameter at the entry (D_x/D_E). Figure 4.65 shows a plot of the dimensionless pressure versus the dimensionless position in the diffuser. P_E is measured at the pressure tap at L = 274 mm (6 mm before the diffuser entry) for experiment E and F (Figure 4.46). The entry pressure for Experiment D is hard to determine since there are a lot of fluctuations around the entry. It is taken at L = 278 mm, so 2 mm before the diffuser entry.

There are large differences between the measured values for the pressure and data obtained from the experiments of Sprenger [8] (4 degree conical diffuser). The experiments from Sprenger showed that the pressure remained rather constant at the entry of the diffuser, after which it experienced a rapid increase and finally approached the theoretical value. This effect is the strongest for low Reynolds numbers. At higher Reynolds numbers, of which the data is not included in Figure 4.65, the pressure distribution in the diffuser was almost similar to the theoretical value. A cause for the difference between Experiment D, E and F may be that the diffuser used in the experiments of Sprenger has a sharper edge at the diffuser entry, which will more likely result in flow separation at the entry. If the flow separates at the entry the pressure remains constant until the flow re-attaches at a certain point. If the Reynolds number is increased, the distance needed for the flow to re-attach will be less, which can be observed in Figure 4.65. Both the experimental results and the data from Sprenger showed a slight peak in underpressure at the entry of the diffuser.

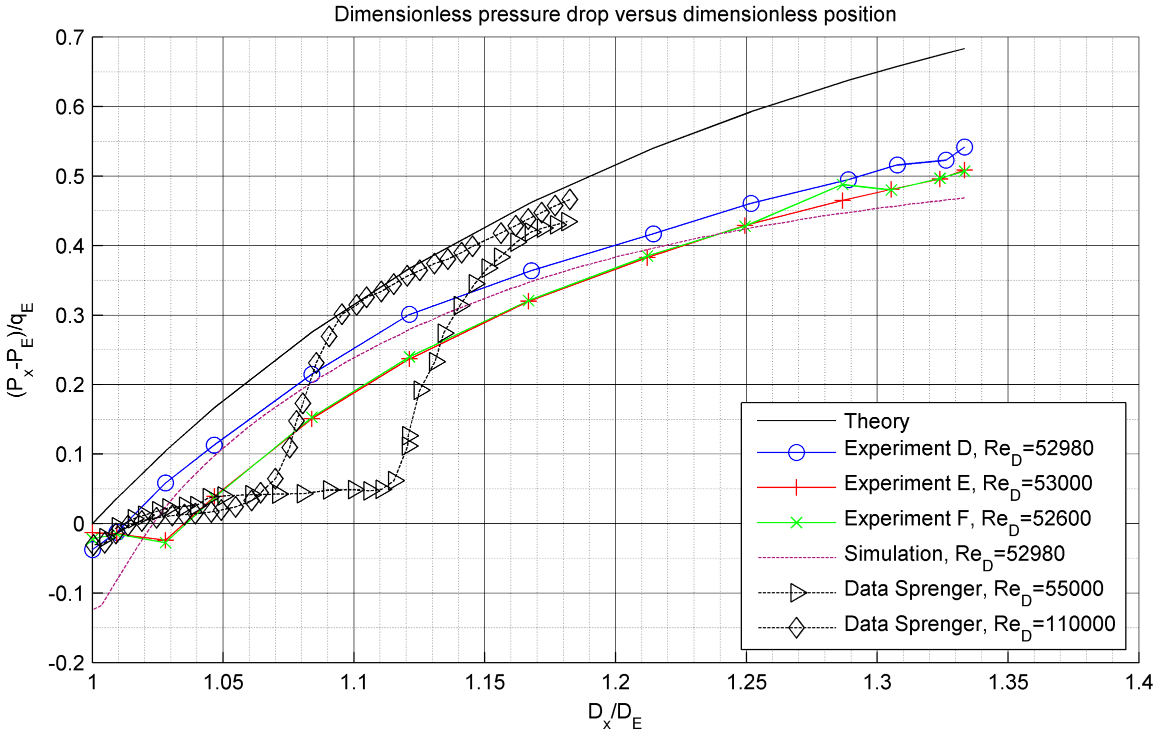

Figure 4.65: Dimensionless pressure versus dimensionless position for the 4 degree diffuser.

4.4.5 Pressure loss

The pressure loss in each diffuser can't be determined straightforwardly by substracting the pressure at the diffuser exit from the pressure at the diffuser entry. The static pressure experiences a decrease around the diffuser entry. At the exit of the diffuser, the static pressure at the wall is not yet fully recovered. Instead, the pressure at the first pressure tap (located 280 mm upstream of the diffuser entry) and at the exit of the set-up (300 mm downstream of the diffuser exit) are used. The pressure at the exit is equal to the atmospheric pressure. The difference between these two pressures, with the substraction of the amount of pressure loss in the sections of entry and exit pipe will be compared with the theoretical pressure increase according to Bernoulli. The pressure loss in the entry and exit pipe is calculated from the Darcy-Weisbach equation (Equation 2.12). An overview of the amount of pressure loss for the diffusers in Experiment F can be found in Table 4.10 to 4.12. It shows that the amount of pressure loss increases as the diverging angle increases.

Re_D	P_1 (Pa)	Pressure loss (Pa)		Theoretical pressure rise (Pa)	Net diffuser Pressure loss (Pa)
		Entry pipe	Exit pipe		
40490	-92.2	49.0	13.3	164.3	9.8
52560	-165.5	77.9	21.1	276.8	12.3
68590	-293	125.4	33.8	471.5	19.2

Table 4.10: Pressure losses in the 4 degree diffuser for different Reynolds numbers. Re_D is determined at the diffuser entry. P_1 is the pressure at the first pressure tap.

Re_D	P_1 (Pa)	Pressure loss (Pa)		Theoretical pressure rise (Pa)	Net diffuser Pressure loss (Pa)
		Entry pipe	Exit pipe		
40010	-87.4	48.5	13.2	162.1	13.1
52130	-158.7	77.6	21.0	275.3	17.9
68410	-283	126.1	34.0	474.0	30.9

Table 4.11: Pressure losses in the 10 degree diffuser for different Reynolds numbers. Re_D is determined at the diffuser entry. P_1 is the pressure at the first pressure tap.

Re_D	P_1 (Pa)	Pressure loss (Pa)		Theoretical pressure rise (Pa)	Net diffuser Pressure loss (Pa)
		Entry pipe	Exit pipe		
39650	-64.8	48.1	13.0	160.4	34.5
52340	-120.5	78.7	21.3	279.4	58.9
66830	-211	121.8	32.9	455.6	89.9

Table 4.12: Pressure losses in the 20 degree diffuser for different Reynolds numbers. Re_D is determined at the diffuser entry. P_1 is the pressure at the first pressure tap.

4.5 Experiment E and F, injection

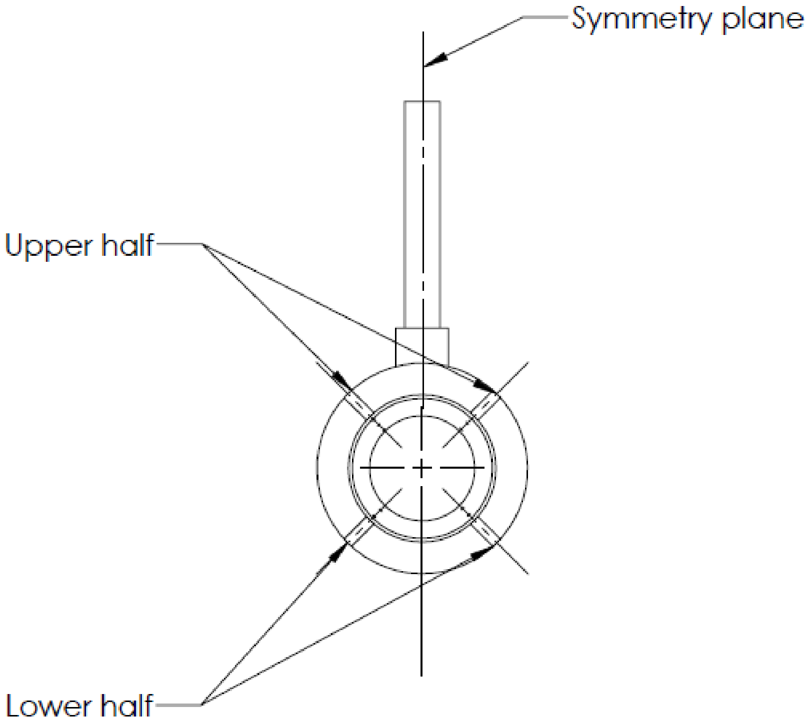

Figure 4.66: Cross-section of the diffuser set-up with gas injection including the symmetry plane and pressure tap locations on the upper and lower half of the diffuser.

The static pressure in the diffusers with air injection was measured at approximately the same Reynolds numbers as in the measurements in Chapter 4.4. Chapter 4.5.1 to 4.5.3 show the measured static pressure distribution for the 4, 10 and 20 degree diffusers. Simulations were performed for the 4 degree diffuser at the highest Reynolds number. Since the pressure distribution is not uniform along the cross-section of the diffusers due to the injection of air, the plots show the pressure measured at the pressure taps on the upper and lower half of the diffuser (Figure 4.66). The flow should by symmetric about the symmetry plane shown in Figure 4.66. The atmospheric conditions during each measurement can be found in Table 4.13. Simulations were performed in ANSYS Fluent using a default $k-\epsilon$ model with resolved wall functions [21].

Property	Dynamic viscosity	Specific gas constant	Pressure	Temperature	Density
Symbol	μ	R_s	P	T	ρ
Unit	Pa s	J kg^{-1}K^{-1}	Pa	K	kg m^{-3}
Experiment E 4° I	$1.79 \cdot 10^{-5}$	287	102200	293.25	1.214
Experiment E 10° I	$1.79 \cdot 10^{-5}$	287	101900	293.85	1.208
Experiment F 4° I	$1.79 \cdot 10^{-5}$	287	101600	292.75	1.209
Experiment F 10° I	$1.79 \cdot 10^{-5}$	287	101100	293.25	1.201
Experiment F 20° I	$1.79 \cdot 10^{-5}$	287	100500	292.95	1.195

Table 4.13: Atmospheric conditions during experiment E and F with air injection (denoted by I).

4.5.1 4 degree diffuser

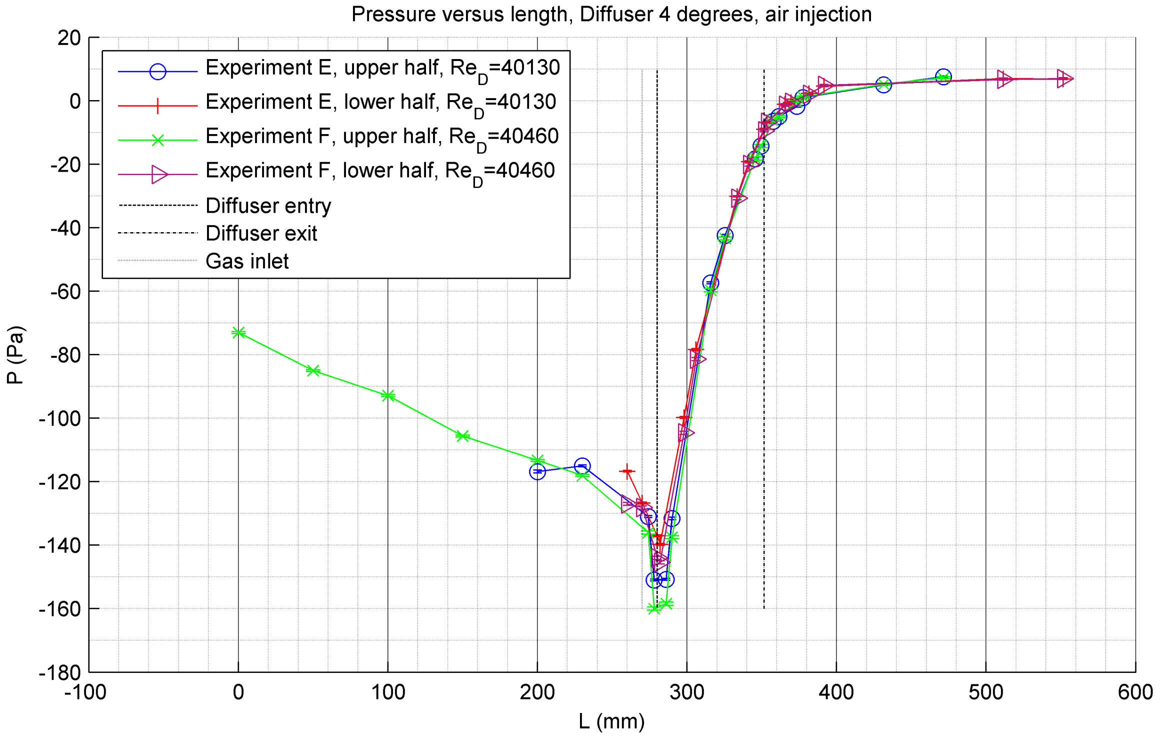

Figure 4.67: Pressure versus length, 4 degree diffuser with gas injection. Re$_D$ corresponds to the Reynolds number before the gas inlet.

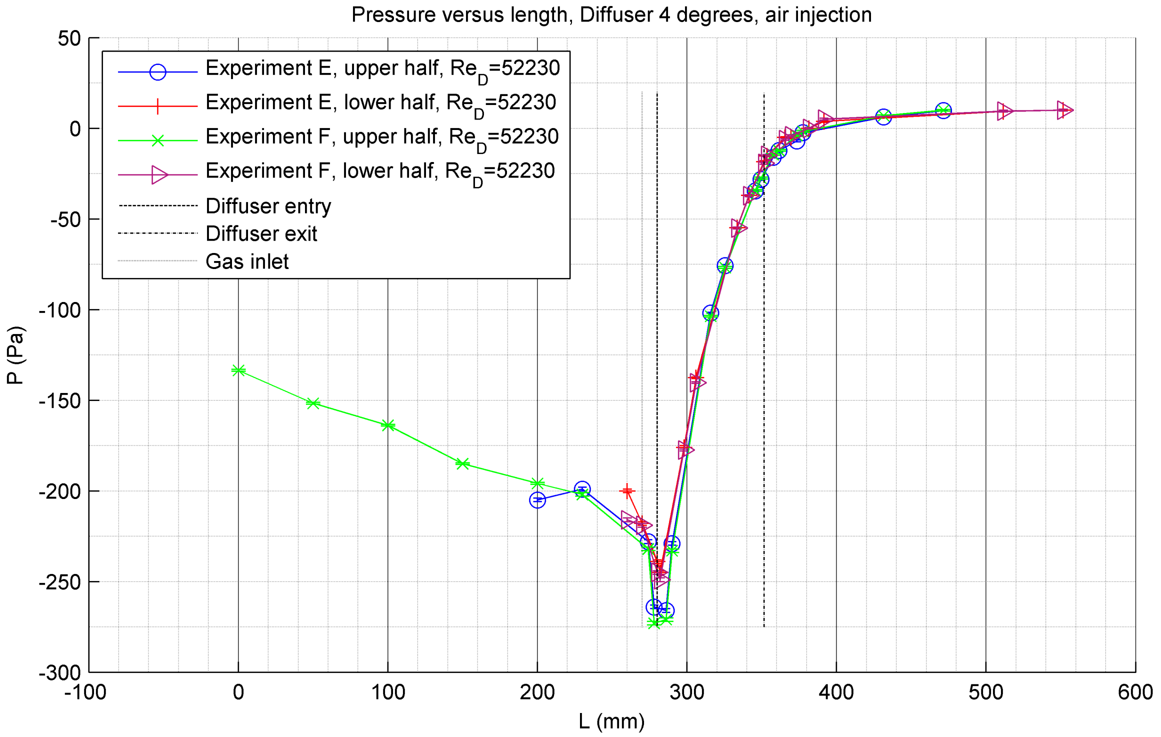

Figure 4.68: Pressure versus length, 4 degree diffuser with gas injection. Re$_D$ corresponds to the Reynolds number before the gas inlet.

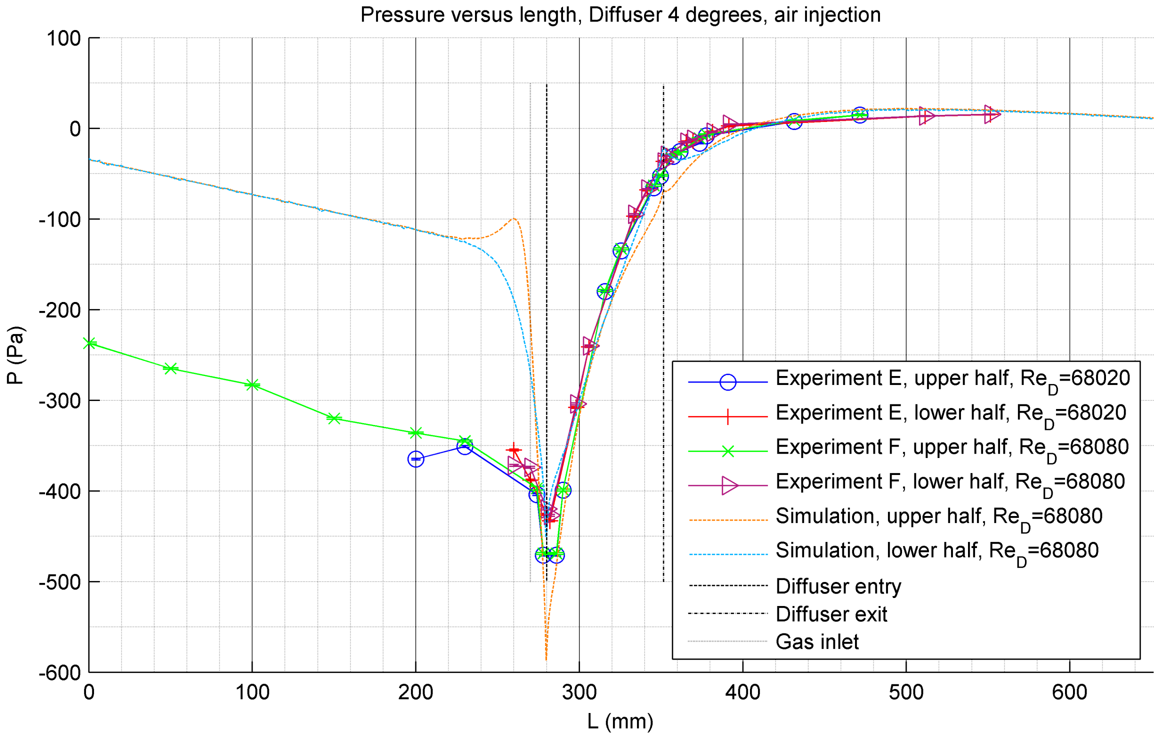

Figure 4.69: Pressure versus length, 4 degree diffuser with gas injection. Re$_D$ corresponds to the Reynolds number before the gas inlet.

4.5.2 10 degree diffuser

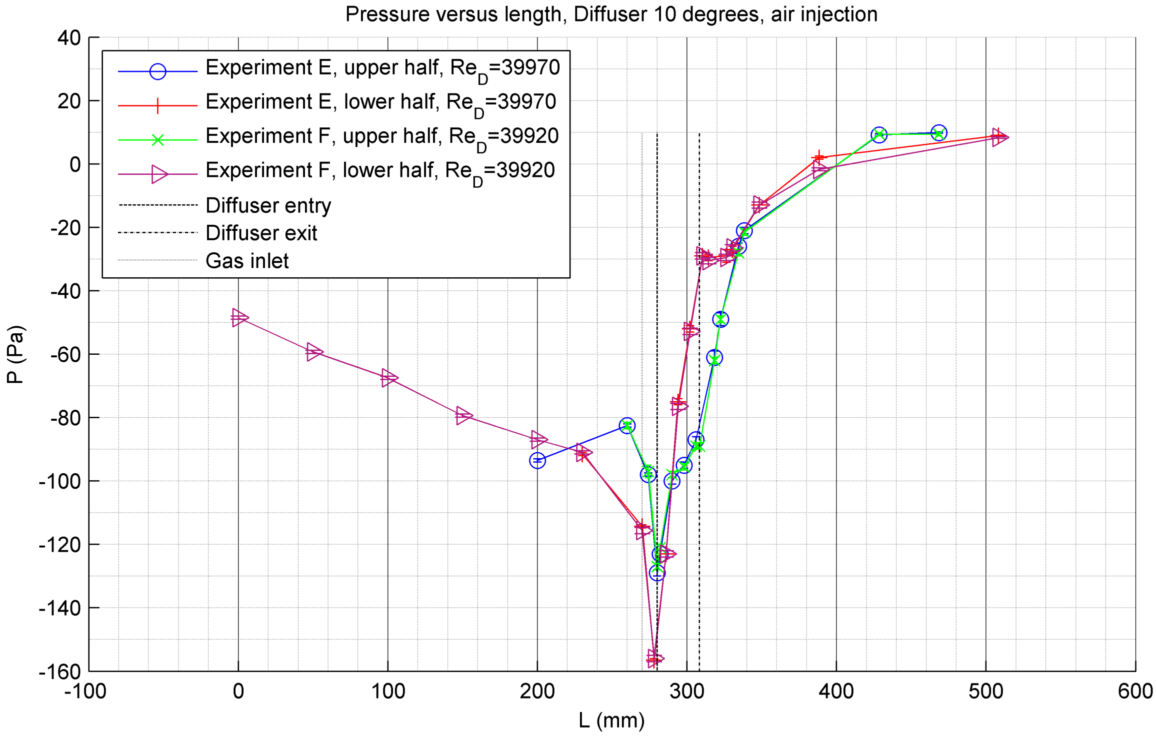

Figure 4.70: Pressure versus length, 10 degree diffuser with gas injection. Re_D corresponds to the Reynolds number before the gas inlet.

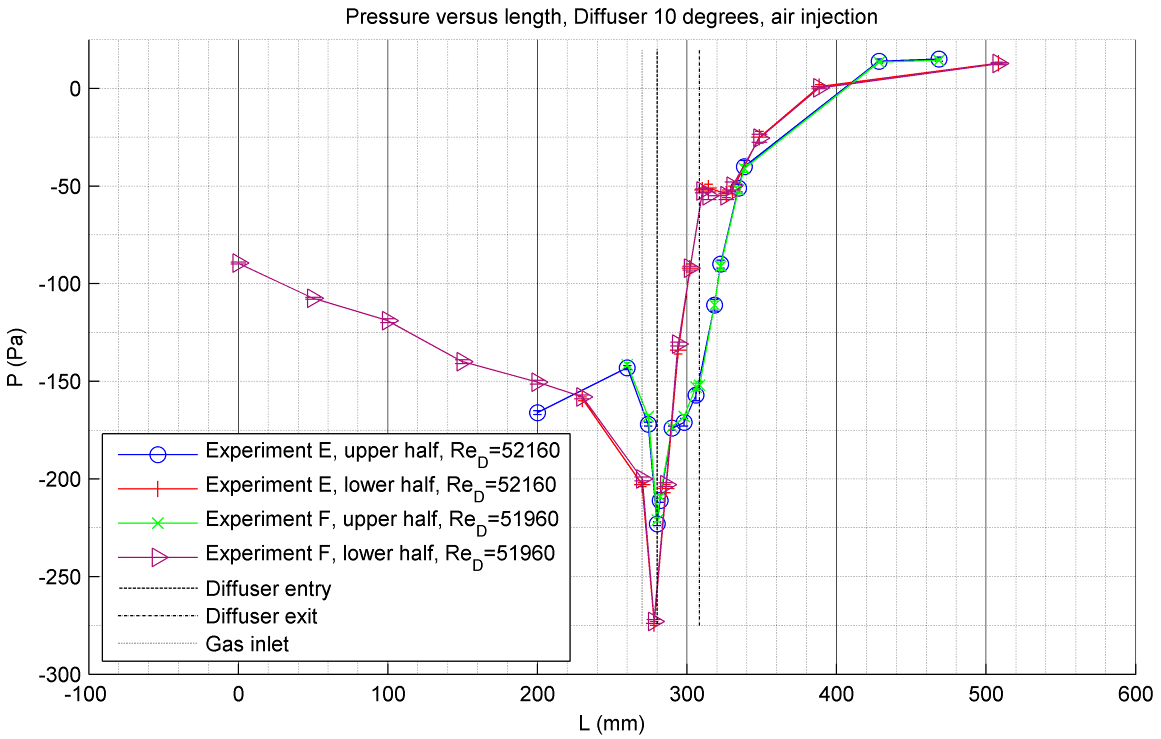

Figure 4.71: Pressure versus length, 10 degree diffuser with gas injection. Re_D corresponds to the Reynolds number before the gas inlet.

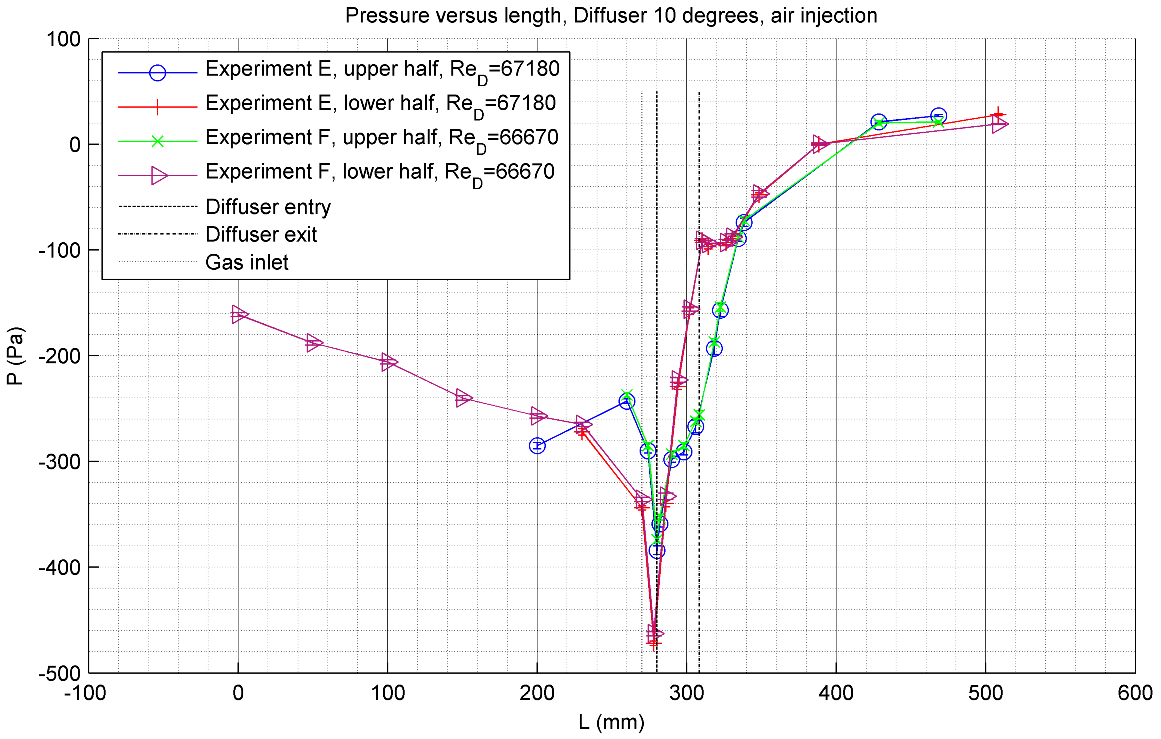

Figure 4.72: Pressure versus length, 10 degree diffuser with gas injection. Re_D corresponds to the Reynolds number before the gas inlet.

4.5.3 20 degree diffuser

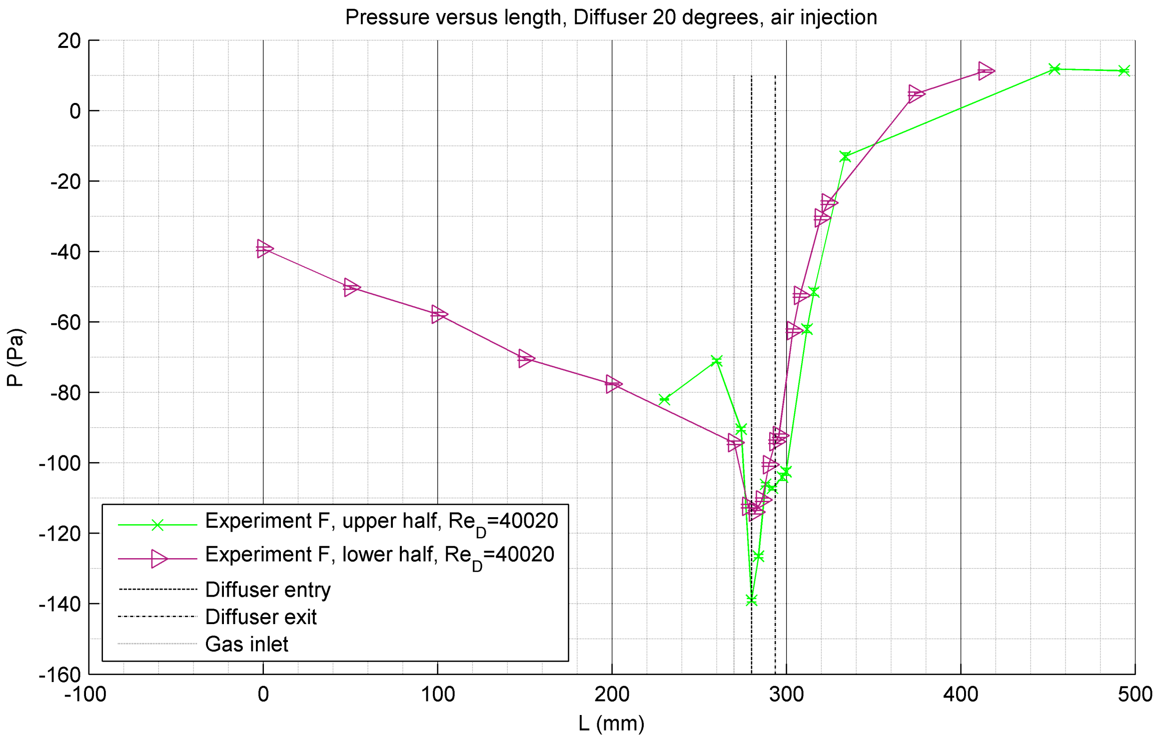

Figure 4.73: Pressure versus length, 20 degree diffuser with gas injection. Re$_D$ corresponds to the Reynolds number before the gas inlet.

4.5.4 Discussion

Figure 4.67 to 4.75 show different pressure distributions for the upper and lower half of the diffusers. This effect becomes stronger when the diverging angle of the diffuser increases. In the region after the gas inlet the pressure in the upper half of the diffuser is lower than in the lower half of the diffuser. This is due to the fact that the gas inlet is closer to the upper half, which means the velocity in the upper half is higher due to the extra amount of mass flow. Figure 4.69 shows that the results from simulations deviate from the measurements. If a closer look is taken at the results of the simulation, the upper and lower half show the same behavior as the measurements. Upstream of the gas inlet the pressure in the upper half rises with respect to the lower half. Downstream of the gas inlet the pressure in the upper half is lower than the pressure in the lower half. The reason for this behavior was explained earlier. The difference with the measurements is the large amount of pressure drop predicted by the simulations.

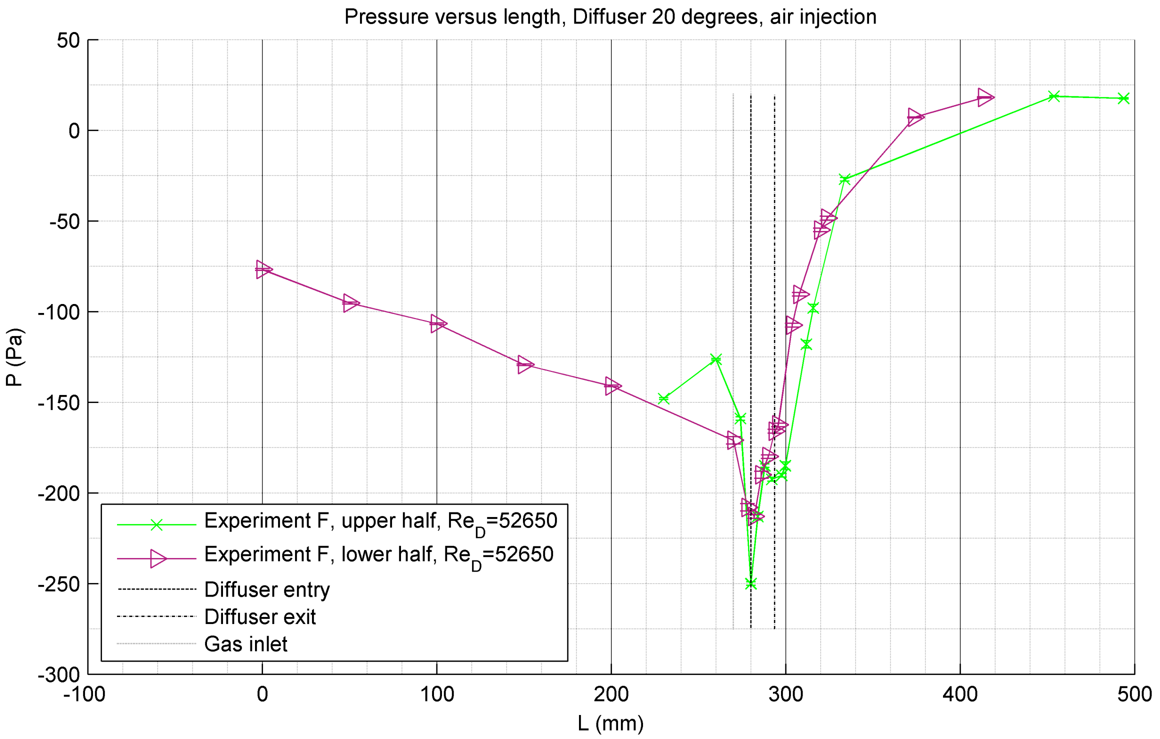

Figure 4.74: Pressure versus length, 20 degree diffuser with gas injection. Re_D corresponds to the Reynolds number before the gas inlet.

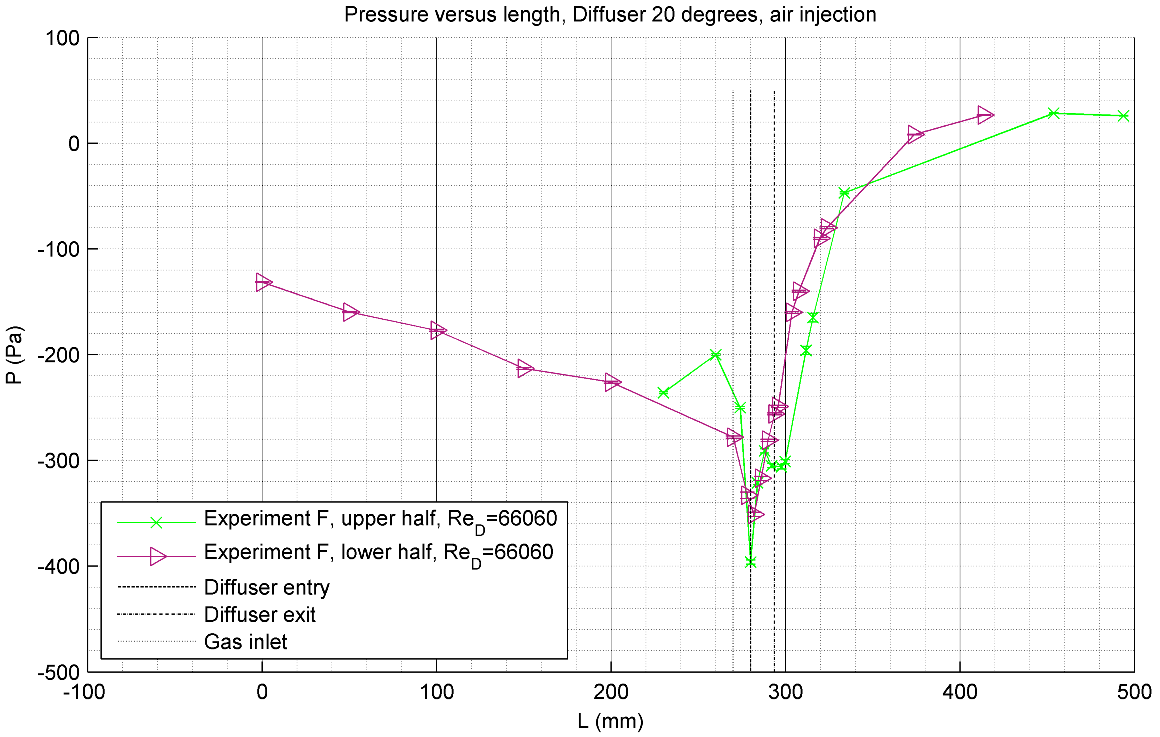

Figure 4.75: Pressure versus length, 20 degree diffuser with gas injection. Re_D corresponds to the Reynolds number before the gas inlet.

4.5.5 Error estimation

The errorbars in the figures in Chapter 4.4 to 4.5 represent fluctuations in the pressure that occurred during the measurements. These fluctuations are due to the fact that the flow was turbulent. The fluctuations were slightly higher at higher Reynolds numbers. The variations in the pressure varied from ± 0.2 Pa to ± 2 Pa. The error in the manometer itself and the resolution of the manometer are negligible, as discussed in Chapter 4.3.1. The error in the pressure tap locations was assumed to be approximately 0.5 mm based on measurements with a caliper. These errors are not displayed as horizontal errorbars in Figure 4.45 to 4.57, as they are negligibly small.

4.6 Experiment F: Air inlet open versus closed

This chapter will compare the results of the diffusers with open gas inlet with the results of the diffusers with closed gas inlet (Figure 4.76 to 4.84). Since Experiment E and F showed similar results, only the results of Experiment F will be treated here since this is the experiment with the most pressure taps. The inlet Reynolds numbers in the entry pipe upstream of the gas inlet are approximately equal for each experiment. Downstream of the gas inlet the Reynolds number of the experiment with open gas inlet differs from the Reynolds number of the experiment with closed gas inlet due to the difference in mass flow.

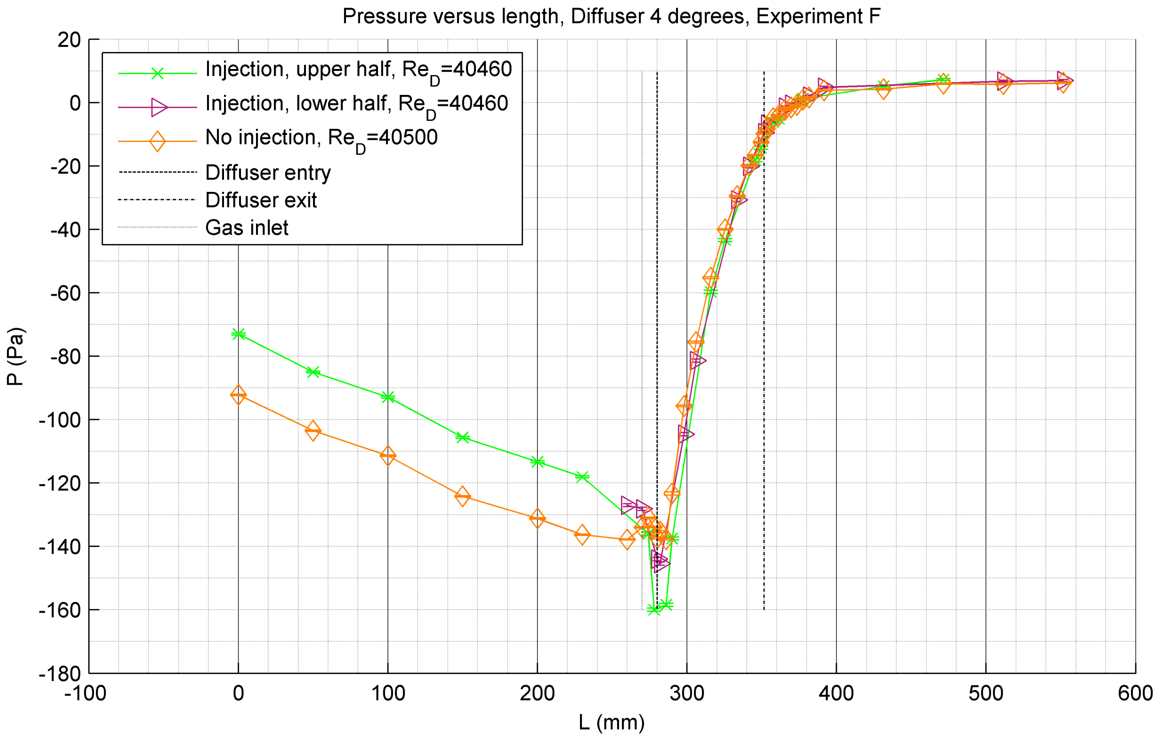

Figure 4.76: Pressure versus length, 4 degree diffuser with and without air injection. Re_D is determined in the entry tube upstream of the gas inlet.

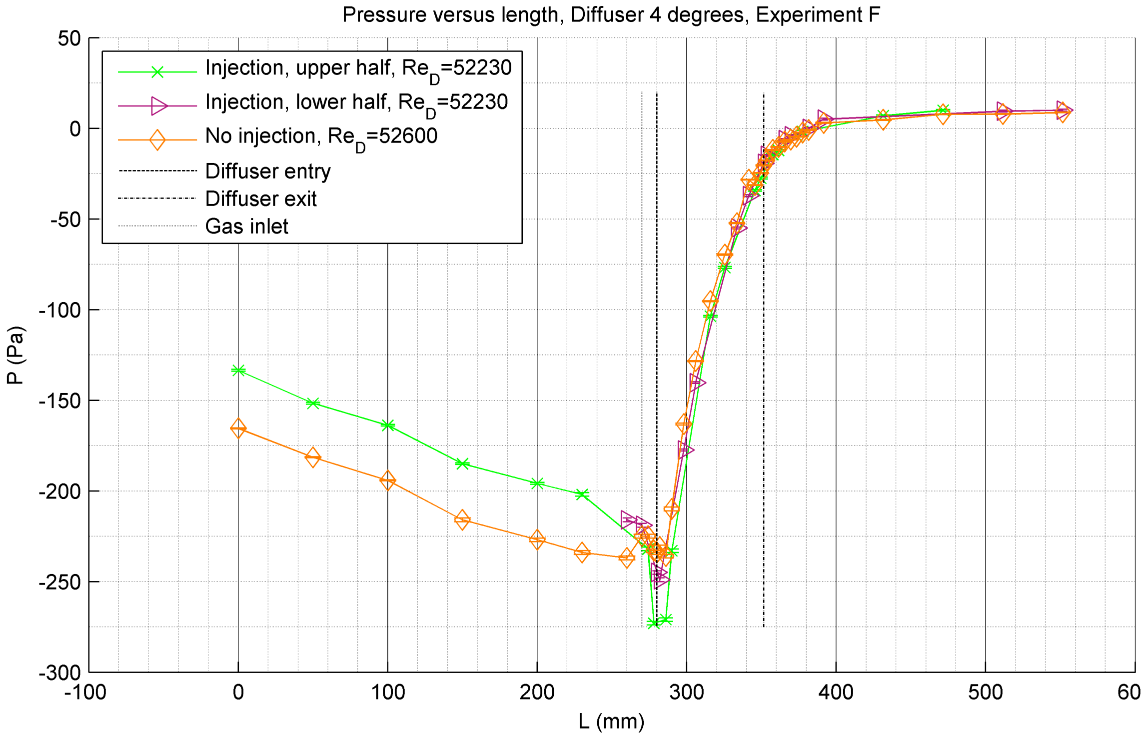

Figure 4.77: Pressure versus length, 4 degree diffuser with and without air injection. Re$_D$ is determined in the entry tube upstream of the gas inlet.

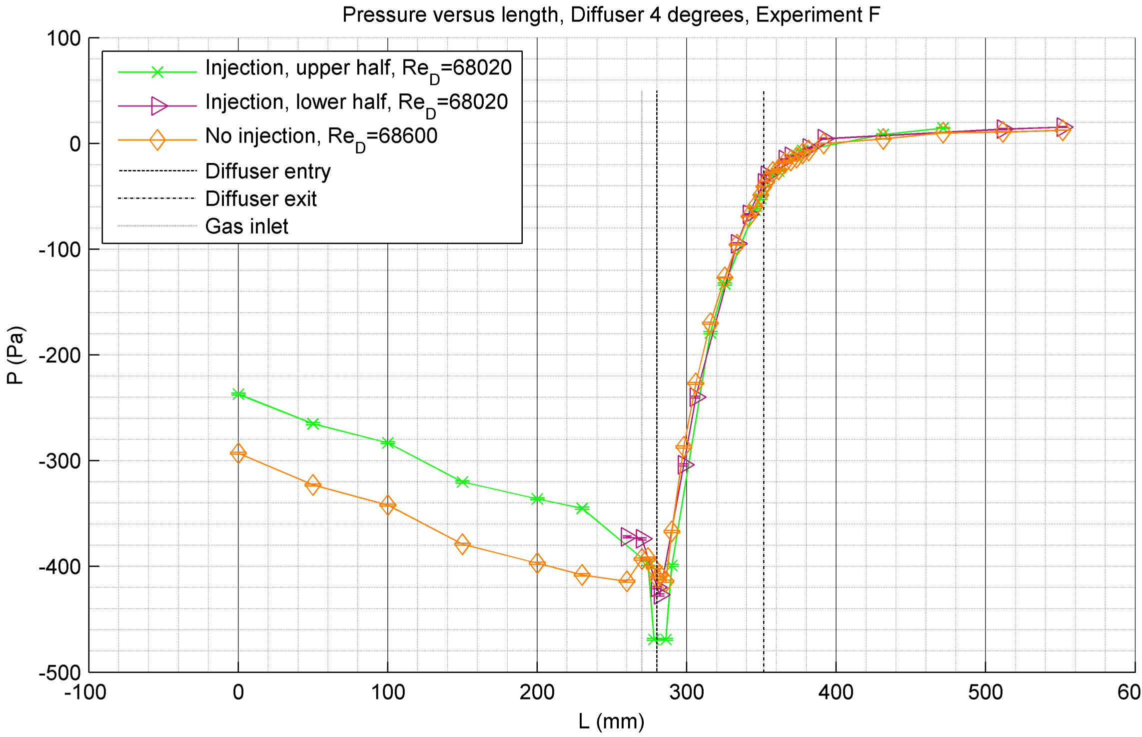

Figure 4.78: Pressure versus length, 4 degree diffuser with and without air injection. Re$_D$ is determined in the entry tube upstream of the gas inlet.

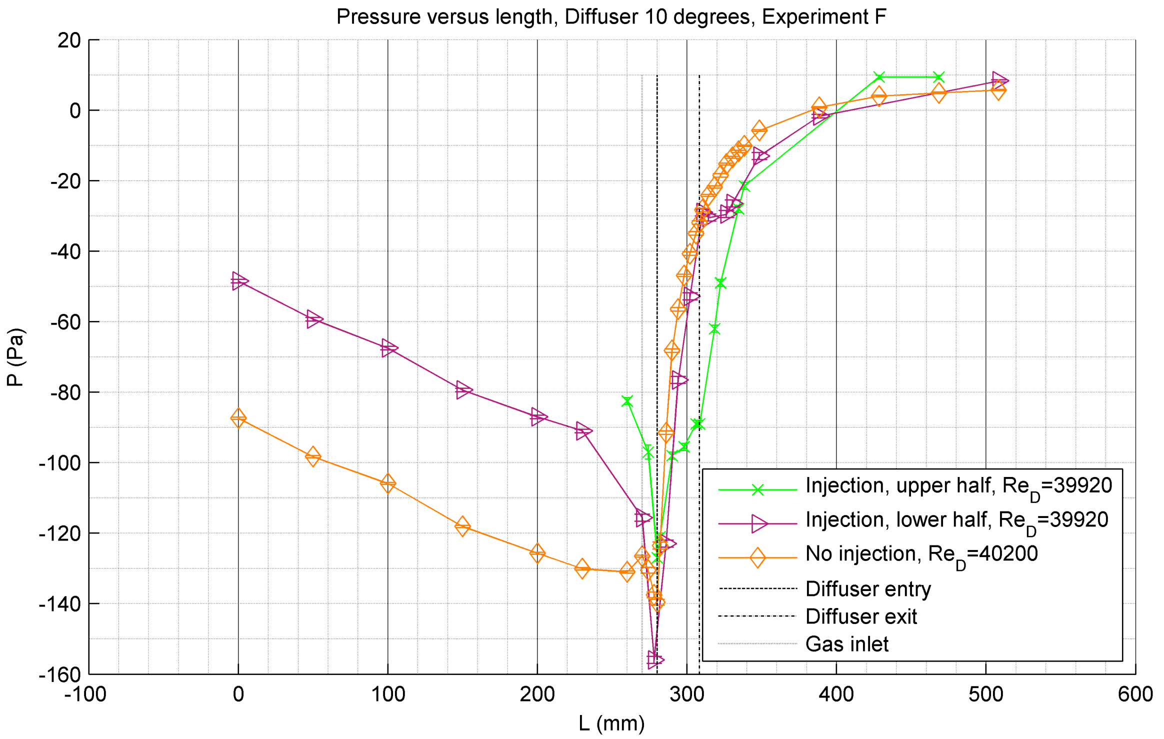

Figure 4.79: Pressure versus length, 10 degree diffuser with and without air injection. Re$_D$ is determined in the entry tube upstream of the gas inlet.

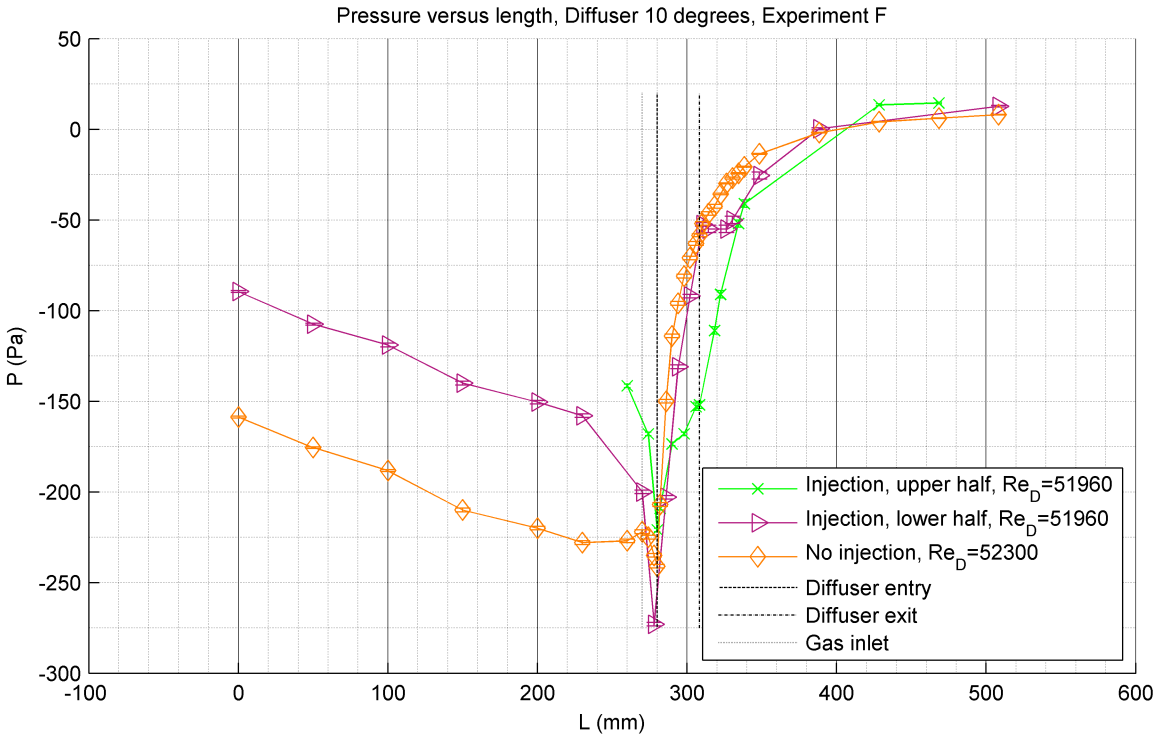

Figure 4.80: Pressure versus length, 10 degree diffuser with and without air injection. Re$_D$ is determined in the entry tube upstream of the gas inlet.

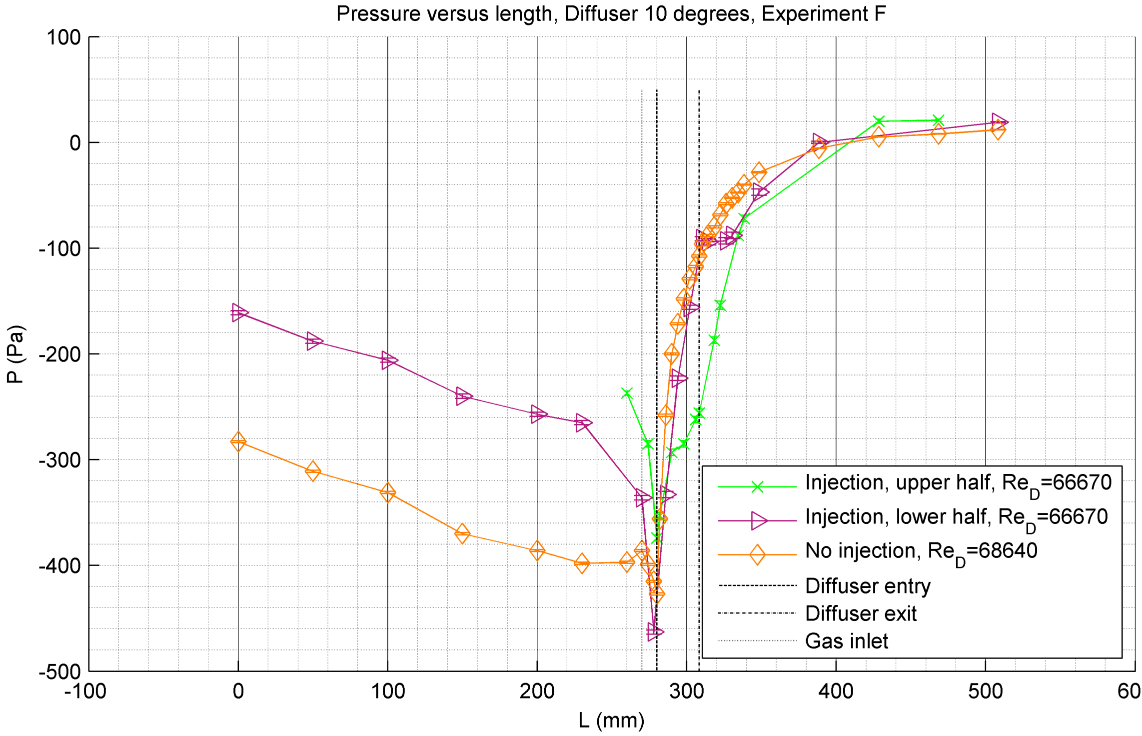

Figure 4.81: Pressure versus length, 10 degree diffuser with and without air injection. Re$_D$ is determined in the entry tube upstream of the gas inlet.

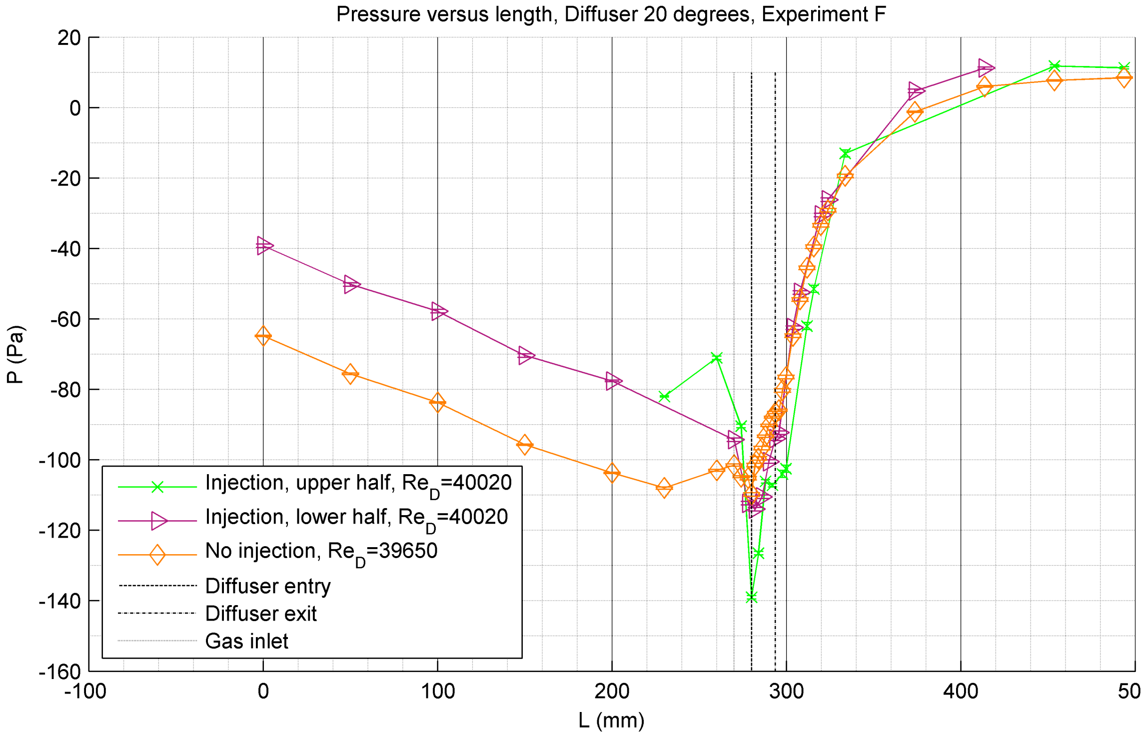

Figure 4.82: Pressure versus length, 20 degree diffuser with and without air injection. Re$_D$ is determined in the entry tube upstream of the gas inlet.

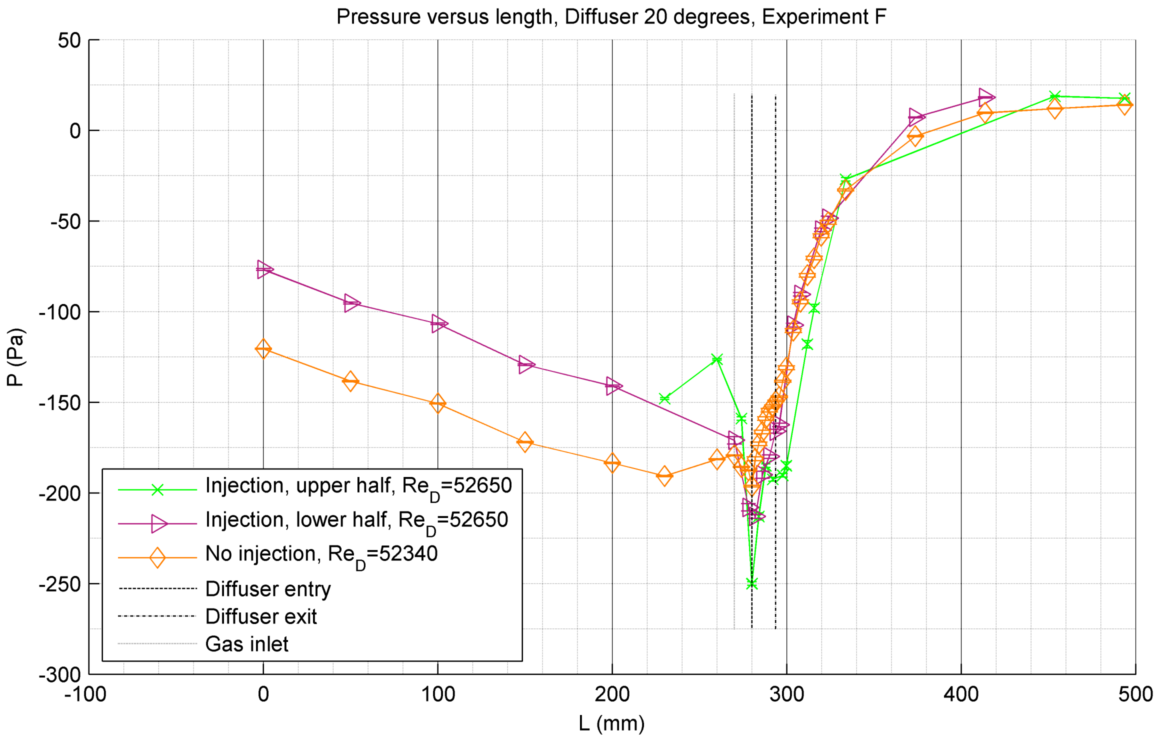

Figure 4.83: Pressure versus length, 20 degree diffuser with and without air injection. Re$_D$ is determined in the entry tube upstream of the gas inlet.

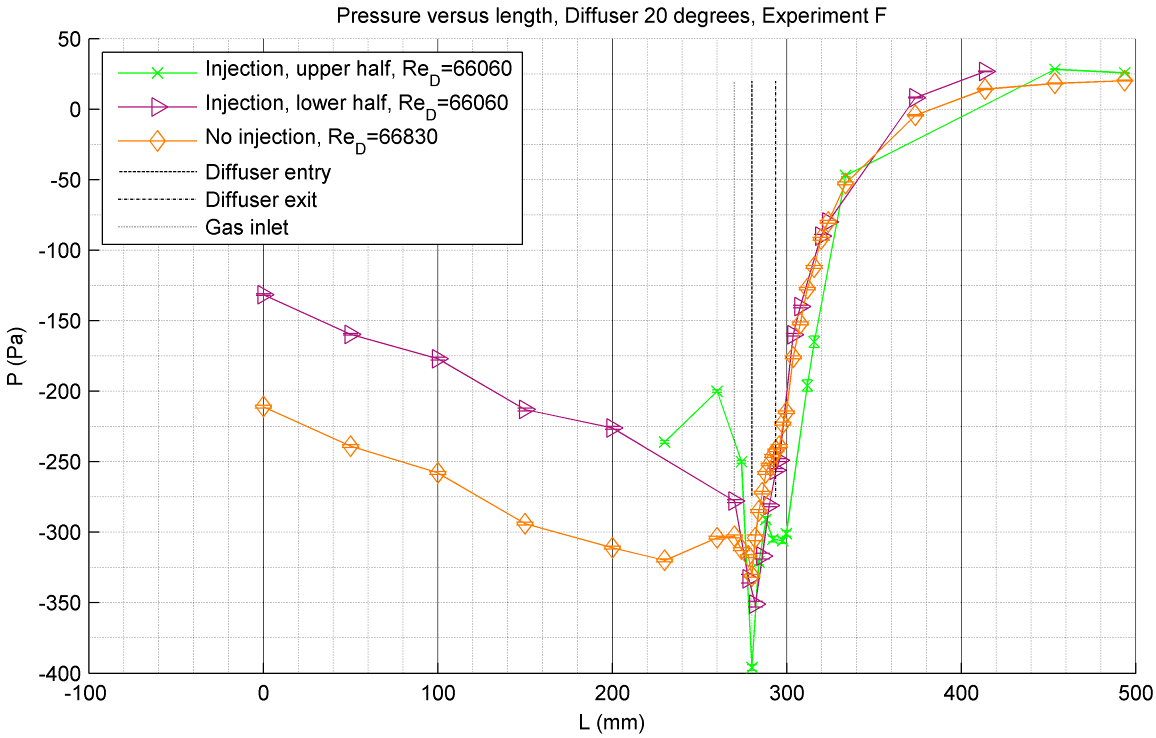

Figure 4.84: Pressure versus length, 20 degree diffuser with and without air injection. Re$_D$ is determined in the entry tube upstream of the gas inlet.

Figure 4.76 to 4.84 show that the diffusers with open air inlet suffer from a greater amount of pressure loss than the diffusers with closed gas inlet. The greatest difference occurs in the 10 degree diffusers. If the air inlet was closed, the 10 degree diffusers did not show any sign of flow separation. However, if the gas inlet was open there were large deviations between the pressure in the upper and lower half of the diffuser. This may be an indication of flow separation, which causes an extra amount of pressure loss. The 20 degree diffuser already had flow separation when the air inlet was closed, so the difference between open and closed air inlet will be smaller. The pressure distribution in the four degree diffusers showed good similarity between open and closed air inlet, resulting in the smallest difference compared to the 10 and 20 degree diffuser.

4.7 Experiment G: WB6 Venturi

The WB6 venturi was tested at three different Reynolds numbers, both with and without the gas inlet. The Reynolds numbers (Re_D) were determined at the exit of the venturi, which has a diameter of $D = 30$ mm. Measurements at a Reynolds number of approximately 32000 have approximately the same flow rate as an appliance with an output power of 30 kW, which is approximately the amount of power needed to supply an average household with hot water. The relation between the flow rate and output power can be determined by calculating the output power which is generated when a mixture of air and methane with an equivalance ratio of 0.8 is burned. This corresponds to a mass flow rate of $0.447 \cdot 10^{-3}$ kg/s/kW. Typically, appliances operate at an efficiency of approximately 97.5 percent, which means a slightly higher mass flow is needed to deliver the same amount of power. Dividing by the efficiency gives a mass flow rate of $0.458 \cdot 10^{-3}$ kg/s/kW. The other measurements were performed at Reynolds numbers of approximately 23500 and 38500, corresponding to an output power of approximately 22 kW and 36 kW. The results and corresponding geometry of the set-up can be found in Figure 4.85 to 4.88. The atmospheric conditions during each measurement can be found in Table 4.14. The numbers 15.0 and 15.3 represent the throat diameter of the venturi. Injection refers to measurements that were done with the gas inlet attached to the venturi, no injection refers to measurements without the gas inlet. The pressure at the throat of the venturi is measured through two static pressure taps, over which the average is taken.

Figure 4.86 to 4.88 show that the lowest throat pressure is achieved by the 15.0 mm venturi with air injection. This is due to the fact that the velocity in the throat with a diameter of 15.0 mm will be higher than the velocity in the throat with a diameter of 15.3 mm if the same flowrate is applied. Since the gas inlet partially blocks the air inlet the surface area decreases and the velocity increases even further. This higher

Property	Dynamic viscosity	Specific gas constant	Pressure	Temperature	Density
Symbol	μ	R_s	P	T	ρ
Unit	Pa s	J kg^{-1}K^{-1}	Pa	K	kg m^{-3}
Experiment G 15.0 Injection	$1.79 \cdot 10^{-5}$	287	100300	293.15	1.192
Experiment G 15.0 No injection	$1.79 \cdot 10^{-5}$	287	101100	294.05	1.198
Experiment G 15.3 Injection	$1.79 \cdot 10^{-5}$	287	100400	292.15	1.197
Experiment G 15.3 No Injection	$1.79 \cdot 10^{-5}$	287	100400	292.15	1.197

Table 4.14: Atmospheric conditions during experiment G.

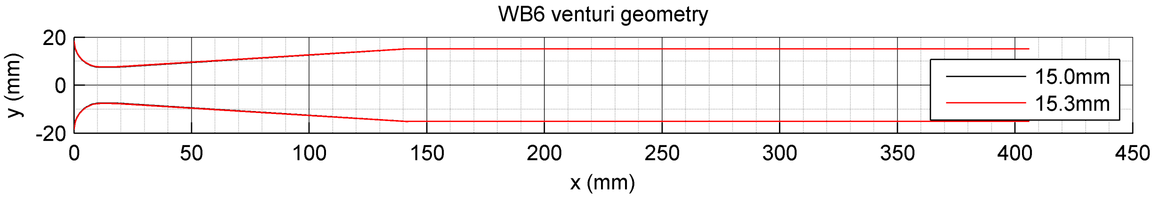

Figure 4.85: Geometry of the WB6 venturi with a throat diameter of 15.0 mm and 15.3 mm.

velocity will result in a lower pressure. The highest amount of pressure recovery is achieved by the 15.3 mm and 15.0 mm venturi without air injection. The venturies with gas injection suffer from slightly more pressure loss. The pressure loss is at its highest for the 15.0 mm venturi with gas injection. This is probably due to the fact that the venturi with gas injection suffers from an additional amount of skin friction.

4.7.1 Error estimation

The errorbars in Figure 4.86 to 4.88 represent fluctutations in the pressure that occurred during measurements, as explained in Chapter 4.5.5. The difference between the two measured pressures at the throat of the venturi is also taken into account in the errorbars. Variations in the pressure varied from ±1 Pa far downstream of the venturi to ±50 Pa at the throat of the venturi. The variations appeared to be smaller when the gas inlet was attached to the venturi. A possible reason for this behavior is that the flow is guided by the gas nozzle, resulting in a more efficient entry flow. The internal error in the manometer is again negligible.

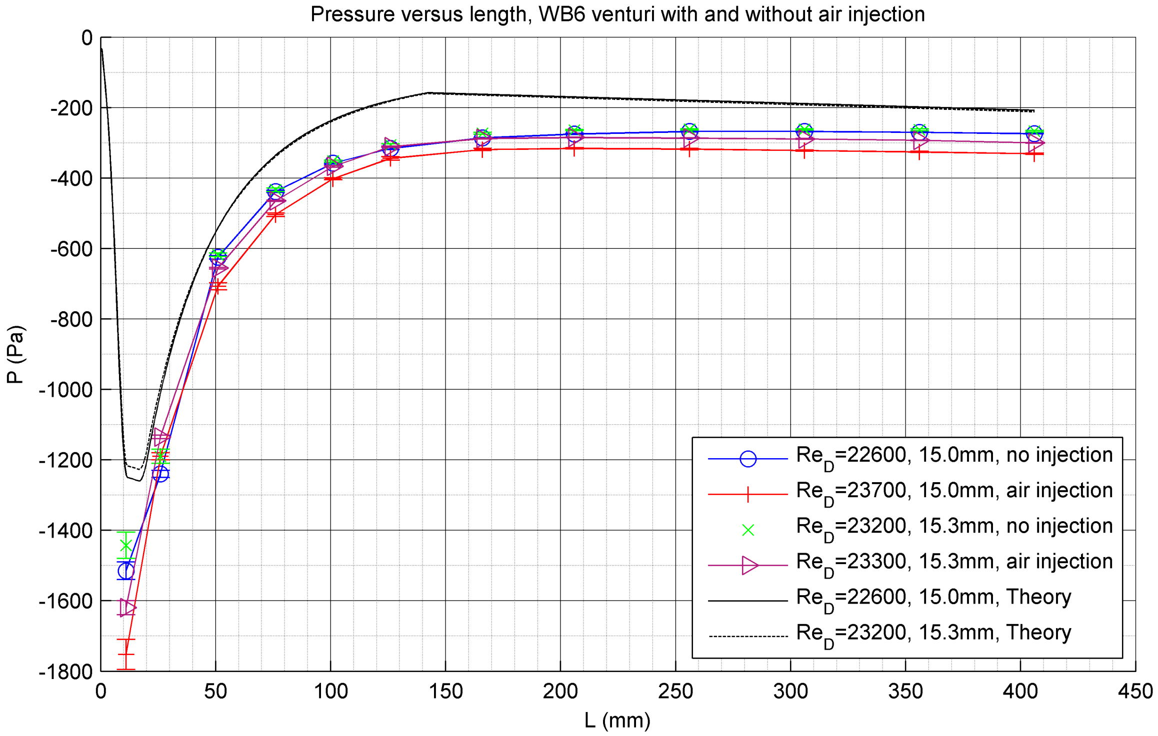

Figure 4.86: Pressure versus length, WB6 venturi with and without air injection. Re$_D$ corresponds to the Reynolds number at the exit of the venturi.

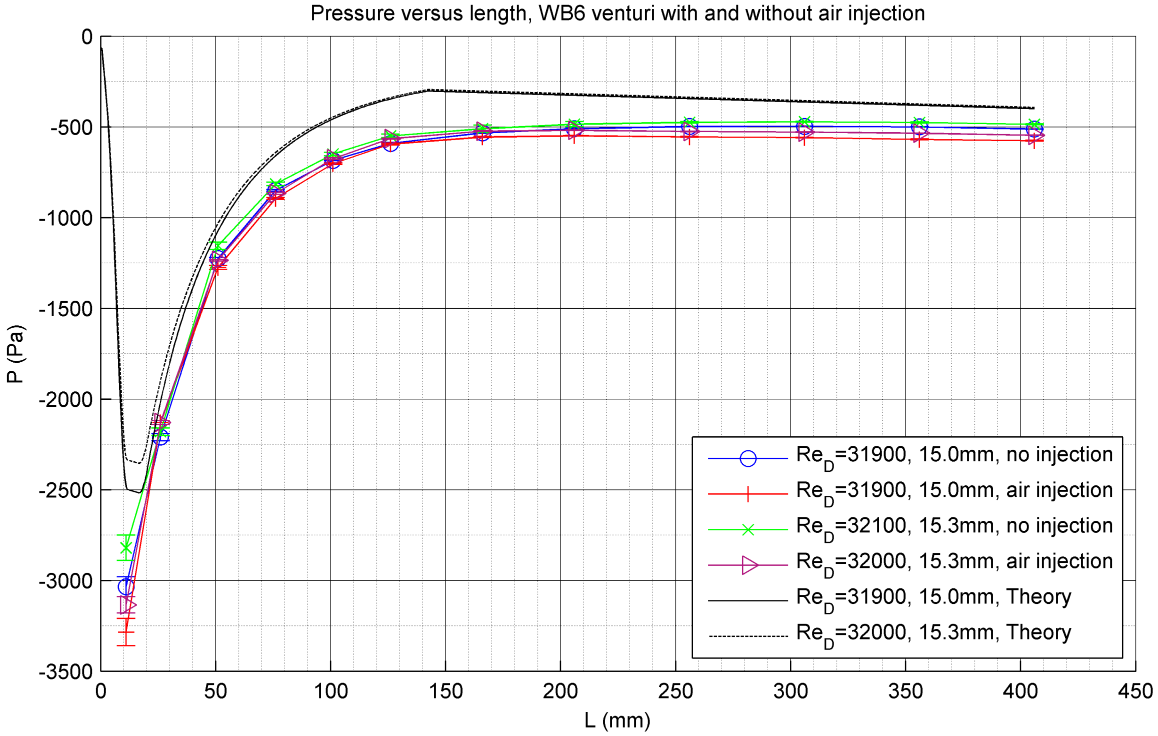

Figure 4.87: Pressure versus length, WB6 venturi with and without air injection. Re$_D$ corresponds to the Reynolds number at the exit of the venturi.

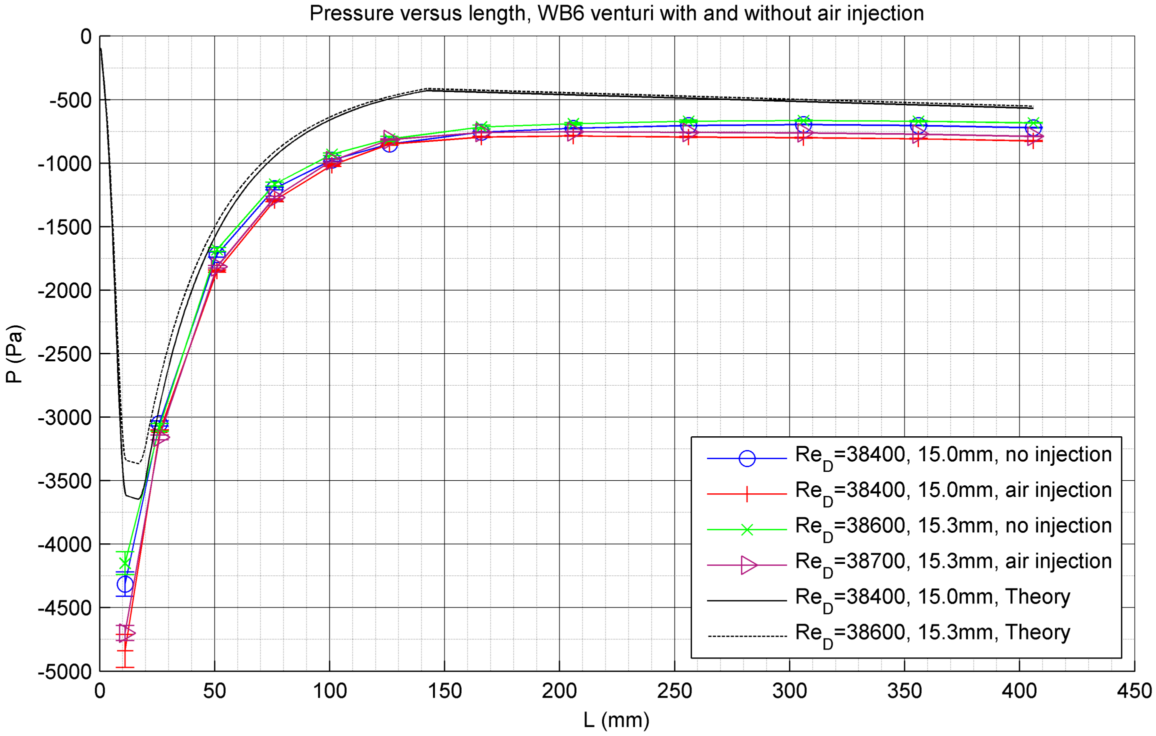

Figure 4.88: Pressure versus length, WB6 venturi with and without air injection. Re_D corresponds to the Reynolds number at the exit of the venturi.

Chapter 5

Conclusions and recommendations

5.1 Conclusions

5.1.1 Pipe pressure drop

First, a set of experiments were performed on a pvc and copper pipe to check the accuracy of the pressure measurements. The pressure measurement of the PVC pipe showed large deviations between the pressure drop over the first and second section of pipe. The set-up was susceptible to bending, which disturbed the measurement.

A copper pipe with more taps was used for the next measurement. Better results were obtained for the pressure drop over a larger section of pipe. However, there were still large deviations in the pressure drop over smaller distances. These deviations were most likely due to defects in the pressure taps. This means the fabrication of the pressure taps should be very accurate on the diffuser to obtain a good result for the pressure distribution.

5.1.2 Diffusers without gas inlet

The pressure distribution in diffusers with an angle of 4, 10 and 20 degrees, both with and without a gas inlet was measured in experiment D, E and F. Experiment D showed the necessity of precise manufacturing of the pressure taps, as fluctuations occurred around the entry and exit of the diffusers. The diffusers from experiment E and F were manufactured with the same geometry as the diffusers from experiment D, with the addition of better pressure taps and a closeable gas inlet. The measurements showed good similarity with the simulations for both the 4 and 10 degree diffuser at three Reynolds numbers. The maximum difference between the measurements and simulations was approximately 10 Pa. The only deviation occurred around the entry of the diffuser. The sudden increase in pressure was due to difference in the internal diameter of the inlet pipe and the diffuser. If the diameters were equal, more pressure loss could be observed. The extra amount of pressure loss is probably due to roughness in the diffusers during the experiments. Pressure measurements in the diffusers were more precise than pressure measurements on the pipes mentioned earlier because of more precise manufacturing of the pressure taps.

5.1.3 Diffusers with gas inlet

The static pressure in the diffusers of experiment E and F with air injection was tested at approximately the same Reynolds numbers as in the measurements without air injection. Due to the locations of the pressure taps the pressure distribution was divided into an upper and lower half. Measurements showed that the pressure in the upper half was lower than in the lower half downstream of the diffuser due to the increase in mass flow and thus velocity caused by the gas inlet. The higher the diverging angle of the diffuser, the stronger this effect was. Simulations done on the 4 degree diffuser did not match the measurements. The pressure drop from simulations was much larger than the pressure drop from measurements. Using a different turbulence model may give better results.

5.1.4 WB6 venturi

In experiment G WB6 venturis with a throat diameter of 15.0 and 15.3 mm were tested at three different Reynolds numbers. Measurements were performed with and without a removable gas injection. The lower the throat diameter, the lower the static pressure in the throat. The gas injection caused the pressure to decrease even further due to the reduced amount of cross-sectional area in the throat of the venturi. There was a large difference between the measured pressure drop in the venturis and the theoretical pressure drop. The theoretical pressure in the throat of the venturi was much lower than the measured pressure. This difference was more than 1000 Pa in some cases. The dimensions of the venturi were checked with a caliper and showed no deviations in the 15.0 and 15.3 mm throat diameter. A possible reason for the lower throat pressure in measurements may be due to a non-uniform pressure distribution over the cross-section of the venturi.

5.2 Recommendations

5.2.1 Improvements

The experiments on the diffusers could be improved by making sure there are as little deviations (in for example the dimensions) as possible, as these deviations cause significant errors in the pressure readout. If more space and fan power is available, experiments can be performed at higher Reynolds numbers and with more entry length before the test section. This will also potentially allow for a settling chamber with screens and honeycombs, resulting in a more homogeneous entry flow. Not each measurement was compared with simulations. Simulations can still be performed on the 10 and 20 degree diffuser with air injection and on the WB6 venturi. Performing these simulations will give better insight in the precision of the simulations.

5.2.2 Future research

This research only covers results regarding the static pressure. A possible next step would be to perform velocity measurements in the diffusers and venturis. This can be done with a Pitot tube or Constant Temperature Anemometry system, or possibly with other techniques like LDV or PIV. Simulations are performed assuming fully developed entry flow. Velocity measurements around the entry of the diffuser can validate this assumption. Velocity measurements in the diverging part of diffusers or venturis will give better insight in the occurrence of possible flow separation and in the development of the velocity profile.

All measurements with gas injection in this report were performed with air as a substitute for natural gas for practical reasons. Performing the measurements with natural gas instead of air could give more insight in the precision of the simulations when natural gas is injected instead of air.

Bibliography

[1] J. D. Anderson Jr., *Fundamentals of Aerodynamics*, 4th ed. Mc Graw Hill, 2005.

[2] A. Rona, “Boundary Layer Trips for Low Reynolds Number Wind Tunnel Tests,” *48th AIAA Aerospace Sciences Meeting*, pp. 1–13, 2010.

[3] H. Schlichting, *Boundary-Layer Theory*, 7th ed. Mc Graw Hill, 1979.

[4] C. Parchen, R. Krishna Prasad, K. Nieuwvelt, “Turbulent flow through pipes and fittings: a literature survey,” Tech. Rep., 1988.

[5] K. Lien, J. Monty, M. Chong, and A. Ooi, “The entrance length for fully developed turbulent channel flow,” *15th Australasian Fluid Mechanics Conference (Sydney, Australia)*, no. December, pp. 1–4, 2004. [Online]. Available: http://www.aeromech.usyd.edu.au/15afmc/proceedings/papers/AFMC00093.pdf

[6] N. Wang, “Automatic adjoint optimization of a venturi mixer, MSc thesis,” University of Twente, Tech. Rep., 2015.

[7] “Flow in pipes,” pp. 321–343, 2004. [Online]. Available: http://www.uio.no/studier/emner/matnat/math/MEK4450/h11/undervisningsmateriale/modul-5/Pipeflow{_}intro.pdf

[8] H. Sprenger, “Experimentelle Untersuchungen an geraden und gekrümmten Diffusoren,” no. 2803, 1959.

[9] R. K. Singh and R. S. Azad, “Measurement of instantaneous flow reversals and velocity field in a conical diffuser,” *Experimental Thermal and Fluid Science*, vol. 10, no. 3, pp. 397–413, 1995. [Online]. Available: http://www.sciencedirect.com/science/article/pii/089417779400083K

[10] E. Spencer, M. Heitor, and I. Castro, “Intercomparison of measurements and computations of flow through a contraction and a diffuser,” *Flow Measurement and Instrumentation*, vol. 6, no. 1, pp. 3–14, 1995. [Online]. Available: http://www.sciencedirect.com/science/article/pii/095559869593452Z

[11] S. Obi, K. Aoki, and S. Masuda, “Experimental and computational study of turbulent separating flow in an asymmetric plane diff user,” in *Ninth symposium on ”Turbulent Shear Flows”*, no. January 1993, 1993.

[12] C. U. Buice and J. K. Eaton, “Experimental Investigation of Flow Through an Asymmetrical Plane Diffuser (report),” *Center for Turbulence Research Annual Research Briefs*, 1996. [Online]. Available: http://me.stanford.edu/groups/thermo/pdf/TSD-107.pdf

[13] J. L. Means, P. C. Glance, and H. A. Klassen, “Analytical Investigation of Conical Diffusers,” Tech. Rep. NASA TM X-2605, 1972.

[14] M. Reader-Harris, *Orifice Plates and Venturi Tubes*. Springer, 2015.

[15] “Unitedsensorcorp.com,” p. Boundary layer probes. [Online]. Available: www.unitedsensorcorp.com/boundary.html

[16] “Dantecdynamics.com,” p. Measurement principle of CTA. [Online]. Available: http://www.dantecdynamics.com/measurement-principles-of-cta

[17] P. Bradshaw and R. Mehta, “Wind tunnel design,” p. Screens. [Online]. Available: http://navier.stanford.edu/bradshaw/tunnel/screen.html

[18] J. Scheiman, “Considerations for the Installation of Honeycomb and Screens To Reduce Wind-Tunnel Turbulence,” *NASA Technical Memorandum 81868*, no. August, 1981.

[19] T. Poinsot and D. Veynante, *Theoretical and Numerical Combustion*, 2nd ed. Edwards, 2005.

[20] David.deKleine@nl.bosch.com, *David de Kleine, Bosch Thermotechniek B.V.*

[21] Nijso.Beishuizen@nl.bosch.com, *Nijso Beishuizen, Bosch Thermotechniek B.V.*

Appendix A

Technical drawings

A.1 Experiment 5: Diffuser with gas inlet

The next pages will show technical drawings of the 4 and 10 degree diffuser with gas inlet and corresponding inlet and outlet pipes. The inlet and outlet pipe can be fitted to both diffusers.

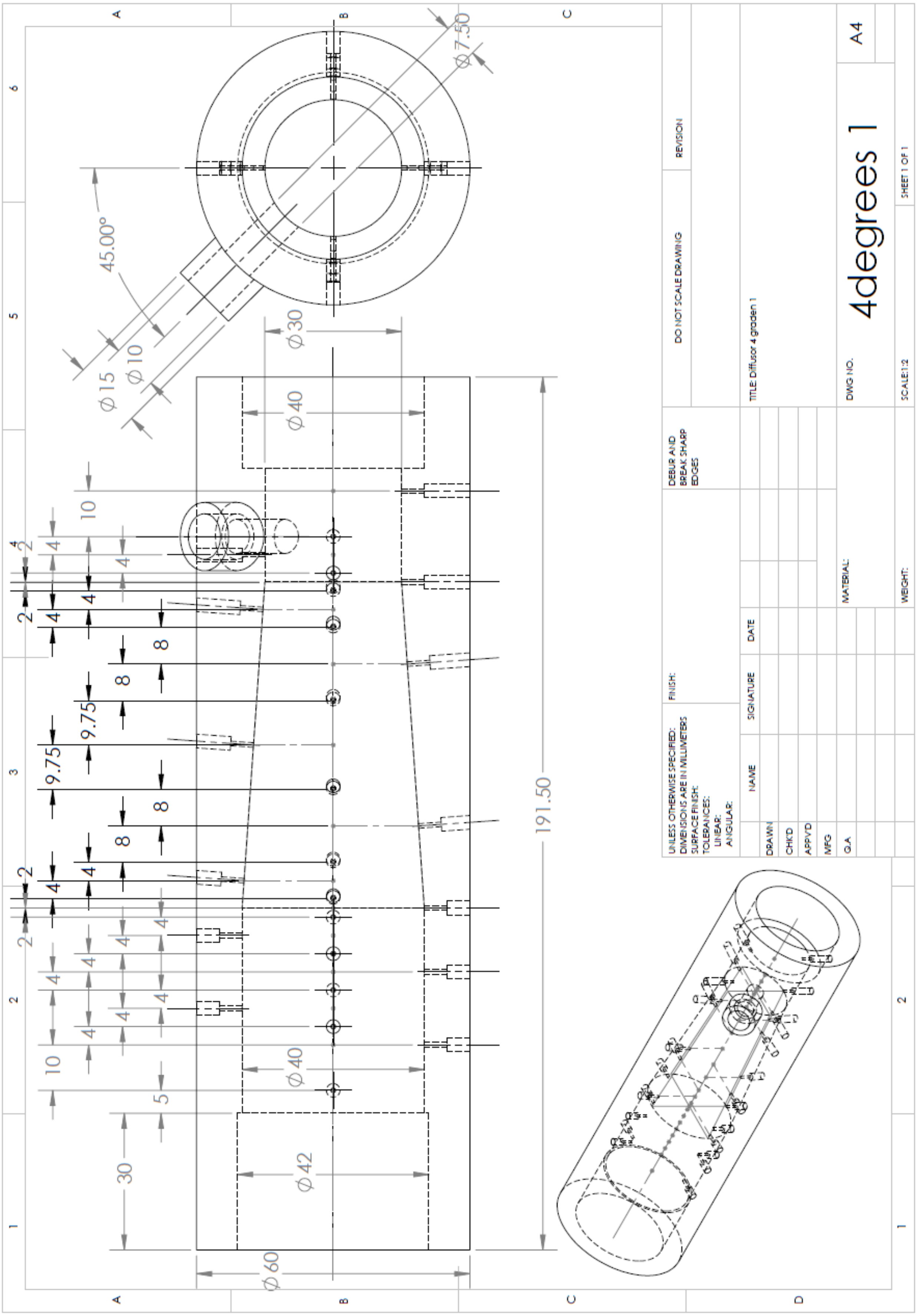
45.00°
Ø7.50
Ø15
Ø10
Ø30
Ø40
Ø40
Ø42
Ø60
191.50
10
4
2
8
9.75
9.75
30
5
UNLESS OTHERWISE SPECIFIED:
DIMENSIONS ARE IN MILLIMETERS
SURFACE FINISH:
TOLERANCES:
LINEAR:
ANGULAR:
FINISH:
DEBUR AND BREAK SHARP EDGES
DO NOT SCALE DRAWING
REVISION
NAME
SIGNATURE
DATE
DRAWN
CHK'D
APPV'D
MFG
Q.A
TITLE: Diffusor 4 graden 1
MATERIAL:
WEIGHT:
DWG NO.
4degrees 1
A4
SCALE:1:2
SHEET 1 OF 1
A
B
C
D
1
2
3
4
5
6

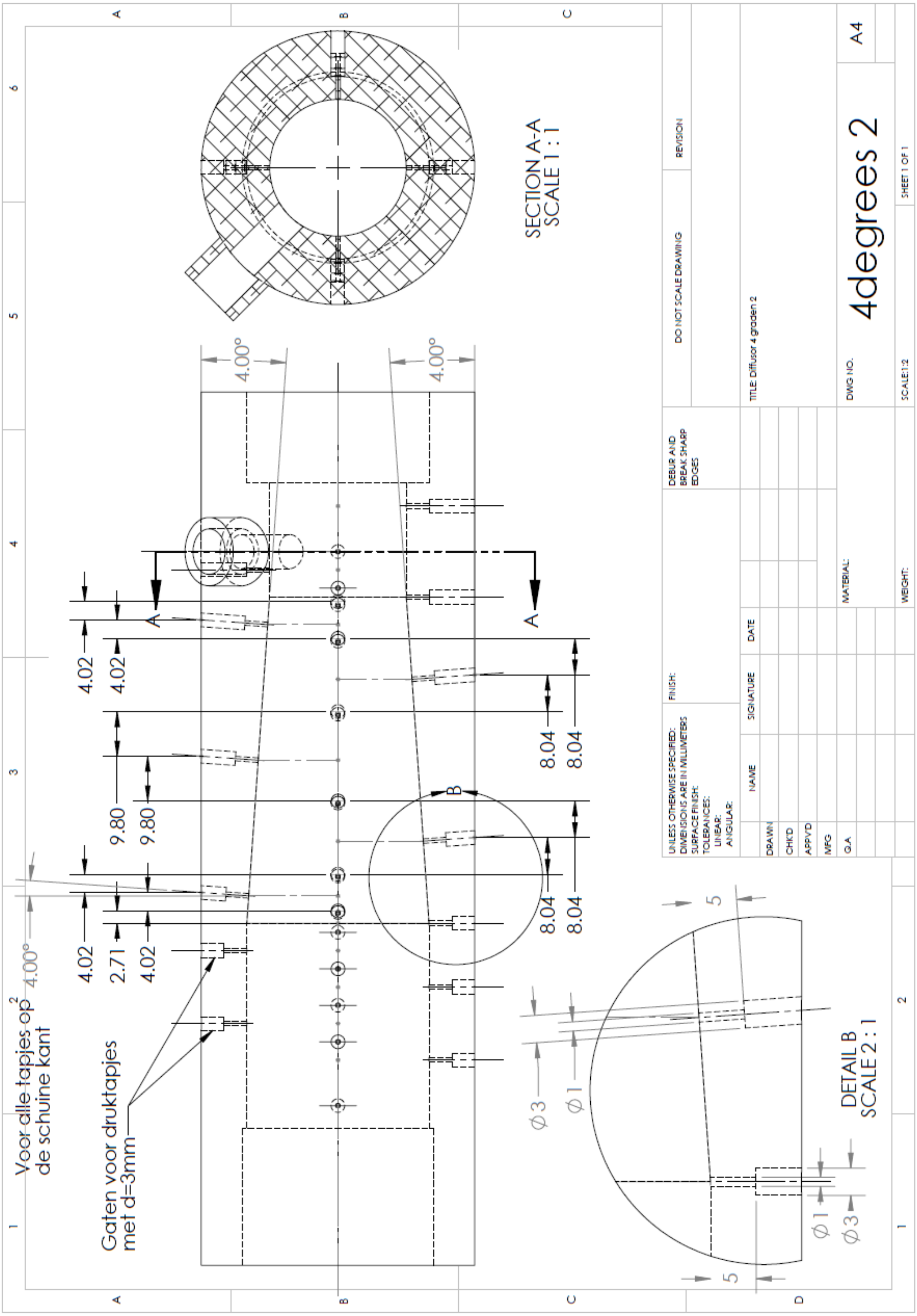
SECTION A-A
SCALE 1 : 1
4.00°
4.00°
4.00°
A
A
B
4.02
4.02
9.80
9.80
4.02
2.71
4.02
8.04
8.04
8.04
8.04
Voor alle tapjes op de schuine kant
Gaten voor druktapjes met d=3mm
5
5
Ø3
Ø1
Ø1
Ø3
DETAIL B
SCALE 2 : 1
DO NOT SCALE DRAWING
REVISION
DEBUR AND BREAK SHARP EDGES
UNLESS OTHERWISE SPECIFIED:
DIMENSIONS ARE IN MILLIMETERS
SURFACE FINISH:
TOLERANCES:
LINEAR:
ANGULAR:
FINISH:
NAME
SIGNATURE
DATE
DRAWN
CHK'D
APPV'D
MFG
Q.A
TITLE: Diffusor 4 graden 2
MATERIAL:
DWG NO.
4degrees 2
A4
WEIGHT:
SCALE:1:2
SHEET 1 OF 1

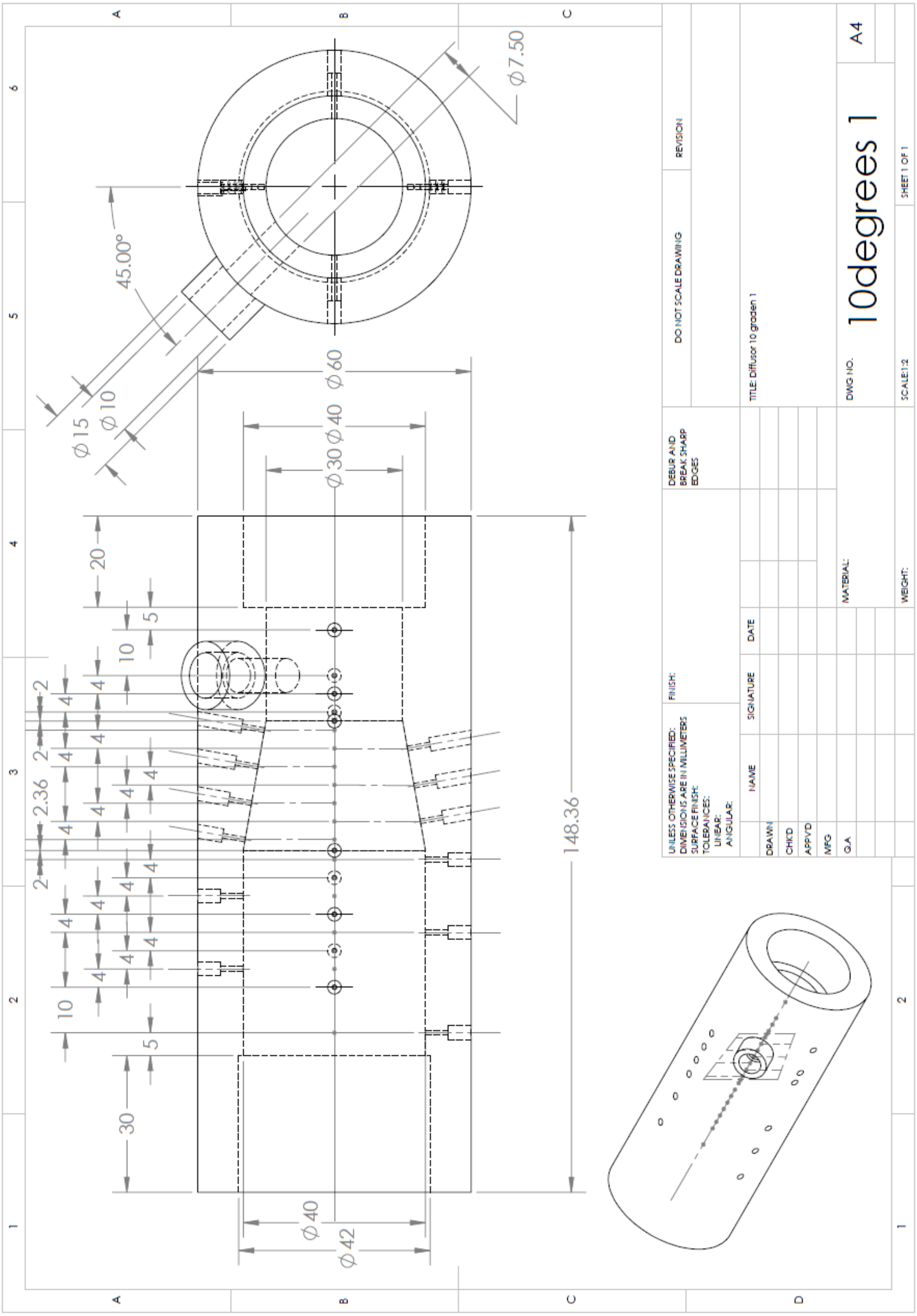
Ø7.50
45.00°
Ø15
Ø10
Ø60
Ø40
Ø30
20
5
10
4
2
2.36
148.36
30
Ø40
Ø42
A
B
C
D
1
2
3
4
5
6
UNLESS OTHERWISE SPECIFIED:
DIMENSIONS ARE IN MILLIMETERS
SURFACE FINISH:
TOLERANCES:
LINEAR:
ANGULAR:
FINISH:
DEBUR AND BREAK SHARP EDGES
DO NOT SCALE DRAWING
REVISION
NAME
SIGNATURE
DATE
DRAWN
CHK'D
APPV'D
MFG
Q.A
TITLE: Diffusor 10 graden 1
MATERIAL:
DWG NO.
10degrees 1
A4
WEIGHT:
SCALE:1:2
SHEET 1 OF 1

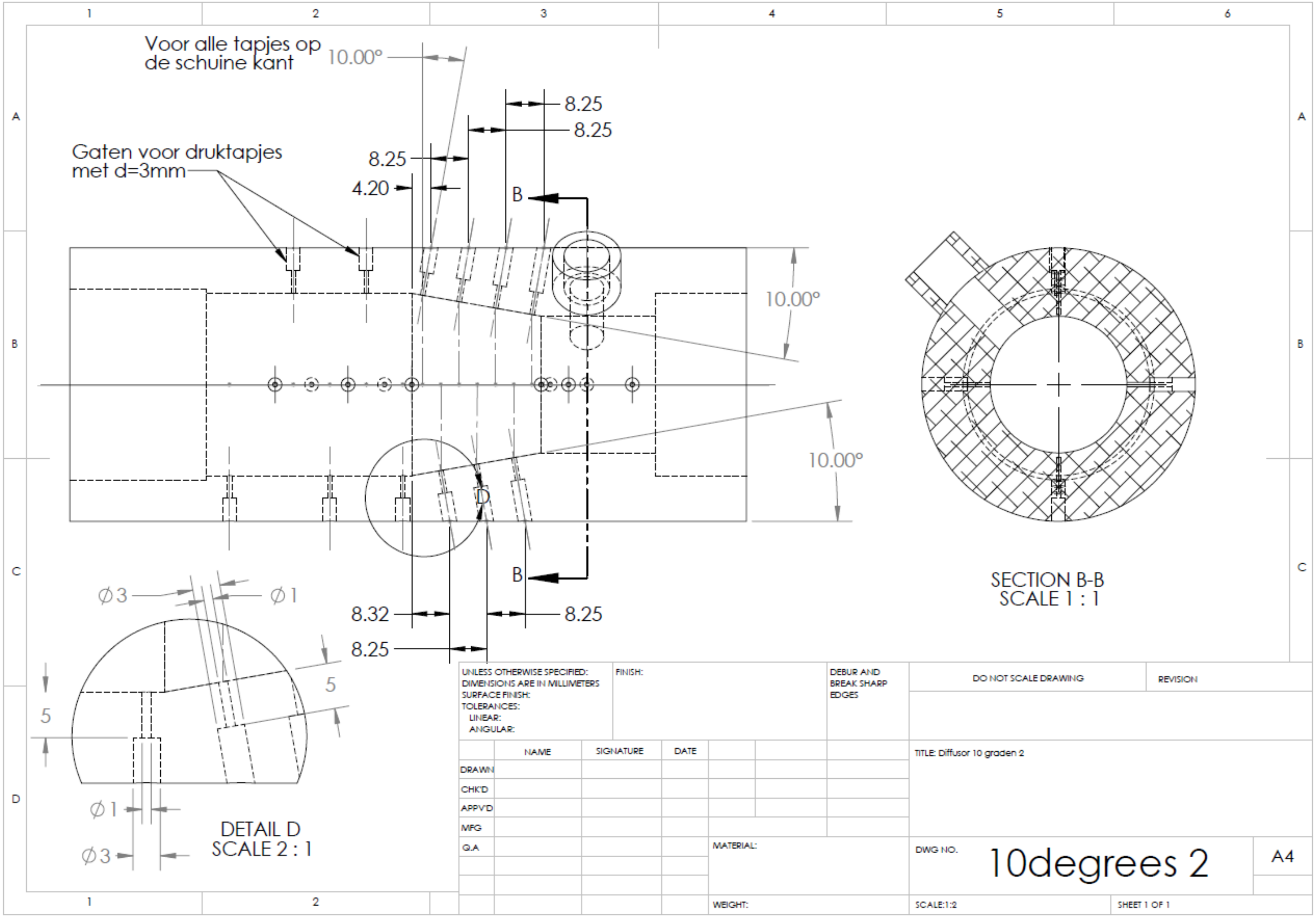
Voor alle tapjes op de schuine kant
10.00°
Gaten voor druktapjes met d=3mm
8.25
8.25
8.25
4.20
B
B
10.00°
10.00°
8.32
8.25
8.25
SECTION B-B
SCALE 1 : 1
Ø3
Ø1
5
5
Ø1
Ø3
DETAIL D
SCALE 2 : 1
D
UNLESS OTHERWISE SPECIFIED:
DIMENSIONS ARE IN MILLIMETERS
SURFACE FINISH:
TOLERANCES:
LINEAR:
ANGULAR:
FINISH:
DEBUR AND BREAK SHARP EDGES
DO NOT SCALE DRAWING
REVISION
NAME
SIGNATURE
DATE
DRAWN
CHK'D
APPV'D
MFG
Q.A
TITLE: Diffusor 10 graden 2
MATERIAL:
DWG NO.
10degrees 2
A4
WEIGHT:
SCALE:1:2
SHEET 1 OF 1
1
2
3
4
5
6
A
B
C
D

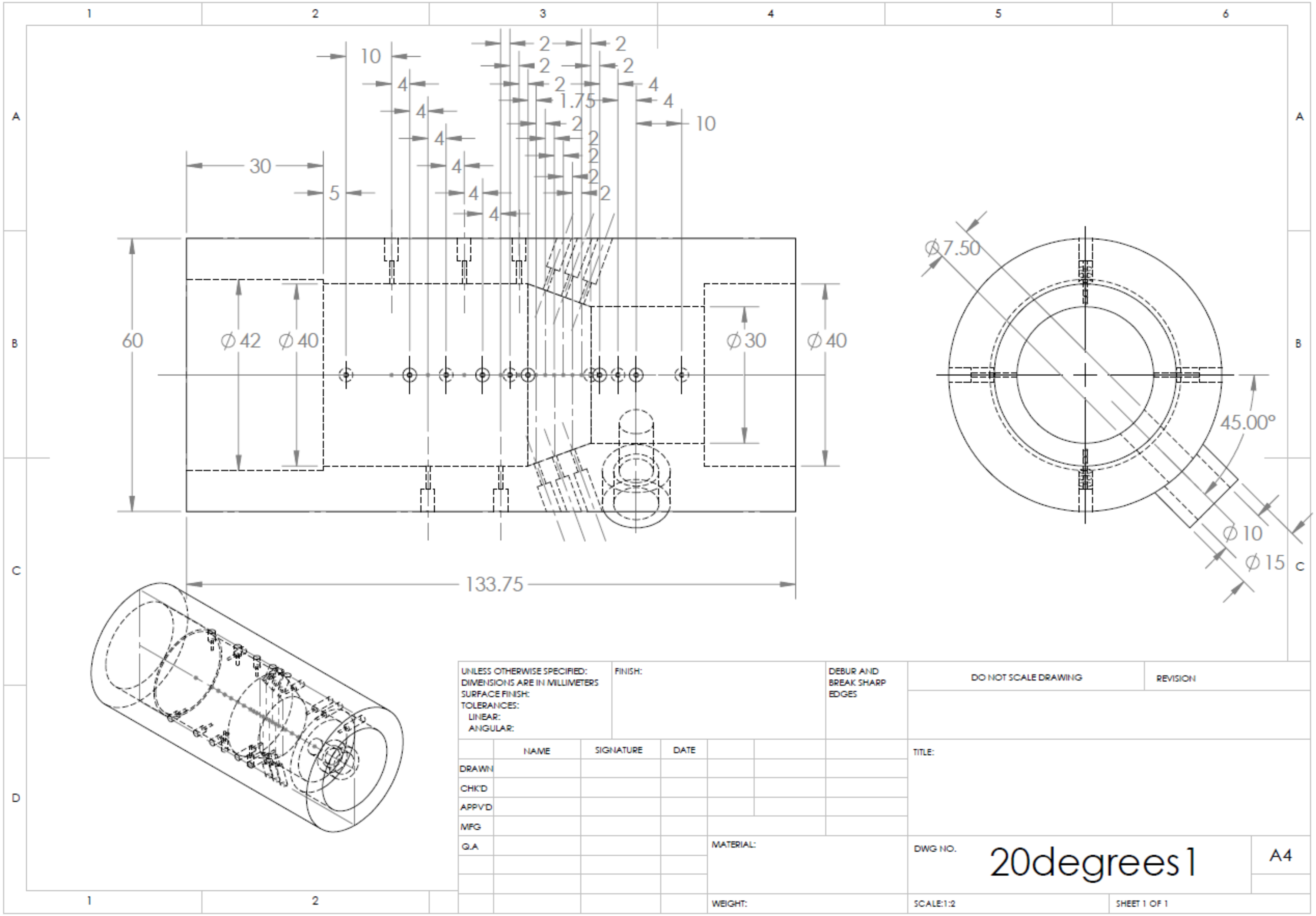
1
2
3
4
5
6
A
B
C
D
10
4
4
4
4
4
4
30
5
2
2
2
2
2
1.75
2
2
2
2
2
4
4
10
60
∅42
∅40
∅30
∅40
133.75
∅7.50
45.00°
∅10
∅15
UNLESS OTHERWISE SPECIFIED:
DIMENSIONS ARE IN MILLIMETERS
SURFACE FINISH:
TOLERANCES:
LINEAR:
ANGULAR:
FINISH:
DEBUR AND BREAK SHARP EDGES
DO NOT SCALE DRAWING
REVISION
NAME
SIGNATURE
DATE
DRAWN
CHK'D
APPV'D
MFG
Q.A
TITLE:
MATERIAL:
DWG NO.
20degrees1
A4
WEIGHT:
SCALE:1:2
SHEET 1 OF 1

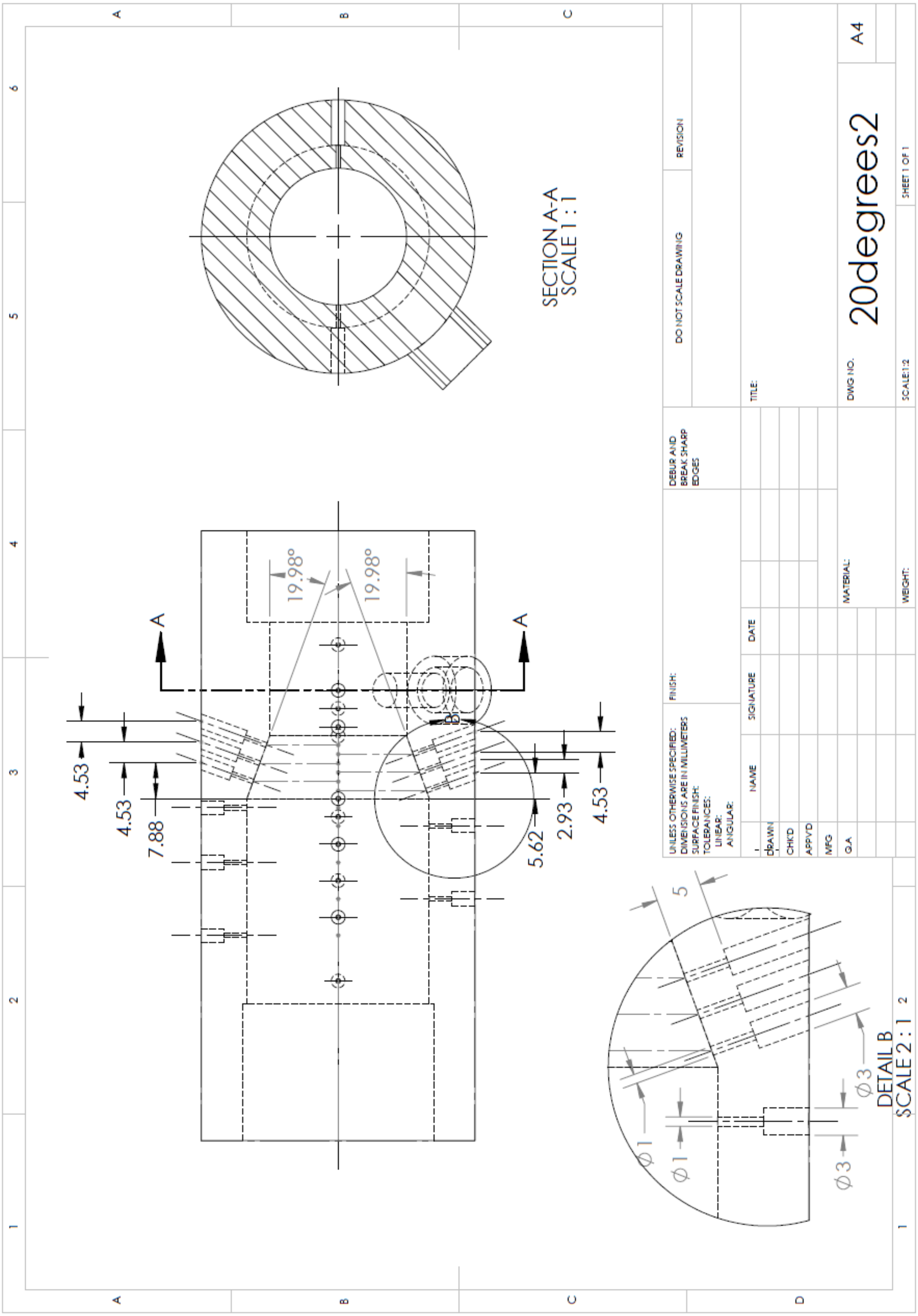
SECTION A-A
SCALE 1 : 1
19.98°
19.98°
A
A
B
4.53
4.53
7.88
5.62
2.93
4.53
DETAIL B
SCALE 2 : 1
5
∅1
∅1
∅3
∅3
UNLESS OTHERWISE SPECIFIED:
DIMENSIONS ARE IN MILLIMETERS
SURFACE FINISH:
TOLERANCES:
LINEAR:
ANGULAR:
FINISH:
DEBUR AND BREAK SHARP EDGES
DO NOT SCALE DRAWING
REVISION
NAME
SIGNATURE
DATE
DRAWN
CHK'D
APPV'D
MFG
Q.A
MATERIAL:
WEIGHT:
TITLE:
DWG NO.
20degrees2
A4
SCALE:1:2
SHEET 1 OF 1
A
B
C
D
1
2
3
4
5
6

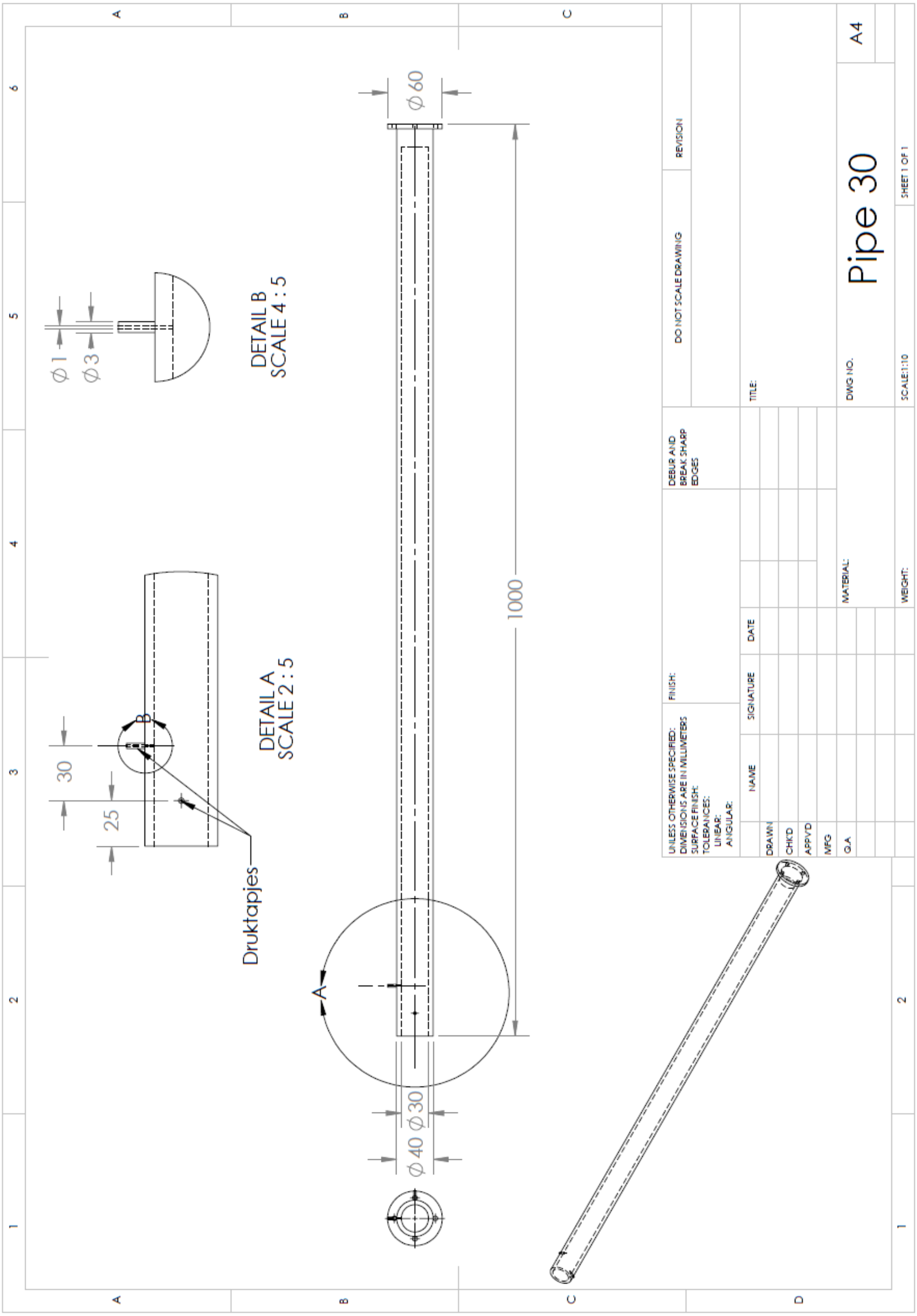
DETAIL B
SCALE 4 : 5
⌀ 1
⌀ 3
DETAIL A
SCALE 2 : 5
30
25
B
Druktapjes
⌀ 60
1000
A
⌀ 40
⌀ 30
UNLESS OTHERWISE SPECIFIED:
DIMENSIONS ARE IN MILLIMETERS
SURFACE FINISH:
TOLERANCES:
LINEAR:
ANGULAR:
FINISH:
DEBUR AND BREAK SHARP EDGES
DO NOT SCALE DRAWING
REVISION
NAME
SIGNATURE
DATE
DRAWN
CHK'D
APPV'D
MFG
Q.A
MATERIAL:
WEIGHT:
TITLE:
Pipe 30
DWG NO.
SCALE:1:10
SHEET 1 OF 1
A4
A
B
C
D
1
2
3
4
5
6

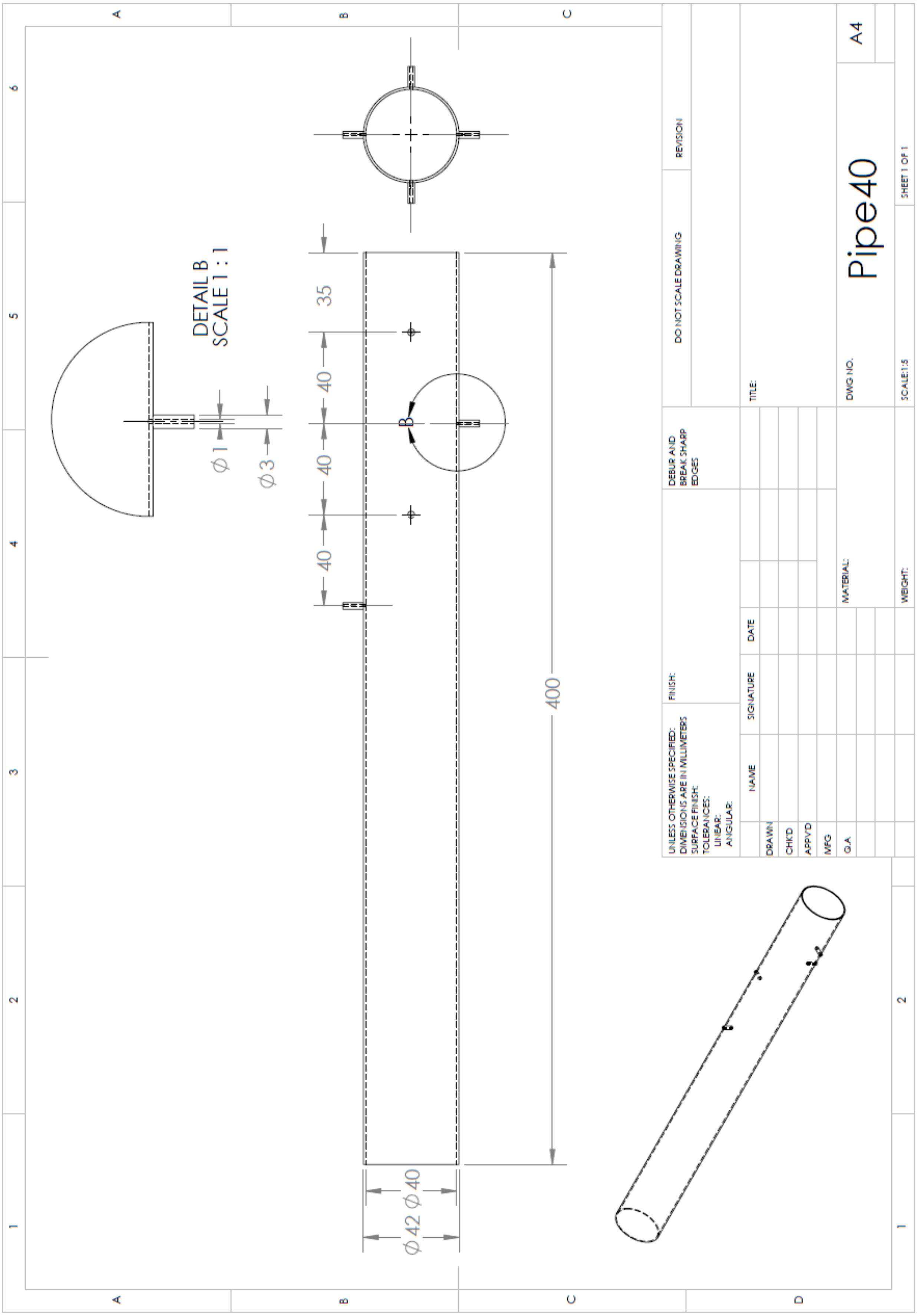
DETAIL B
SCALE 1 : 1
Ø1
Ø3
35
40
40
40
400
B
Ø42
Ø40
UNLESS OTHERWISE SPECIFIED:
DIMENSIONS ARE IN MILLIMETERS
SURFACE FINISH:
TOLERANCES:
LINEAR:
ANGULAR:
FINISH:
DEBUR AND BREAK SHARP EDGES
DO NOT SCALE DRAWING
REVISION
NAME
SIGNATURE
DATE
DRAWN
CHK'D
APPV'D
MFG
Q.A
TITLE:
MATERIAL:
DWG NO.
Pipe40
A4
WEIGHT:
SCALE:1:5
SHEET 1 OF 1
A
B
C
D
1
2
3
4
5
6

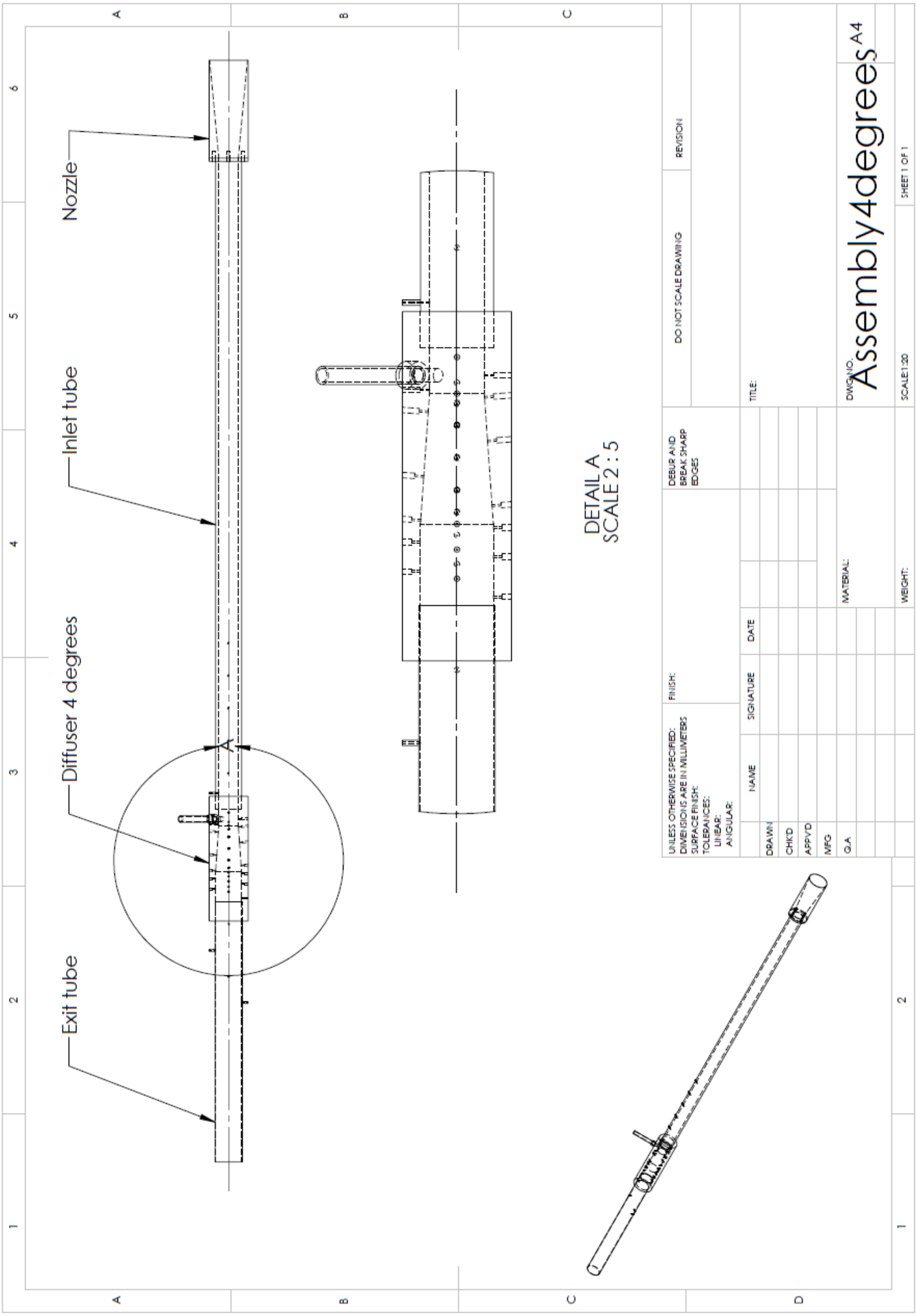
Nozzle
Inlet tube
Diffuser 4 degrees
Exit tube
A
DETAIL A
SCALE 2 : 5
UNLESS OTHERWISE SPECIFIED:
DIMENSIONS ARE IN MILLIMETERS
SURFACE FINISH:
TOLERANCES:
LINEAR:
ANGULAR:
FINISH:
DEBUR AND BREAK SHARP EDGES
DO NOT SCALE DRAWING
REVISION
NAME
SIGNATURE
DATE
DRAWN
CHK'D
APPV'D
MFG
Q.A
MATERIAL:
WEIGHT:
TITLE:
DWG NO.
Assembly4degrees
A4
SCALE:1:20
SHEET 1 OF 1
A
B
C
D
1
2
3
4
5
6

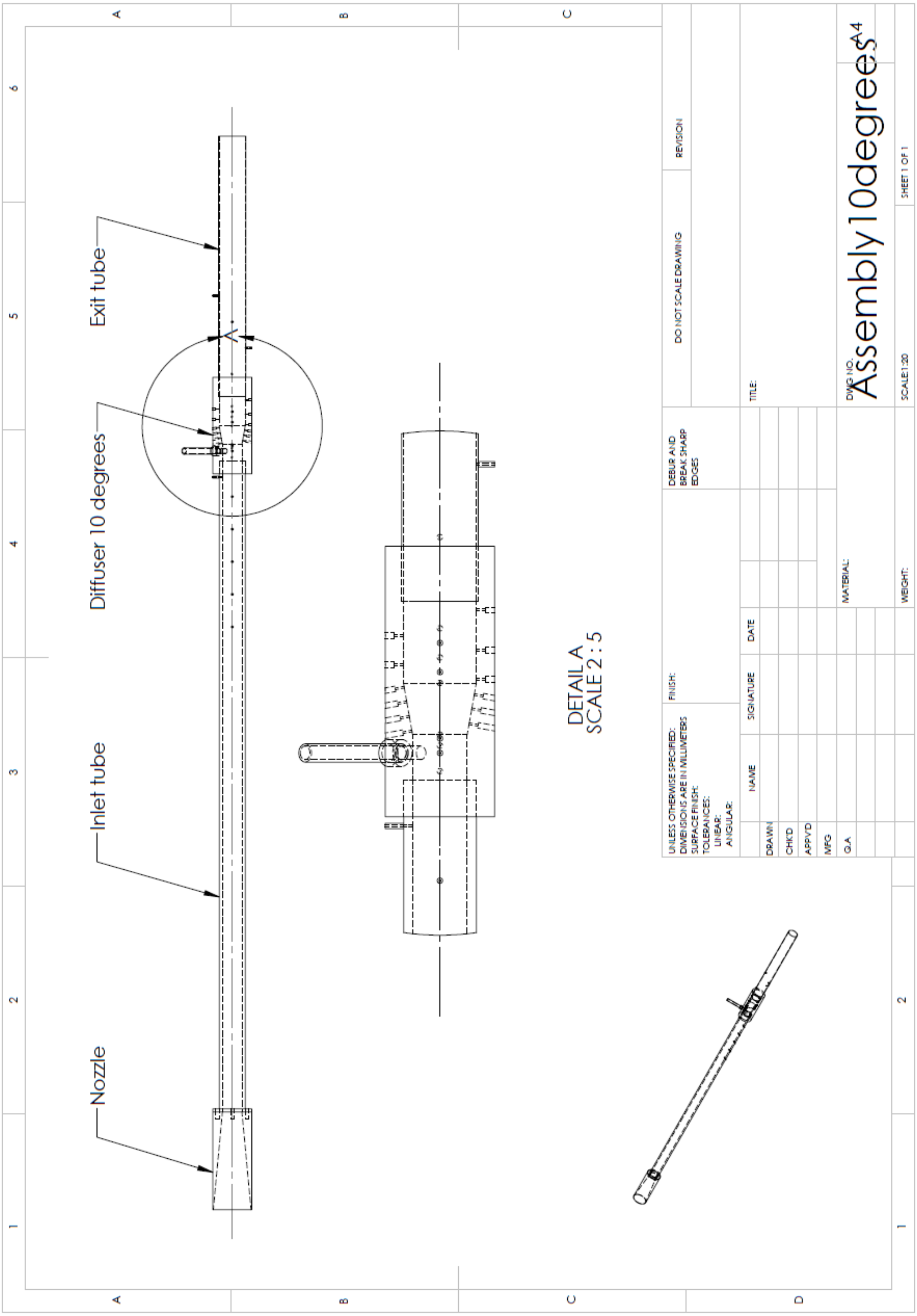
Exit tube
Diffuser 10 degrees
Inlet tube
Nozzle
DETAIL A
SCALE 2 : 5
A
B
C
D
1
2
3
4
5
6
UNLESS OTHERWISE SPECIFIED:
DIMENSIONS ARE IN MILLIMETERS
SURFACE FINISH:
TOLERANCES:
LINEAR:
ANGULAR:
FINISH:
DEBUR AND BREAK SHARP EDGES
DO NOT SCALE DRAWING
REVISION
NAME
SIGNATURE
DATE
DRAWN
CHK'D
APPV'D
MFG
Q.A
TITLE:
MATERIAL:
DWG NO.
Assembly10degrees
A4
WEIGHT:
SCALE:1:20
SHEET 1 OF 1

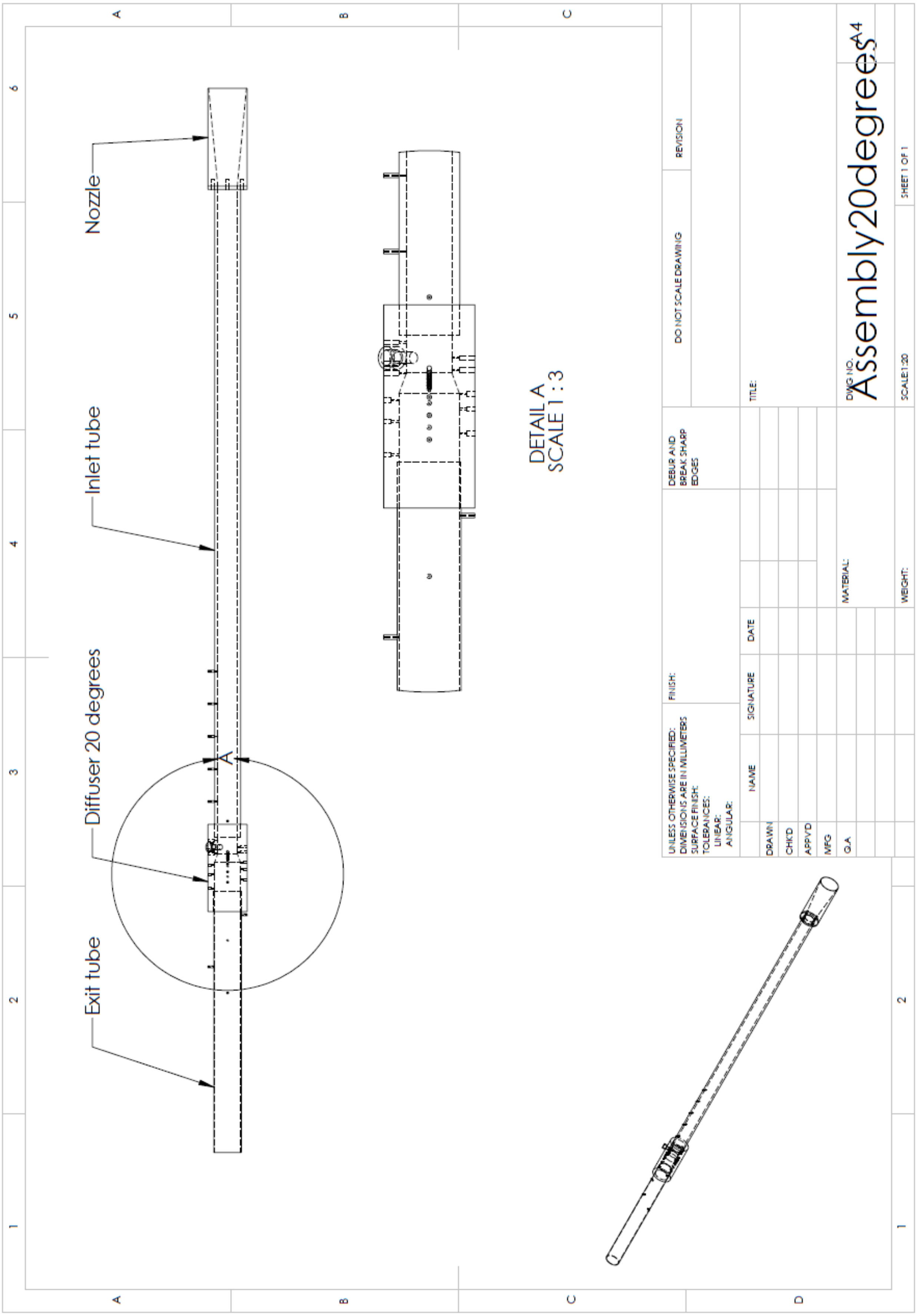
Nozzle
Inlet tube
Diffuser 20 degrees
Exit tube
A
DETAIL A
SCALE 1 : 3
UNLESS OTHERWISE SPECIFIED:
DIMENSIONS ARE IN MILLIMETERS
SURFACE FINISH:
TOLERANCES:
LINEAR:
ANGULAR:
FINISH:
DEBUR AND BREAK SHARP EDGES
DO NOT SCALE DRAWING
REVISION
NAME
SIGNATURE
DATE
DRAWN
CHK'D
APPV'D
MFG
Q.A
MATERIAL:
WEIGHT:
TITLE:
DWG NO.
Assembly20degrees
A4
SCALE:1:20
SHEET 1 OF 1
A
B
C
D
1
2
3
4
5
6

Appendix B

Experimental Data

The following chapters contain the experimental data of Experiment A to G.

B.1 Experiment A

Table B.1 to B.3 contain the experimental data of Experiment A. Figure B.1 shows the corresponding geometry of the test-section.

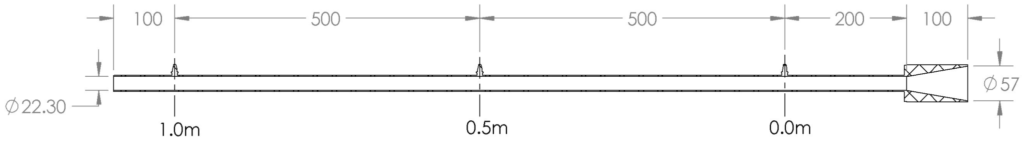

Figure B.1: Geometry of the test section of Experiment A.

Measurement A1				**Measurement A2**				**Measurement A3**			
Re $(\cdot 10^4)$	Pressure (Pa)			Re $(\cdot 10^4)$	Pressure (Pa)			Re $(\cdot 10^4)$	Pressure (Pa)		
2.354	166.8	105.0	24.5	2.358	166.8	104.0	26.5	2.370	-375.7	-294.3	-221.7
3.066	292.3	167.8	43.2	3.074	295.3	169.7	45.1	3.121	-637.7	-499.3	-383.6
3.630	410.1	225.6	61.8	3.640	410.1	226.6	62.8	3.693	-878.0	-682.8	-529.7
4.092	523.9	281.5	82.4	4.092	521.9	281.5	78.5	4.185	-1108.5	-869.2	-678.9
4.439	617.0	326.7	94.2	4.483	614.1	327.7	92.2	4.526	-1297.9	-1025.1	-795.6
4.750	701.4	367.9	108.9	4.760	704.4	369.8	112.8	4.843	-1463.7	-1157.6	-903.5
4.963	765.2	398.3	123.6	4.982	764.2	399.3	120.7	5.082	-1608.8	-1265.5	-989.8
5.298	868.2	449.3	140.3	5.325	871.1	452.2	137.3	5.474	-1852.1	-1446.0	-1144.8
x (mm)	0	500	1000		0	500	1000		0	500	1000

Table B.1: Static pressure and Reynolds numbers for Measurement A1, A2 and A3.

Measurement A4				**Measurement A5**				**Measurement A6**			
Re ($\cdot 10^4$)	Pressure (Pa)			Re ($\cdot 10^4$)	Pressure (Pa)			Re ($\cdot 10^4$)	Pressure (Pa)		
2.391	-387.5	-300.2	-227.6	2.349	-396.3	-297.2	-224.6	2.370	-390.4	-299.2	-228.6
3.153	-657.3	-513.1	-396.3	3.072	-667.1	-508.2	-391.4	3.121	-661.2	-510.1	-395.3
3.733	-905.5	-704.4	-548.4	3.693	-927.0	-711.2	-551.3	3.693	-905.5	-696.5	-542.5
4.232	-1149.7	-892.7	-696.5	4.185	-1175.2	-908.4	-704.4	4.185	-1151.7	-882.9	-697.5
4.613	-1339.1	-1045.7	-817.2	4.548	-1373.4	-1054.6	-826.0	4.526	-1344.0	-1041.8	-814.2
4.904	-1520.6	-1182.1	-929.0	4.843	-1550.0	-1201.7	-934.9	4.843	-1532.3	-1175.2	-927.0
5.159	-1659.9	-1294.9	-1018.3	5.072	-1699.0	-1309.6	-1023.2	5.082	-1657.9	-1291.0	-1021.2
5.563	-1892.3	-1495.0	-1177.2	5.465	-1950.2	-1508.8	-1185.0	5.474	-1913.0	-1484.3	-1181.1
x (mm)	0	500	1000		0	500	1000		0	500	1000

Table B.2: Static pressure and Reynolds numbers for Measurement A4, A5 and A6.

Measurement A7				**Measurement A8**				**Measurement A9**			
Re ($\cdot 10^4$)	Pressure (Pa)			Re ($\cdot 10^4$)	Pressure (Pa)			Re ($\cdot 10^4$)	Pressure (Pa)		
2.706	175	108	29	2.427	175	107	27	2.427	174	107	27
3.507	300	171	45	3.145	301	172	45	3.161	300	171	45
4.151	427	233	63	3.723	427	233	61	3.723	429	234	63
4.706	550	292	80	4.209	547	291	82	4.221	549	293	80
5.106	649	338	96	4.579	650	339	95	4.601	652	340	94
3.628	733	380	109	4.891	736	381	109	4.901	740	383	109
3.796	803	413	118	5.107	802	413	117	5.117	808	415	119
4.018	895	459	134	5.415	894	462	134	5.442	905	466	136
x (mm)	0	500	1000		0	500	1000		0	500	1000

Table B.3: Static pressure and Reynolds numbers for Measurement A7, A8 and A9.

B.2 Experiment B

Table B.4 to B.9 contain the experimental data of Experiment B. Figure B.2 shows the corresponding geometry of the test-section.

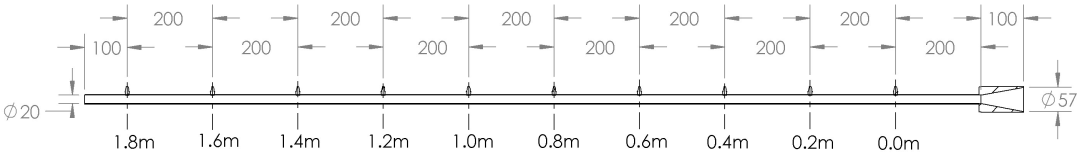

Figure B.2: Geometry of the test section of Experiment B and C.

Measurement B1

Re ($\cdot 10^4$)	Pressure (Pa)									
2.706	-388.5	-357.1	-327.7	-307.1	-283.5	-256.0	-226.6	-211.9	-185.4	-160.9
3.507	-686.7	-627.8	-567.0	-531.7	-500.3	-460.1	-407.1	-383.6	-336.5	-297.2
4.151	-964.3	-880.9	-797.6	-750.5	-714.2	-647.5	-578.8	-539.6	-479.7	-424.8
4.706	-1229.2	-1131.1	-1011.4	-957.5	-904.5	-823.1	-750.5	-706.3	-626.9	-560.2
5.106	-1438.1	-1324.4	-1187.0	-1118.3	-1064.4	-969.2	-871.1	-830.9	-735.8	-658.3
3.628	-1628.5	-1485.2	-1349.9	-1273.3	-1201.7	-1115.4	-994.7	-951.6	-838.8	-750.5
3.796	-1784.4	-1628.5	-1469.5	-1409.7	-1320.4	-1219.4	-1079.1	-1043.8	-920.2	-836.8
4.018	-2020.9	-1844.3	-1667.7	-1574.5	-1499.0	-1387.1	-1231.2	-1180.1	-1049.7	-951.6
x (mm)	0	200	400	600	800	1000	1200	1400	1600	1800

Table B.4: Static pressure and Reynolds numbers for Measurement B1.

Measurement B2

Re ($\cdot 10^4$)	Pressure (Pa)									
1.806	252.1	236.4	204.0	186.4	161.9	124.6	94.2	67.7	37.3	7.8
2.337	427.7	393.4	316.9	292.3	250.2	192.3	144.2	103.0	54.9	9.8
2.800	597.4	533.7	427.7	394.4	338.4	259.0	192.3	139.3	71.6	10.8
3.180	757.3	674.9	535.6	496.4	425.8	323.7	236.4	170.7	85.3	11.8
3.445	875.1	782.8	622.9	569.0	495.4	370.8	276.6	198.2	98.1	11.8
3.691	992.8	870.1	698.5	637.7	552.3	417.9	307.1	223.7	107.9	11.8
3.858	1075.2	945.7	753.4	699.5	604.3	450.3	332.6	242.3	115.8	10.8
4.075	1178.2	1053.6	824.0	771.1	664.1	502.3	367.9	268.8	125.6	9.8
x (mm)	0	200	400	600	800	1000	1200	1400	1600	1800

Table B.5: Static pressure and Reynolds numbers for Measurement B2.

Measurement B3

Re ($\cdot 10^4$)	Pressure (Pa)									
1.837	258.0	240.3	206.0	188.4	161.9	123.6	94.2	67.7	38.3	9.8
2.395	424.8	388.5	317.8	291.4	251.1	193.3	145.2	105.0	54.9	10.8
2.842	591.5	521.9	419.9	386.5	332.6	253.1	189.3	137.3	70.6	11.8
3.207	760.3	671.0	539.6	495.4	427.7	325.7	242.3	173.6	87.3	12.8
3.516	878.0	781.9	625.9	576.8	497.4	377.7	279.6	202.1	100.1	13.7
3.750	995.7	882.9	701.4	645.5	557.2	419.9	312.0	225.6	110.9	13.7
3.909	1082.0	959.4	761.3	700.4	606.3	456.2	336.5	243.3	117.7	12.8
4.150	1196.8	1069.3	840.7	774.0	666.1	500.3	370.8	267.8	127.5	12.8
x (mm)	0	200	400	600	800	1000	1200	1400	1600	1800

Table B.6: Static pressure and Reynolds numbers for Measurement B3.

Measurement B4

Re ($\cdot 10^4$)	Pressure (Pa)									
1.936	-465.0	-427.7	-384.6	-362.0	-338.4	-308.0	-273.7	-253.1	-220.7	-192.3
2.569	-792.6	-721.0	-653.3	-620.0	-582.7	-531.7	-475.8	-442.4	-388.5	-341.4
3.090	-1126.2	-1020.2	-922.1	-877.0	-828.0	-760.3	-683.8	-637.7	-561.1	-494.4
3.516	-1432.3	-1304.7	-1177.2	-1120.3	-1057.5	-971.2	-870.1	-823.1	-721.0	-639.6
3.831	-1687.3	-1530.4	-1388.1	-1304.7	-1250.8	-1147.8	-1025.1	-973.2	-863.3	-765.2
4.106	-1920.8	-1736.4	-1574.5	-1506.8	-1422.5	-1310.6	-1172.3	-1110.5	-983.0	-884.9
4.308	-2079.7	-1873.7	-1697.1	-1618.7	-1540.2	-1412.6	-1265.5	-1196.8	-1059.5	-951.6
4.594	-2315.2	-2089.5	-1893.3	-1805.0	-1716.8	-1579.4	-1412.6	-1344.0	-1196.8	-1069.3
x (mm)	0	200	400	600	800	1000	1200	1400	1600	1800

Table B.7: Static pressure and Reynolds numbers for Measurement B4.

Measurement B5

Re ($\cdot 10^4$)	Pressure (Pa)									
1.899	264	246	211	194	167	128	98	71	39	9
2.483	464	413	333	306	265	202	152	109	58	12
2.971	641	565	453	419	363	276	206	149	76	13
3.388	801	707	566	521	452	341	255	184	92	13
3.724	947	835	663	614	531	399	296	215	105	12
4.000	1072	948	752	697	602	451	334	243	117	11
4.184	1169	1033	817	758	656	489	362	263	125	10
4.458	1309	1159	910	844	730	545	404	293	136	8
x (mm)	0	200	400	600	800	1000	1200	1400	1600	1800

Table B.8: Static pressure and Reynolds numbers for Measurement B5.

Measurement B6

Re ($\cdot 10^4$)	Pressure (Pa)									
1.965	-475	-435	-394	-374	-348	-317	-282	-264	-231	-202
2.559	-803	-733	-660	-629	-592	-542	-484	-456	-404	-358
3.096	-1156	-1055	-952	-906	-857	-783	-703	-665	-592	-525
3.534	-1485	-1349	-1216	-1162	-1106	-1011	-906	-848	-766	-690
3.856	-1748	-1589	-1434	-1371	-1303	-1195	-1073	-1023	-911	-825
4.123	-1989	-1802	-1635	-1566	-1483	-1370	-1230	-1176	-1049	-952
4.330	-2190	-1970	-1794	-1717	-1635	-1500	-1346	-1290	-1150	-1035
4.610	-2430	-2220	-2020	-1931	-1840	-1692	-1522	-1456	-1303	-1179
x (mm)	0	200	400	600	800	1000	1200	1400	1600	1800

Table B.9: Static pressure and Reynolds numbers for Measurement B6.

B.3 Experiment C

Table B.10 to B.12 contain the experimental data of Experiment B. Figure B.2 shows the corresponding geometry of the test-section.

Measurement C1

Re ($\cdot 10^4$)	Pressure (Pa)									
1.873	248	231	200	185	160	124	95	68	38	9
2.423	427	393	320	295	254	195	147	106	56	11
2.867	604	535	432	399	345	265	198	143	73	12
3.267	765	674	539	498	431	326	244	171	87	13
3.554	890	783	625	581	502	379	281	204	100	12
3.819	1013	891	708	658	569	428	315	229	110	11
4.006	1100	970	769	716	619	465	344	250	119	12
4.270	1226	1083	857	797	691	518	383	278	130	10
x (mm)	0	200	400	600	800	1000	1200	1400	1600	1800

Table B.10: Static pressure and Reynolds numbers for Measurement C1.

Measurement C2

Re ($\cdot 10^4$)	Pressure (Pa)									
1.873	243	223	198	183	158	122	93	67	37	9
2.398	412	381	311	288	248	191	144	103	55	12
2.824	586	521	421	389	335	256	192	138	71	13
3.211	744	653	525	485	419	318	237	171	86	13
3.520	868	766	609	566	490	370	275	199	98	13
3.755	978	864	686	638	552	415	308	224	108	12
3.929	1065	940	744	693	599	451	334	243	115	12
4.184	1190	1051	826	773	668	501	369	270	127	11
x (mm)	0	200	400	600	800	1000	1200	1400	1600	1800

Table B.11: Static pressure and Reynolds numbers for Measurement C2.

Measurement C3

Re ($\cdot 10^4$)	Pressure (Pa)									
1.938	263	245	211	193	166	129	98	71	39	10
2.474	449	411	333	309	266	203	153	110	58	12
2.951	633	559	449	417	359	273	204	147	75	13
3.341	793	699	558	517	449	339	253	183	90	13
3.639	924	816	649	606	523	395	293	213	103	14
3.898	1050	928	733	684	590	444	329	239	114	12
4.081	1139	1007	794	740	637	482	354	259	121	12
4.355	1277	1130	887	829	717	539	397	289	134	10
x (mm)	0	200	400	600	800	1000	1200	1400	1600	1800

Table B.12: Static pressure and Reynolds numbers for Measurement C3.

B.4 Experiment D

Table B.13 contains the experimental data of Experiment D. Figure B.3 and B.4 show the corresponding geometry of the test-section.

Experiment D, 4 degree diffuser				**Experiment D, 10 degree diffuser**			
x (mm)	Pressure (Pa)			x (mm)	Pressure (Pa)		
190	-137	-242	-424	190	-130	-226	-400
220	-135	-236	-408	220	-128	-220	-386
250	-138	-240	-412	250	-132	-227	-398
260	-146	-259	-444	260	-139	-239	-421
270	-147	-257	-438	270	-139	-240	-425
274	-155	-275	-472	274	-136	-233	-405
278	-138	-243	-414	278	-150	-261	-456
280	-147	-257	-435	280	-143	-248	-433
282	-141	-246	-416	282	-148	-257	-440
286	-124	-214	-360	286	-103	-171	-292
290	-111	-195	-330	290	-75	-127	-222
298	-86.5	-154	-262	294	-61	-106	-186
306	-65.9	-118	-201	298	-51.5	-91	-164
316	-51	-93.3	-160	302	-43	-77	-140
326	-38.2	-71.3	-123	306	-36	-65	-118
334	-27.6	-52.6	-92.6	308	-33.3	-62	-113
342	-19.5	-38	-69	310	-33.5	-62	-117
346	-14.5	-29.5	-54.6	314	-28.5	-54	-99.6
350	-12.8	-27	-50.3	318	-24	-44.5	-85
352	-8.3	-19	-39	322	-22	-42	-80
354	-10	-22.5	-42.7	326	-22	-42	-79
358	-8.9	-19.7	-39.6	330	-20.5	-37.5	-72
362	-7.3	-17.5	-35.3	334	-14.8	-29.5	-56
366	-6.9	-16.5	-32.8	338	-12	-24	-47.5
370	-5.5	-14	-29.5	348	-8.7	-18	-37
374	-4.9	-13	-27.6	388	0	-3	-8
378	-4.2	-12	-25.8	428	3.6	3.8	4.3
382	-1.7	-7	-16	468	4.8	6	8
392	-0.8	-5	-12.6	508	5.6	8	11
432	4	4	4.4				
472	5.6	7.3	9.5				
512	5.7	8	10.9				
552	5.7	8.9	12.7				
Re $(\cdot 10^4)$	4.028	5.298	6.837		4.017	5.223	6.806

Table B.13: Static pressure and Reynolds number for Experiment D.

B.5 Experiment E

Table B.14 and B.15 contain the experimental data of Experiment E. Figure B.3 and B.4 show the corresponding geometry of the test-section.

Experiment D, 4 degree diffuser no air injection				**Experiment D, 10 degree diffuser no air injection**			
x (mm)	Pressure (Pa)			x (mm)	Pressure (Pa)		
200	-130.0	-239.0	-411.0	200	-130.6	-231.0	-407.0
230	-128.5	-232.0	-395.0	230	-129.5	-226.0	-394.0
260	-125.0	-224.0	-380.0	260	-129.0	-225.0	-390.0
270	-127.5	-229.0	-388.0	270	-125.5	-219.0	-382.0
274	-126.5	-226.0	-384.0	274	-129.0	-226.0	-392.0
278	-126.5	-226.0	-385.0	278	-135.2	-237.0	-414.0
280	-129.5	-232.0	-399.0	280	-138.0	-241.0	-426.0
282	-130.0	-233.0	-398.0	282	-122.3	-208.0	-357.0
286	-132.0	-237.0	-403.0	286	-89.9	-149.0	-255.0
290	-117.5	-209.0	-355.0	290	-67.4	-114.2	-201.0
298	-91.5	-163.0	-278.0	294	-55.8	-96.0	-171.0
306	-71.7	-129.0	-221.0	298	-47.0	-81.5	-147.0
315.75	-52.5	-95.0	-165.0	302	-40.2	-71.0	-129.0
325.5	-38.1	-69.5	-121.6	306	-34.0	-62.0	-117.0
333.5	-27.4	-51.7	-91.8	308.36	-31.2	-57.0	-108.0
341.5	-19.0	-36.5	-65.7	310.36	-27.5	-52.0	-97.0
345.5	-15.4	-31.3	-56.5	314.36	-23.6	-45.0	-87.0
349.5	-11.9	-24.1	-46.3	318.36	-21.6	-41.5	-79.5
351.5	-8.9	-20.2	-39.0	322.36	-18.0	-35.5	-67.0
353.5	-7.7	-17.6	-35.0	326.36	-15.0	-29.6	-58.0
357.5	-3.9	-12.1	-26.0	330.36	-13.0	-26.2	-52.5
361.5	-3.2	-10.7	-23.0	334.36	-11.5	-23.5	-47.0
365.5	-1.2	-6.9	-17.5	338.36	-9.7	-20.0	-40.8
369.5	-0.5	-6.3	-16.0	348.36	-5.6	-13.1	-27.5
373.5	-1.3	-6.9	-16.3	388.36	1.3	-1.5	-6.0
377.5	1.2	-2.3	-8.5	428.36	4.8	4.7	5.5
381.5	2.4	-0.5	-6.3	468.36	5.2	6.0	8.1
391.5	3.7	3.0	-0.5	508.36	5.9	7.8	12.0
431.5	4.3	4.9	4.3	508	5.6	8	11
471.5	5.9	8.3	10.0				
511.5	5.8	7.9	10.7				
551.5	6.0	9.1	12.5				
Re $(\cdot 10^4)$	3.979	5.255	6.771		4.024	5.231	6.864

Table B.14: Static pressure and Reynolds numbers for Experiment E without air injection.

Experiment D, 4 degree diffuser injection				**Experiment D, 10 degree diffuser injection**			
x (mm)	Pressure (Pa)			x (mm)	Pressure (Pa)		
200	-116.8	-205.0	-365.0	200	-93.5	-166.0	-285.0
230	-115.0	-199.0	-351.0	230	-91.5	-159.0	-272.0
260	-116.7	-200.0	-355.0	260	-82.5	-143.0	-243.0
270	-126.7	-218.0	-388.0	270	-114.3	-203.0	-344.0
274	-131.0	-228.0	-404.0	274	-98.0	-172.0	-290.0
278	-151.0	-264.0	-471.0	278	-156.5	-274.0	-472.0
280	-137.0	-239.0	-426.0	280	-129.0	-223.0	-384.0
282	-139.8	-245.0	-433.0	282	-123.0	-211.0	-359.0
286	-150.8	-266.0	-471.0	286	-123.0	-205.0	-340.0
290	-131.6	-229.0	-399.0	290	-100.0	-174.0	-298.0
298	-99.8	-176.0	-308.0	294	-75.0	-134.0	-229.0
306	-78.4	-137.6	-241.0	298	-95.0	-171.0	-291.0
315.75	-57.4	-101.8	-180.0	302	-52.0	-92.0	-158.0
325.5	-42.4	-75.7	-135.0	306	-87.0	-157.0	-267.0
333.5	-30.1	-54.8	-97.0	308.36	-85.0	-151.0	-262.0
341.5	-19.2	-37.0	-68.0	310.36	-29.0	-52.0	-91.0
345.5	-18.3	-34.6	-65.5	314.36	-29.5	-51.0	-97.0
349.5	-14.3	-28.2	-53.0	318.36	-61.0	-111.0	-193.0
351.5	-9.0	-18.4	-36.5	322.36	-49.0	-90.0	-157.0
353.5	-6.9	-15.2	-30.5	326.36	-29.0	-54.0	-93.0
357.5	-6.5	16.0	-31.0	330.36	-27.0	-52.0	-89.0
361.5	-5.0	-12.3	-25.5	334.36	-26.0	-51.0	-89.0
365.5	-1.2	-5.1	-15.0	338.36	-21.0	-40.0	-74.0
369.5	-0.5	-5.0	-13.5	348.36	-13.0	-25.0	-48.0
373.5	-1.8	-7.0	-16.5	388.36	2.0	1.0	0.0
377.5	1.0	-2.4	-8.2	428.36	9.2	14.0	21.0
381.5	2.3	0.0	-4.0	468.36	9.9	15.0	27.0
391.5	4.6	3.8	2.5	508.36	9.0	13.0	28.0
431.5	5.0	6.2	7.5	508	5.6	8	11
471.5	7.5	9.8	14.8				
511.5	6.9	9.3	13.5				
551.5	6.8	10.0	15.2				
Re $(\cdot 10^4)$	4.013	5.223	6.802		3.997	5.216	6.718

Table B.15: Static pressure and Reynolds numbers for Experiment E with air injection.

B.6 Experiment F

Table B.16 and **??** contain the experimental data of Experiment F. Figure B.3 to B.5 show the corresponding geometry of the test-section.

Experiment D, 4 degree diffuser no air injection				**Experiment D, 10 degree diffuser no air injection**				**Experiment D, 20 degree diffuser no air injection**	
x (mm)	Pressure (Pa)			x (mm)	Pressure (Pa)			x (mm)	Pressure (Pa)
0	-92.2	-165.5	-293.0	0	-87.4	-158.7	-283.0		
50	-103.5	-181.5	-323.0	50	-98.3	-175.6	-311.0		
100	-111.4	-194.2	-342.0	100	-105.9	-188.3	-331.0		
150	-124.2	-216.0	-379.0	150	-118.1	-210.0	-370.0		
200	-131.2	-227.0	-397.0	200	-125.7	-220.0	-386.0		
230	-136.3	-234.0	-408.0	230	-130.1	-228.0	-398.0		
260	-137.8	-237.0	-414.0	260	-131.0	-227.0	-397.0		
270	-134.0	-225.0	-393.0	270	-126.5	-222.0	-386.0		
274	-131.0	-225.0	-392.0	274	-130.5	-225.0	-399.0		
278	-133.9	-233.0	-401.0	278	-137.5	-235.0	-415.0		
280	-137.3	-234.0	-411.0	280	-139.6	-241.0	-427.0		
282	-135.3	-231.0	-408.0	282	-123.5	-207.0	-356.0		
286	-137.7	-236.0	-414.0	286	-91.5	-150.0	-258.0		
290	-123.3	-210.0	-367.0	290	-68.2	-114.0	-200.0		
298	-95.7	-163.2	-287.0	294	-56.5	-96.0	-171.5		
306	-75.6	-128.4	-227.0	298	-46.9	-81.0	-148.0		
315.75	-55.3	-95.4	-170.0	302	-40.7	-71.0	-129.0		
325.5	-40.0	-69.7	-126.8	306	-35.0	-63.0	-117.5		
333.5	-29.5	-52.3	-95.7	308.36	-31.9	-58.5	-107.5		
341.5	-19.9	-28.3	-69.1	310.36	-28.3	-52.0	-96.0		
345.5	-16.6	-31.4	-59.8	314.36	-24.2	-46.5	-88.0		
349.5	-12.6	-24.6	-48.9	318.36	-21.8	-42.5	-80.0		
351.5	-9.8	-20.5	-41.0	322.36	-18.5	-35.7	-68.5		
353.5	-8.3	-17.8	-36.0	326.36	-15.3	-29.9	-58.0		
357.5	-5.0	-12.0	-27.2	330.36	-13.4	-27.0	-52.5		
361.5	-4.1	-10.4	-24.6	334.36	-11.7	-24.3	-47.5		
365.5	-2.4	-7.4	-18.5	338.36	-10.1	-20.7	-40.0		
369.5	-1.6	-6.3	-16.3	348.36	-5.8	-13.6	-28.3		
373.5	-0.7	-4.7	-13.3	388.36	0.8	-1.9	-5.5		
377.5	0.9	-2.4	-9.5	428.36	4.0	4.1	5.2		
381.5	1.6	-1.0	-6.8	468.36	4.9	6.1	8.0		
391.5	3.8	3.0	0.0	508.36	5.7	8.1	12.0		
431.5	4.2	4.6	4.2						
471.5	5.9	7.7	10.1						
511.5	5.8	7.8	10.8						
551.5	6.2	8.7	12.4						
Re ($\cdot 10^4$)	3.979	5.255	6.771		4.024	5.231	6.864		

Table B.16: Static pressure and Reynolds numbers for Experiment F without air injection.

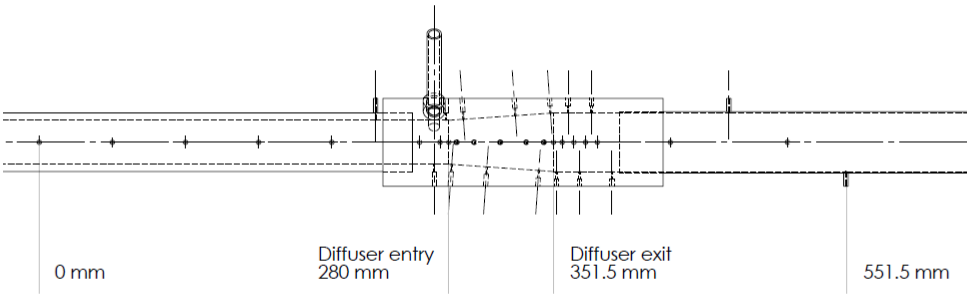

Figure B.3: Geometry of the test section for Experiment D, E, and F with 4 degree diffuser. Experiment D and E have been done without the first four pressure taps.

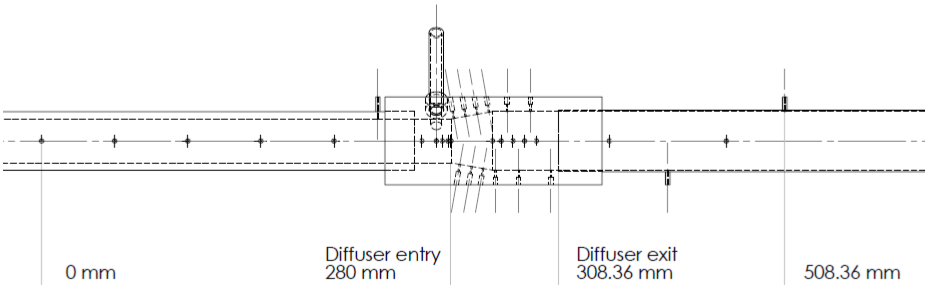

Figure B.4: Geometry of the test section for Experiment D, E, and F with 10 degree diffuser. Experiment D and E have been done without the first four pressure taps.

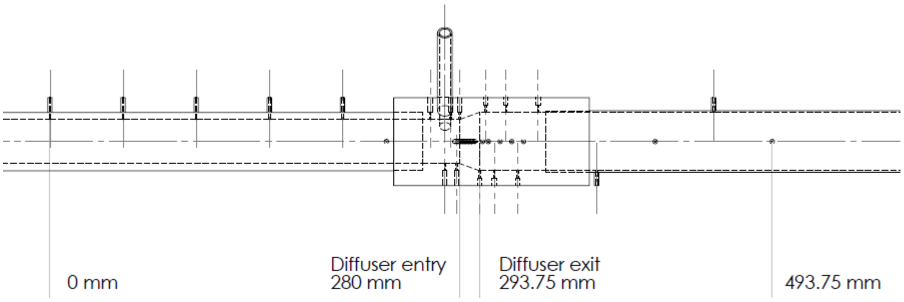

Figure B.5: Geometry of the test section for Experiment F with 20 degree diffuser.

B.7 Experiment G

Table B.17 and B.18 contain the experimental data of Experiment F. Figure B.6 shows the corresponding geometry of the test-section.

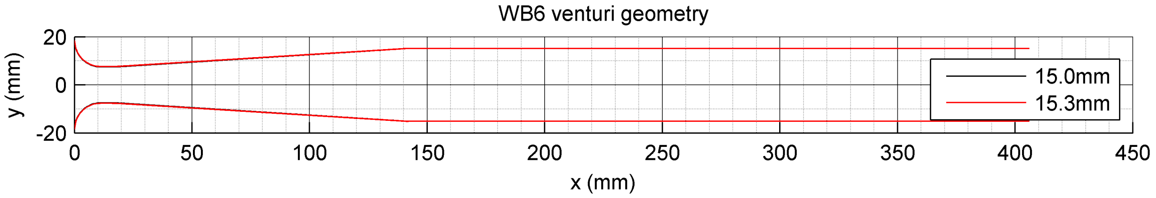

Figure B.6: Geometry of the WB6 venturi with a throat diameter of 15.0 mm and 15.3 mm.

15.0 mm, injection				**15.0 mm, no injection**			
x (mm)	Pressure (Pa)			x (m)	Pressure (Pa)		
11	-1785	-3350	-4940	11	-1530	-3070	-4390
11	-1720	-3220	-4740	11	-1500	-3000	-4240
26	-1190	-2130	-3120	26	-1240	-2210	-3050
51	-707	-1275	-1850	51	-625	-1225	-1720
76	-504	-895	-1293	76	-438	-850	-1200
101	-402	-703	-1015	101	-358	-684	-975
126	-344	-595	-850	126	-316	-591	-850
166	-319	-556	-795	166	-286	-533	-755
206	-316	-549	-785	206	-275	-510	-725
256	-318	-555	-795	256	-268	-498	-704
306	-322	-559	-800	306	-268	-497	-696
356	-326	-569	-808	356	-270	-500	-703
406	-331	-576	-825	406	-274	-512	-721
Re $(\cdot 10^4)$	2.370	3.190	3.842		2.262	3.192	3.842

Table B.17: Static pressure and Reynolds numbers for Experiment G, WB6 venturi with 15.0 mm throat diameter.

15.3 mm, injection				**15.3 mm, no injection**			
x (mm)	Pressure (Pa)			x (m)	Pressure (Pa)		
11	-1610	-3110	-4660	11	-1425	-2780	-4110
11	-1630	-3160	-4740	11	-1460	-2860	-4190
26	-1135	-2130	-3160	26	-1190	-2180	-3080
51	-656	-1235	-1815	51	-618	-1155	-1680
76	-465	-867	-1270	76	-433	-815	-1165
101	-367	-675	-980	101	-352	-650	-930
126	-311	-565	-815	126	-306	-550	-810
166	-288	-523	-758	166	-273	-510	-715
206	-285	-519	-753	206	-264	-485	-690
256	-287	-525	-758	256	-262	-475	-670
306	-289	-529	-762	306	-262	-472	-665
356	-293	-535	-772	356	-263	-476	-670
406	-300	-546	-789	406	-267	-486	-683
Re $(\cdot 10^4)$	2.330	3.197	3.870		2.318	3.214	3.857

Table B.18: Static pressure and Reynolds numbers for Experiment G, WB6 venturi with 15.3 mm throat diameter.